GRADUATE AERONAUTICAL LABORATORIES

CALIFORNIA INSTITUTE OF TECHNOLOGY

Chemical Reactions in Turbulent Mixing Flows

Paul E. Dimotakis*, James E. Broadwell** and Anthony Leonard†

Air Force Office of Scientific Research
Grant No. 83-0213
Final Report for the period ending 31 December 1988

1 June 1989

Firestone Flight Sciences Laboratory

Guggenheim Aeronautical Laboratory

Karman Laboratory of Fluid Mechanics and Jet Propulsion

Pasadena

Unclassified
SECURITY CLASSIFICATION OF THIS PAGE

REPORT DOCUMENTATION PAGE

Form Approved OMB No. 0704-0188

1a. REPORT SECURITY CLASSIFICATION: Unclassified	1b. RESTRICTIVE MARKINGS: None.
2a. SECURITY CLASSIFICATION AUTHORITY	3. DISTRIBUTION/AVAILABILITY OF REPORT: Approved for public release; distribution is unlimited.
2b. DECLASSIFICATION/DOWNGRADING SCHEDULE	
4. PERFORMING ORGANIZATION REPORT NUMBER(S)	5. MONITORING ORGANIZATION REPORT NUMBER(S): AFOSR-TR- 89-1035
6a. NAME OF PERFORMING ORGANIZATION: California Institute of Technology; 6b. OFFICE SYMBOL (If applicable)	7a. NAME OF MONITORING ORGANIZATION: AFOSR/NA
6c. ADDRESS (City, State, and ZIP Code): Pasadena, California 91125	7b. ADDRESS (City, State, and ZIP Code): Building 410, Bolling AFB DC 20332-6448
8a. NAME OF FUNDING/SPONSORING ORGANIZATION: AFOSR/NA; 8b. OFFICE SYMBOL (If applicable): NA	9. PROCUREMENT INSTRUMENT IDENTIFICATION NUMBER: AFOSR 83-0213
8c. ADDRESS (City, State, and ZIP Code): Building 410, Bolling AFB DC 20332-6448	10. SOURCE OF FUNDING NUMBERS: PROGRAM ELEMENT NO. 61102F; PROJECT NO. 2308; TASK NO. A2; WORK UNIT ACCESSION NO.

11. TITLE (Include Security Classification)

(U) Chemical Reactions in Turbulent Mixing Flows

12. PERSONAL AUTHOR(S)

Paul E. Dimotakis, James E. Broadwell, Anthony Leonard

13a. TYPE OF REPORT	13b. TIME COVERED	14. DATE OF REPORT (Year, Month, Day)	15. PAGE COUNT
Final Scientific	FROM 86/01/01 TO 12/88	1989, June, 1	131

16. SUPPLEMENTARY NOTATION 88/12/31

17. COSATI CODES			18. SUBJECT TERMS (Continue on reverse if necessary and identify by block number)
FIELD	GROUP	SUB-GROUP	
20	04		Turbulence, shear flow, combustion
21	01		

19. ABSTRACT (Continue on reverse if necessary and identify by block number)

The purpose of this research has been to conduct fundamental investigations of turbulent mixing, chemical reaction and combustion processes in turbulent, subsonic and supersonic flows. Progress in this effort thus far has uncovered important deficiencies in conventional modeling of these phenomena, and offered alternative suggestions and formulations to address some of these deficiences. This program is comprised of an experimental effort, an analytical modeling effort, a computational effort, and a diagnostics development and data acquisition effort, the latter as dictated by specific needs of our experiments.

Our approach has been to carry out a series of detailed theoretical and experimental studies primarily in two, well-defined, fundamentally important flow fields: free shear layers and axisymmetric jets. To elucidate molecular transport effects, experiments and theory concern themselves with both liquids and gases. Modeling efforts have been focused on both shear layers and turbulent jets, with an effort to include the physics of the

(continued on back of this page)

20. DISTRIBUTION/AVAILABILITY OF ABSTRACT: ☒ UNCLASSIFIED/UNLIMITED ☒ SAME AS RPT. ☐ DTIC USERS	21. ABSTRACT SECURITY CLASSIFICATION: Unclassified
22a. NAME OF RESPONSIBLE INDIVIDUAL: Julian M Tishkoff	22b. TELEPHONE (Include Area Code): (202) 767-[illegible] 4465; 22c. OFFICE SYMBOL: AFOSR/NA

DD Form 1473, JUN 86 Previous editions are obsolete. SECURITY CLASSIFICATION OF THIS PAGE

14

Unclassified

Block 19, Abstract, continued.

molecular transport processes, as well as formulations of models that permit the full chemical kinetics of the combustion process to be incorporated. The computational studies are at present, focused at fundamental issues pertaining to the computational simulation of both compressible and incompressible flows.

This report includes an outline discussion of work completed under the sponsorship of this Grant, with six papers, which have not previously been included in past reports, or transmitted in reprint form, appended.

GRADUATE AERONAUTICAL LABORATORIES
CALIFORNIA INSTITUTE of TECHNOLOGY
Pasadena, California 91125

Chemical Reactions in Turbulent Mixing Flows

Paul E. Dimotakis*, James E. Broadwell** and Anthony Leonard†

Air Force Office of Scientific Research
Grant No. 83-0213
Final Report for the period ending 31 December 1988

1 June 1989

---

* Professor, Aeronautics & Applied Physics.

** Senior Scientist, Aeronautics.

† Professor, Aeronautics.

Abstract

The purpose of this research has been to conduct fundamental investigations of turbulent mixing, chemical reaction and combustion processes in turbulent, subsonic and supersonic flows. Progress in this effort thus far has uncovered important deficiencies in conventional modeling of these phenomena, and offered alternative suggestions and formulations to address some of these deficiencies. This program is comprised of an experimental effort, an analytical modeling effort, a computational effort, and a diagnostics development and data-acquisition effort, the latter as dictated by specific needs of our experiments.

Our approach has been to carry out a series of detailed theoretical and experimental studies primarily in two, well-defined, fundamentally important flow fields: free shear layers and axisymmetric jets. To elucidate molecular transport effects, experiments and theory concern themselves with both liquids and gases. Modeling efforts have been focused on both shear layers and turbulent jets, with an effort to include the physics of the molecular transport processes, as well as formulations of models that permit the full chemical kinetics of the combustion process to be incorporated. The computational studies are, at present, focused at fundamental issues pertaining to the computational simulation of both compressible and incompressible flows.

This report includes an outline discussion of work completed under the sponsorship of this Grant, with six papers, which have not previously been included in past reports, or transmitted in reprint form, appended.

1. Introduction

This effort has been directed towards issues involving mixing and chemical reactions in turbulent shear flows at moderate to high Reynolds numbers. More specifically, the effort has been directed towards addressing generic issues in these flows and their dependence on the various parameters of the flow/chemical system, such as

1. entrainment and mixing of the entrained fluids, and their dependence on
   a. Reynolds number,
   b. Schmidt number,
   c. differential diffusion effects,
   d. free stream density ratio,
   e. dilatation owing to combustion heat release,

   and, during the last year, or so, extending the studies to
   f. compressibility, as measured by the convective Mach number in shear layers;

and

2. chemistry of the combusting reactants comprising the entrained fluids, including effects of stoichiometry and chemical kinetics.

Experimental, analytical and theoretical/modeling efforts undertaken as part of this program have focused on the mixing in turbulent shear layers and jets to provide the arena in which to address such issues. The computational effort has concentrated on fundamental issues in both compressible and incompressible flows and has not addressed mixing and chemical reactions, *per se*, to date.

Progress in the effort reported here has been realized in all of these areas, with significant work completed in:

a. non-reacting, gas phase, turbulent jets[‡];

b. chemically reacting, gas phase, subsonic shear layers with unequal free stream densities;

c. hydrodynamic linear stability analysis of homogeneous compressible free (unbounded) shear layers;

and in

d. the design of the supersonic shear layer combustion facility.

Other work in progress* includes:

---

‡ The investigations of turbulent mixing and combustion in turbulent jets are co-sponsored, in part, by the Gas Research Institute.

* Continuing under AFOSR (URI) Contract No. F49620-86-C-0113 and AFOSR Grant No. 88-0155.

e. fabrication of the new supersonic shear layer facility;

f. investigations of gas phase, chemically reacting jets;

g. liquid phase jet mixing and interface topology studies;

h. analysis of the effects of compressibility using linear hydrodynamic stability methods;

i. the development of jet mixing models that permit the inclusion of full chemical kinetics calculations;

j. the development of lagrangian computational methods for compressible, unsteady flows;

and

k. the development of efficient algorithms for vortex dynamics calculations.

We should note that this effort is part of a larger effort at the Graduate Aeronautical Laboratories of the California Institute of Technology to investigate turbulent entrainment, and mixing — with or without chemical reactions and combustion — with contributions from students faculty and staff, not cited in this report, in a broad variety of contexts. While the Air Force Office of Scientific Research support represents the larghest single contribution to the sponsorship of this effort, parts of the larger effort are co-sponsored by the Gas Research Institute, the Office of Naval Research, the Department of Energy, and the National Bureau of Standards, with additional contributions by both Industry (Rockwell, Rocketdyne) and the California Institute of Technology.

2. Mixing and combustion in turbulent shear layers

The experimental effort directed towards subsonic shear layer mixing and combustion was being brought to a close during the last year of this Grant, in preparation for the conversion of the H_2/F_2 shear layer combustion facility to supersonic flow operation.

2.1 Heat release effects

A first documentation of the previously completed research on subsonic shear layer heat release effects was published in the *AIAA J.* (Hermanson, Mungal & Dimotakis 1987). A copy of the paper is included as Appendix A. An archival documentation of that effort has just appeared in the *J. Fluid Mechanics* (Hermanson & Dimotakis 1989).

2.2 Free stream density ratio effects

A preliminary discussion of these effects was included in the previous annual report (Dimotakis, Broadwell & Leonard 1987). A first documentation was presented at the 1^{st} *National Fluid Dynamics Congress* (Frieler & Dimotakis 1988). A copy of that paper is included as Appendix B.

2.3 A cascade model for shear layer mixing and chemical reactions

A brief discussion of this model was included in the previous annual report (Dimotakis, Broadwell & Leonard 1987) and was presented at the *U.S.–France Workshop on Turbulent Reactive Flows*. This model seems able to capture a variety of the features of the data in low heat release, fast kinetics chemically reacting shear layer data. It has since been published (Dimotakis 1987). A copy is included as Appendix C.

2.4 Finite kinetics effects on shear layer combustion

The issue of finite kinetics (Damköhler number) effects in chemical product formation was addressed as part of this effort experimentally and theoretically in the context of the model proposed by Broadwell & Breidenthal (1982). The conclusion of this experimental (Mungal & Frieler 1988) and modeling effort (Broadwell & Mungal 1986, 1988) was that a Damköhler number of approximately 40 is required, based on the ratio of the turbulent flow convection time,

$$\tau_c \equiv \frac{x}{U_c} ,$$

for the large scale shear layer structures to reach a station x, with U_c the large scale structure convection velocity, to the chemical reaction time τ_χ required for the chemical reaction. The latter was estimated using a constant mass, finite kinetics calculation of a homogeneous reactor and the $H_2/NO/F_2$ chemical system, with the aid of the CHEMKIN chemical kinetics package made available to us by the SANDIA laboratories at Livermore (Kee *et al.* 1980).

A more simplified mixing model, which can be considered nearly correct in the limit of slow chemistry, was attempted by Dimotakis & Hall, which permitted, however, the computation of the full chemical kinetic system (using CHEMKIN) by modeling the shear layer as a homogeneous reactor into which the reactants are introduced at the correct total rate and ratio, as dictated by our understanding of these quantities for the shear layer (*e.g.* Dimotakis 1986). This analysis was also extended into the compressible flow regime, using the available information at the time, as part of the design effort for the new supersonic shear layer combustion facility. We subsequently decided that the results of this analysis might be of interest in a broader context and they were presented at the 23^{rd} *Joint Propulsion Meeting* (Dimotakis & Hall 1987). They are included in this report as Appendix D.

2.5 Hydrodynamic stability of compressible shear layers

A first calculation of the hydrodynamic stability characteristics of compressible, free and unbounded shear layers was presented at the 1^{st} *National Fluid Dynamics Congress* (Zhuang, Kubota & Dimotakis 1988). A copy is included as Appendix E. This effort is continuing with calculations of the effect of different free stream densities, static temperatures, molecular weights, ratios of specific heats, *etc.*, presently in progress.

2.6 Supersonic shear layer combustion facility

The design of the supersonic shear layer combustion facility was completed (Hall *et al.* 1988; an updated version of this document is in preparation). A significant advance has been realized, in our opinion, in the design of the throttling valve and associated control system, which will regulate the pressure in the supersonic stream plenum during the expected 3 *sec* run time by means of an active feedback loop with sufficient bandwidth and resolution to meet the flow quality specifications.

Fabrication and assembly begun last summer, with many of the major components in place at this writing. The initial configuration is with a (low) supersonic ($M_1 = 1.5$) high speed free stream and a subsonic ($M_2 = 0.2$) low speed stream. High speed stream nozzles for $M_1 = 2.5$ and $M_1 = 3.2$ have also been fabricated. Please note, however, that the low speed stream gas supply section is capable of providing supersonic flow for the low speed stream also, should that prove an issue in the future. We expect a first, non-reacting run, with this initial configuration, sometime this summer.

3. Mixing and combustion in turbulent jets

The part of the research effort dealing with mixing, chemical reactions and combustion in turbulent jets is co-sponsored by the Gas Research Institute**.

3.1 Gas phase mixing in turbulent non-reacting jets

The work on moderate Reynolds number ($5,000 < Re < 40,000$) non-reacting turbulent jet mixing, using high time and space resolution laser Rayleigh scattering diagnostic techniques was completed. A first presentation of the low Reynolds number data ($Re = 5,000$) from this work was made at the 1^{st} *National Fluid Dynamics Congress* (Dowling & Dimotakis 1988) and has since been submitted to the *AIAA J.* for publication. A copy of that paper is included as Appendix F. A thesis documenting a large part of this work was also completed (Dowling 1988) last spring. An archival documentation of part of the effort, dealing with the similarity properties of the far field of the jet fluid concentration field in gas-phase turbulent jets, including the results of experiments that were completed subsequent to the thesis, has been submitted for publication (Dowling & Dimotakis 1989).

** GRI Contract No. 5087-260-2467 (1-Jan-87 to 31-Dec-89).

3.2 High Pressure jet Combustion Facility

The fabrication of this facility (Dimotakis, Broadwell & Leonard 1988, Sec. 3.2) is nearing completion at this writing. Recall that it is designed to address a series of issues regarding the dependence of turbulent jet (molecular) mixing on such flow/chemistry parameters as reactant stoichiometry, Reynolds number, heat release (with or without buoyancy effects), and Damköhler number. Its main capability is in that it permits the study of turbulent jet mixing with chemical reactions and combustion to be studied over a range of pressures of $0.1\,atm < p_0 < 10\,atm$, permitting a range of two decades of Reynolds number to be covered. Depending on other constraints imposed on the flow/chemical system, as much as additional decade might be achievable. This effort is part of the Ph.D. research of Mr. Richard Gilbrech.

Some delays in the final assembly and testing were incurred in order to improve the jet fluid delivery system so as to shorten the flow start-up time. The first hot runs are expected sometime during June 1989.

3.3 Turbulent structure and mixing in high Schmidt number jets

We are continuing investigations of the fine scale turbulent structure in a liquid phase (high Schmidt number), axisymmetric jet. Laser-induced fluorescence (LIF) concentration measurements have been performed at Reynolds numbers of 10,000 and 20,000, both on the centerline and at several radial locations. While keeping the moderate Reynolds numbers in mind, we have made several *findings to date:*

1. No -1 slope is observed in the power spectrum at scales below the Kolmogorov scale, as would have been expected (Batchelor 1959)[†]. This reflects on the structure of the straining field at these scales, which aer important for molecular diffusion and mixing, and has interesting ramifications for jet modeling for both gas phase and liquid phase jet mixing modeling.
2. The behavior of the inertial range of the spectrum suggests that the turbulence has in some sense not reached its asymptotic behavior at these Reynolds numbers (as evidenced by an incipient, but possibly underdeveloped, $-5/3$ slope). This may be significant in as much as this range of Reynolds numbers is typically considered as corresponding to fully developed flow, as least in terms of measured flame lengths (*e.g.* Dahm & Dimotakis 1987).
3. As reported previously in gas phase jets (Dowling 1988), the inertial range spectrum power law exponent depends on the radial measurement location $r/(x - x_0)$ in the jet. Unless the variation can be attributed to differences between temporal and spatial data, this would suggest that qualitative differences may exist in the turbulent field as a function of radial position.

[†] We appreciate that measurements of very high spatial and temporal resolution, as well as very high signal-to-noise ratio, are required to make this claim. We have made advances in our LIF technique, however, and abandoned imaging diagnostics, for the time being, in the interest of observing these specifications.

4. Calculations have been performed on both two-dimensional image data, and very long records of high spatial and temporal resolution single-point scalar data, to investigate the validity of a fractal dimension description of the iso-scalar surfaces in the jet, as has been suggested (*e.g.* Sreenivasan & Meneveau 1986, Gouldin 1988). Our data suggest that *no such fractal dimension exists*. On the other hand, our data suggest that the geometry can be described in terms a similarity relation, which is not a power law, however.

It has been determined that measurements at still higher Reynolds number should have sufficient resolution to address many of these questions. A new jet plenum and flow control system are being constructed which will permit operation up to $Re = 100,000$. Such measurements will allow us to address issues concerning Reynolds number effects.

This effort is part of the Ph.D. research of Mr. Paul Miller.

4. Computational effort

The computational effort undertaken under the sponsorship of this Grant has focused on two main problems.

The first, conducted as part of the Ph.D. research of Mr. Francois Pepin, deals with the improvement of the efficiency of vortex element methods for the use in incompressible ($M \to 0$) flow. As reported previously (see Dimotakis *et al.* 1987, Sec. 4), an improvement from the typical N^2, with N the number of computational vortex elements, to $N \log N$ has been achieved. As yet, no documentation of this work[‡] is available.

The second, conducted as part of the Ph.D. research of Mr. Tasso Lappas, has focused on the development of Lagrangian methods, suitable for the simulation of both compressible and incompressible flows. To date, one-dimensional unsteady gasdynamic flows have been simulated successfuly, with considerable improvements, relative to established methods, in the manner in which shocks, and their associated entropy production, are captured by the new scheme. Specifically, the improvement in the Lagrangian description obviates the usual flux-corrected-transport fixes to remove the oscillations in the computed flow field. A documentation of this effort should be available sometime this Fall. This work will be extended[‡] to unsteady, two-dimensional flow.

[‡] Continuing under co-sponsorship of AFOSR Grant 88-0155.

5. Personnel

In addition to the Principal Investigators:

P. E. Dimotakis: Professor, Aeronautics & Applied Physics;

J. E. Broadwell: Senior Scientist, Aeronautics;

A. Leonard: Professor, Aeronautics;

personnel who have participated directly in the effort sponsored by this Grant are listed below:

E. Dahl: Member of the technical Staff, Aeronautics;

W. J. A. Dahm: Graduate Research Assistant, Aeronautics[1];

D. R. Dowling: Graduate Research Assistant, Aeronautics[2];

C. E. Frieler: Graduate Research Assistant, Aeronautics;

R. J. Gilbrech: Graduate Research Assistant, Aeronautics;

J. A. Hall: Graduate Research Assistant, Aeronautics;

J. C. Hermanson: Graduate Research Assistant, Aeronautics[3];

D. B. Lang: Staff Engineer, Aeronautics;

M. M. Koochesfahani: Senior Research Fellow, Aeronautics[4];

T. Kubota: Professor, Aeronautics;

R. Miake-Lye: Senior Research Fellow, Aeronautics;

P. L. Miller: Graduate Research Assistant, Applied Physics;

M. G. Mungal: Senior Research Fellow, Aeronautics[5];

M. Zhuang: Graduate Research Assistant, Aeronautics;

---

[1] Presently, Assistant Professor, U. Michigan.

[2] Presently, Staff Engineer, Boeing.

[3] Presently, Staff Engineer, United Technologies Research Center.

[4] Presently, Assistant Professor, Dept. Mechanical Engineering, Michigan State University.

[5] Presently, Assistant Professor, Dept. Mechanical Engineering, Stanford University.

6. References

A left margin bullet in the text reference list below denotes a publication of work completed under sponsorship, or co-sponsorship, of this Grant. Other publications of research sponsored by this Grant are listed separately below.

BATCHELOR, G. K. [1959] "Small-scale variation of convected quantities like temperature in turbulent fluid. Part 1. General discussion and the case of small conductivity", *J. Fluid Mech.* **5**, 113–133.

BROADWELL, J. E. and BREIDENTHAL, R. E. [1982] "A Simple Model of Mixing and Chemical Reaction in a Turbulent Shear Layer", *J. Fluid Mech.* **125**, 397–410.

- BROADWELL, J. E. and MUNGAL, M. G. [1986] "The effects of Damköhler number in a turbulent shear layer", GALCIT Report FM86-01.

- BROADWELL, J. E. and MUNGAL, M. G. [1988] "Molecular Mixing and Chemical Reactions in Turbulent Shear Layers", 22nd *International Symposium of Combustion* (Seattle, Wash.), 14–18 August 1988 (to appear).

- DAHM, W. J. A. and DIMOTAKIS, P. E. [1987] "Measurements of Entrainment and Mixing in Turbulent Jets", *AIAA J.* **25**(9), 1216–1223.

- DIMOTAKIS, P. E. [1986] "Two-Dimensional Shear-Layer Entrainment", *AIAA J.* **24**(11), 1791–1796.

- DIMOTAKIS, P. E. [1987] "Turbulent shear layer mixing with fast chemical reactions", US-France Workshop on Turbulent Reactive Flows (Rouen, France), 7–10 July 1987. *Turbulent Reactive Flows*, (eds.) R. Borghi and S. N. B. Murthy *Lecture Notes in Engineering* **40** (Springer-Verlag, New York, 1989), 417–485. See Appendix C.

- DIMOTAKIS, P. E., BROADWELL, J. E. and LEONARD, A. [1987] "Chemical Reactions in Turbulent Mixing Flows", California Institute of Technology, AFOSR-83-0213 Annual Report.

- DIMOTAKIS, P. E. and HALL, J. L. [1987] "A simple model for finite chemical kinetics analysis of supersonic turbulent shear layer combustion", AIAA/SAE/ASME/ASEE 23rd Joint Propulsion Meeting (La Jolla, CA), 29 June – 1 July 1987, AIAA Paper 87-1879. See Appendix D.

- DOWLING, D. R. [1988] *Mixing in gas phase turbulent jets*, Ph.D. thesis, California Institute of Technology.

- DOWLING, D. R. and DIMOTAKIS, P. E. [1988] "On Mixing and Structure of the Concentration Field of Turbulent Jets", Proceedings, *First National Fluid Dynamics Congress*, 25–28 July 1988 (Cincinatti, Ohio), II, 982–988. See Appendix F.

- DOWLING, D. R. and DIMOTAKIS, P. E. [1989] "Similarity of the concentration field of

gas-phase turbulent jets", submitted for publication to the *J. Fluid Mech.*

- FRIELER, C. E. and DIMOTAKIS, P. E. [1988] "Mixing and Reaction at Low Heat Release in the Non-Homogeneous Shear Layer", *First National Fluid Dynamics Congress*, 24-28 July 1988 (Cincinatti, Ohio), AIAA Paper 88-3626. See Appendix B.

GOULDIN, F. C. [1988] "Interpretation of Jet Mixing Using Fractals", *AIAA J.* **26**(11), 1405-1407.

- HALL, J., DIMOTAKIS, P., PAPAMOSCHOU, D. and FRIELER, C. [1988] "Design Overview of the Supersonic Hydrogen-Fluorine Facility (V3.0)", GALCIT Internal Report (6 May 1988).

- HERMANSON, J. C. and DIMOTAKIS, P. E. [1989] "Effects of heat release in a turbulent reacting shear layer", *J. Fluid Mech.* **199**, 333-375.

- HERMANSON, J. C., MUNGAL, M. G. and DIMOTAKIS, P. E. [1987] "Heat Release Effects on Shear Layer Growth and Entrainment", *AIAA J.* **25**(4), 578-583 (AIAA Paper 85-0142). See Appendix A.

KEE, R. J., MILLER, J. A. and JEFFERSON, T. H. [1980] "CHEMKIN: A General Purpose, Problem-independent, Transportable, Fortran Chemical Kinetics Code Package", SANDIA Report SAND80-8003.

- MUNGAL, M. G. and FRIELER, C. E. [1988] "The Effects of Damköhler Number in a Turbulent Shear Layer", *Comb. & Flame* **71**, 23-34.

SREENIVASAN, K. R. and MENEVEAU, C. [1986] "The Fractal Facets of Turbulence", *J. Fluid Mech.* **173**, 357-386.

- ZHUANG, M., KUBOTA, T. and DIMOTAKIS, P. E. [1987] "On the Stability of Inviscid, Compressible Free Shear Layers", Proceedings, *First National Fluid Dynamics Congress*, 25-28 July 1988 (Cincinatti, Ohio), **II**, 768-773. See Appendix E.

Other publications of work sponsored/co-sponsored under this Grant

The listing below includes publications of work that has been discussed in previous annual reports. It is included here, for the purposes of the final Grant Report, to provide a documentation of other work sponsored by this Grant.

- BROADWELL, J. E. [1987] "Molecular Mixing and Chemical Reactions in Turbulent Shear Flows", NATO Summer Institute on Disorder and Mixing (unpublished), 14-28 June 1987 (Corsica, France).

- BROADWELL, J. E. [1987] "A Model for Reactions in Turbulent Jets: Effects of Reynolds, Schmidt, and Damköhler Numbers", US-France Workshop on Turbulent Reactive Flows (Rouen, France), 7-10 July 1987. *Turbulent Reactive Flows*, (eds.) R. Borghi and S. N. B.

Murthy *Lecture Notes in Engineering* **40** (Springer-Verlag, New York, 1989), 257–277.

- BROADWELL, J. E., DAHM, W. J. A. and MUNGAL, M. G. [1984] "Blow-Out of Turbulent Diffusion Flames", *20th International Symposium on Combustion* (Ann Arbor, Michigan), 303-310.

- BROADWELL, J. E. and DIMOTAKIS, P. E. [1986] "Implications of Recent Experimental Results for Modeling Reactions in Turbulent Flows", *AIAA J.* **24**(6), 885-889.

- DAHM, W. J. A. [1985] *Experiments on Entrainment, Mixing and Chemical Reactions in Turbulent Jets at Large Schmidt Numbers*, Ph.D. thesis, California Institute of Technology.

- DAHM, W. J. A., DIMOTAKIS, P. E. and BROADWELL, J. E. [1984] "Non-premixed turbulent jet flames", AIAA 22nd Aerospace Sciences Meeting (Reno, Nevada), AIAA Paper No. 84-0369.

- DIMOTAKIS, P. E., BROADWELL, J. E. and LEONARD, A. [1986] "Chemical Reactions in Turbulent Mixing Flows", AFOSR-83-0123 Annual Scientific Report (AFOSR-TR-86-2123, 15-Jun-86).

- HERMANSON, J. C. [1985] *Heat Release Effects in a Turbulent, Reacting Shear Layer* Ph.D. thesis, California Institute of Technology.

- HERMANSON, J. C., MUNGAL, M. G. and DIMOTAKIS, P. E. [1987] "Heat Release Effects on Shear Layer Growth and Entrainment", *AIAA J.* **25**(4), 578–583 (AIAA Paper 85-0142).

- KOOCHESFAHANI, M. M. [1984] *Experiments on Turbulent Mixing and Chemical Reactions in a Liquid Mixing Layer* Ph.D. thesis, California Institute of Technology.

- KOOCHESFAHANI, M. M. and DIMOTAKIS, P. E. [1985] "Laser Induced Fluorescence Measurements of Mixed Fluid Concentration in a Liquid Plane Shear Layer", *AIAA J.* **23**(11), 1700-1707.

- KOOCHESFAHANI, M. M. and DIMOTAKIS, P. E. [1986] "Mixing and chemical reactions in a turbulent liquid mixing layer", *J. Fluid Mech.* **170**, 83–112.

- KOOCHESFAHANI, M. M and FRIELER, C. E. [1987] "Inviscid Instability Characteristics of Free Shear Layers with non-Uniform Density", 25^{th} *AIAA Aerospace Sciences Meeting*, 12–15 January 1987 (Reno, Nevada), AIAA Paper 87-0047.

- MIAKE-LYE, R. C. and TONER, S. J. [1987] "Laser Soot-Scattering Imaging of a Large Buoyant Diffusion Flame", *Comb. & Flame* **67**(1), 9-26.

- MUNGAL, M. G. [1983] *Experiments on Mixing and Combustion with Low Heat Release in a Turbulent Shear Flow*, Ph.D. thesis, California Institute of Technology.

- MUNGAL, M. G. and DIMOTAKIS, P. E. [1984] "Mixing and combustion with low he·t

release in a turbulent mixing layer", *J. Fluid Mech.* **148**, 349-382.

- MUNGAL, M. G, HERMANSON, J. C. and DIMOTAKIS, P. E. [1985] "Reynolds Number Effects on Mixing and Combustion in a Reacting Shear Layer", *AIAA J.* **23**(9), 1418-1423.

Please note that this list does not include several internal reports, as well as brief seminars and presentations (*e.g. Am. Phys. Soc.* meeting Bulletins). The material in the latter references is documented in the lists above.

Appendix A

HERMANSON, J. C., MUNGAL, M. G. and DIMOTAKIS, P. E. [1987] "Heat Release Effects on Shear Layer Growth and Entrainment", *AIAA J.* **25**(4), 578-583 (AIAA Paper 85-0142).

Heat Release Effects on Shear-Layer Growth and Entrainment

J. C. Hermanson, M. G. Mungal, P. E. Dimotakis

Reprinted from
AIAA Journal
Volume 25, Number 4, April 1987, Page 578
AMERICAN INSTITUTE OF AERONAUTICS AND ASTRONAUTICS • 1633 BROADWAY • NEW YORK, N.Y. 10019

Heat Release Effects on Shear-Layer Growth and Entrainment

J. C. Hermanson,* M. G. Mungal,† and P. E. Dimotakis‡
California Institute of Technology, Pasadena, California

The effects of heat release were studied in a planar, gaseous reacting mixing layer formed between two subsonic freestreams; one containing hydrogen in an inert diluent, the other containing fluorine in an inert diluent. Sufficiently high concentrations of hydrogen and fluorine reactants were employed to produce adiabatic flame temperature rises of up to 940 K (adiabatic flame temperature of 1240 K absolute). Although the displacement thickness of the layer for a zero streamwise pressure gradient showed an increase with increasing heat release, the actual thickness of the mixing layer at a given downstream location was not observed to increase and, in fact, was characterized by a slight thinning. The overall entrainment into the layer was seen to be substantially reduced by heat release. The large-scale vortical nature of the flow appeared to persist over all levels of heat release in this investigation. Imposition of a favorable pressure gradient, though resulting in additional thinning of the layer, was observed to have no resolvable effect on the amount of chemical product formation and hence on the mixing.

I. Introduction

THIS investigation was concerned with heat-release effects in a subsonic, gas-phase, turbulent, plane, reacting shear layer at high Reynolds number. The work was an extension of earlier work in the same facility.[1-3] The flow consisted of a two-dimensional mixing layer with gas-phase freestreams; one stream carrying a given concentration of hydrogen in an inert diluent, the other carrying fluorine in an inert diluent. The reaction $H_2 + F_2 - 2HF$ is highly exothermic so that reactant concentrations of 1% H_2 and 1% F_2, each in an N_2 diluent, produce an adiabatic flame temperature rise of 93 K above ambient. Results will be presented here corresponding to fluorine concentrations of up to 6% and hydrogen concentrations of up to 24%, with a maximum adiabatic flame temperature rise of 940 K (corresponding to an adiabatic flame temperature of 1240 K absolute).

In earlier, low heat release work by Mungal et al.[1-3] with flame temperature rises of up to 165 K, no coupling of heat release with the fluid mechanics could be observed, as manifested by the layer growth rate, entrainment, and discernible large-scale structure dynamics. In those works, the chemical reaction could be considered as a diagnostic used to infer the amount of molecular mixing without disturbing the overall properties of the layer. In the work reported here, the heat release was much larger and the effects of the heat release itself on the properties of the shear layer were investigated. The highest heat-release cases reported here produced a time-averaged temperature change sufficient to reduce the mean density in the center of the layer by a factor of nearly 3, assuming constant pressure conditions.

Presented as Paper 85-0142 at the AIAA 23rd Aerospace Sciences Meeting, Reno, NV, Jan. 14-17, 1985; received Sept. 18, 1985; revision received Sept. 15, 1986.

*Graduate Student, Aeronautics; currently Engineer, Applied Physics Laboratory, University of Washington. Member AIAA.

†Research Fellow, Aeronautics; currently, Assistant Professor, Mechanical Engineering Department, Stanford University. Member AIAA.

‡Professor, Aeronautics and Applied Physics. Member AIAA.

II. Experimental Facility and Instrumentation

The experimental apparatus is described in detail by Mungal and Dimotakis[2] and also by Hermanson.[4] It is a blowdown facility in which premixed volumes of fluorine in an inert diluent and hydrogen in an inert diluent are discharged through sonic orifices to maintain a constant mass flux. Each stream enters a settling and contraction section for turbulence suppression with the high-speed stream emerging from a 6:1 contraction with an exit area of 5×20 cm, and the low-speed stream emerging from a 4:1 contraction with a 7.5×20-cm exit area. The two streams meet at the tip of a splitter plate, with a trailing edge included angle of 3.78 deg. The high-speed freestream turbulence level was measured[2] to be about 0.6% rms.

To offset the freestream density difference, which results from large amounts of hydrogen in one stream, the densities of the freestreams were matched, for most cases, by using as diluent a mixture of nitrogen and a small amount of helium on the fluorine side, and a mixture of nitrogen with a small amount of argon on the hydrogen side. This also served to match the heat capacities of the two freestreams to an accuracy of approximately 6-10%, as the freestream absolute reactant concentrations were estimated to be accurate to 3-5% by Mungal and Dimotakis.[2]

Runs were performed with a nominal high-speed flow velocity of 22 m/s and a freestream speed ratio of $U_2/U_1 \approx 0.4$. In practice, the high-speed flow velocity varied from run to run up to about 5% from the nominal high-speed velocity; the corresponding variation in the low-speed stream velocity was typically less than 6%. The freestream speed ratio for each run was typically within 4% of the nominal value. These variations were a result of differences in gas constants of the various mixtures, although the sonic metering orifices were adjusted for each run to minimize these variations. The measuring station was positioned at $x = 45.7$ cm downstream of the splitter-plate trailing edge. The Reynolds number at the measuring station was typically $Re_{\delta_1} \approx 6 \times 10^4$, based on the freestream velocity difference, the 1% thickness of the mean temperature profile, and the cold freestream kinematic viscosity. The 1% thickness, δ_1, of the temperature or concentration field[2,5] is defined here as the transverse width of the layer at which the time-averaged temperature rise is 1% of the maximum time-averaged temperature rise and was used in this investigation as the

principal measure of layer width. The quality δ_1 has been shown[2] to correlate well with the visual thickness δ_{vis} (Ref. 6) of the layer. The value of the Reynolds number based on δ_1 is well above that for the mixing transition as reported by Bernal et al.,[7] Breidenthal,[8] and Konrad.[9] The corresponding Reynolds number based on the high-speed freestream velocity and on the downstream distance was $Re_x \approx 6 \times 10^5$. A diagram of the shear-layer geometry is shown in Fig. 1.

Temperature data were recorded with a rake of eight 2.5-μm-diam platinum-10% rhodium cold wires, with a typical wire span of 1.5 mm, welded to Inconel prongs. For some runs, a rake of 25-μm-diam Chromel-Alumel thermocouples was employed. It was found that the 2.5 μm resistance wires in the hottest regions did not survive in runs in which the adiabatic flame temperature rise exceeded approximately 600 K. Both the cold wire and thermocouple probe rakes were positioned across the transverse extent of the layer. The probes were equally spaced at nominal intervals of 1 cm, which sufficed to capture the mean temperature rise profile. The total data rate for the resistance wires was 80 kHz, corresponding to 10 kHz per probe. The thermocouples were sampled at 500 Hz each, for a total data rate of 4 kHz; their considerably lower frequency response not warranting a higher rate.

Thermocouples produce a voltage proportional to the junction temperature and normally do not require calibration. The resistance wires were calibrated as described previously[1,2] using a hot and cold jet of known temperature. The two measurements provided calibration constants to convert voltage to temperature rise. An additional correction was applied to the output signal voltage in the present experiments to account for the nonlinearity in the resistivity of the platinum-10% rhodium wire element at elevated temperatures.[10] It was determined that for neither the thermocouples nor the resistance wires was there significant radiation error for the temperatures in this investigation.[11] Both probes, however, were influenced by heat conduction to the support prongs, which could have resulted in excursions from the mean temperature being in error by as much as 10-20% for the cold wires and up to 40% for the thermocouples. Both diagnostics, however, produced accurate mean temperatures, as during a small fraction of the course of the run (before data acquisition began) the tips of the support prongs equilibrated to the local mean value. Good agreement (typically within 5%) was obtained in runs in which both sets of probes were employed. Errors resulting from differences in the thermal conductivities between the freestreams were established to be small.[4]

In addition to the temperature probes, a schlieren system was utilized for concurrent flow visualization. The beam width utilized was sufficient to illuminate a 25-cm length of the shear layer. A circular source mask and a circular hole spatial filter were used in place of the conventional source slit and knife edge in an effort to give equal weights to gradients in index of refraction in all directions and to better resolve the large-scale structure of the flow. The hole sizes were increased with increasing flow temperature to optimize (reduce) sensitivity as needed. High time-resolution spark schlieren photographs were taken with a spark source ($\sim$3-μs duration), synchronized with a motor-driven 35-mm camera, at a rate of approximately three frames per second.

The mean velocity profile was measured for most runs by a pitot probe rake of 15 probes connected to a miniature manometer bank filled with fluorine-resistant oil (Hooker Chemical Fluorolube FS-5) with a time response of 2-3 s, adequate to yield a reliable mean dynamic pressure profile during each 6-s run. The bank was photographed by a second motor-driven 35-mm camera. The photographic data were digitized and reduced to mean velocity profiles. This technique of measuring the pitot pressure was estimated to be accurate to 5%. Rebollo[12] estimated that the accuracy of extracting mean velocities from pitot pressures in nonconstant density flows is about 4-5%. This estimate was made for a shear flow with a freestream density ratio of $\rho_2/\rho_1 = 7$. In the present experiment, the density ratio of the cold freestreams to the hot layer center was at most 3, suggesting that the Rebollo error estimate represents an upper bound under these conditions.

Finally, the streamwise static pressure gradient was monitored by measuring the pressure difference between two downstream locations on the low-speed sidewall with a Datametrics type 573 fluorine-resistant Barocel sensor. The high-speed sidewall was kept horizontal for all runs and the low-speed sidewall was adjusted for the desired streamwise pressure gradient. The wedge-like geometry of the planar shear-layer displacement allows this simple means of accommodating or imposing any desired pressure gradient. Most of the runs in the present investigation were performed with the low-speed sidewall adjusted to the requisite divergence angle to ensure a zero streamwise pressure gradient. For some runs at high heat release, the walls were left fixed at the angle required for zero pressure gradient at zero heat release, producing a favorable streamwise pressure gradient (accelerating flow) as a result of the combustion displacement effects due to volume expansion.

III. Chemistry

The chemical reaction utilized in the present investigation is effectively

$$H_2 + F_2 - 2HF, \quad \Delta Q = -130 \text{ kcal/mole}$$

This yields a temperature rise of 93 K for 1% F_2 and 1% H_2 in N_2 diluent under constant pressure, adiabatic conditions (this is the so-called adiabatic flame temperature rise). The chemical reaction is actually comprised of two second-order chain reactions:

$$H_2 + F - HF + H, \quad \Delta Q = -32 \text{ kcal/mole}$$

$$H + F_2 - HF + F, \quad \Delta Q = -98 \text{ kcal/mole}$$

Proper chain initiation requires some free F atoms, which were generated in these experiments by premixing a trace amount of nitric oxide into the hydrogen-carrying stream. This allows the reaction

$$F_2 + NO - NOF + F$$

which provides the required small F atom concentration in the layer to sustain proper ignition and combustion. For all runs in this investigation, the NO concentration was maintained at 3% of the freestream fluorine concentration.

For all flows reported here, the resulting chemical time scales were fast compared with the fluid mechanical time scales. The chemical time scales for the reaction, over the entire range of concentrations, were determined using the CHEMKIN chemical kinetics program.[13] The chemical rate

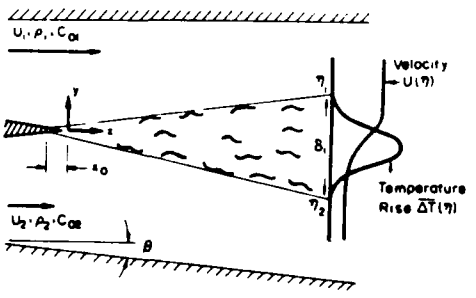

Fig. 1 Turbulent shear-layer geometry.

data for the reactions involved were taken from Refs. 14 and 15. The Damköhler number (ratio of mixing time to chemical time) based on the local, large-scale characteristic time ($\delta_\omega/\Delta U$, where ΔU is the freestream velocity difference) ranged from 25 to 130 with increasing reactant concentrations. The Damköhler number based on the time of flight from the location of the mixing transition to the measuring station [$(x-x_t)/U_c$, where U_c is the mean convection speed, $(U_1+U_2)/2$] varied from 95 to 470. Taking the transition Reynolds number to be $Re_{\delta_\omega}=2\times10^4$ gives $x_t=14.2$ cm. The recent work of Mungal and Frieler[16] suggests that the chemistry can be regarded as being fast when the Damköhler numbers exceed 10 and 40 for the large scales and time of flight, respectively. Chemical kinetics are, consequently, not an issue in the present investigation, where the chemistry is much faster as a result of the higher reactant concentrations and combustion temperatures.

The stoichiometric mixture ratio ϕ is defined here as the volume of high-speed fluid required to react completely with a unit volume of low-speed fluid. This is the same as the ratio of the low-speed freestream molar concentration c_{02} to the high-speed freestream molar concentration c_{01} divided by the low- to high-speed stoichiometric ratio, i.e.

$$\phi=\frac{c_{02}/c_{01}}{(c_{02}/c_{01})_s}=c_{02}/c_{01}$$

In this case the molar stoichiometric ratio for the hydrogen-fluorine reaction is unity.

IV. Results and Discussion

A. Growth Rate and Entrainment

The low-speed sidewall divergence required for zero streamwise pressure gradient is a direct measure of the displacement thickness of the layer δ^*, where $\delta^*/(x-x_0)$ indicates the tangent of the angle β by which the low-speed freestream line is shifted owing to the presence of the shear layer (see Fig. 1). Note that the displacement thickness is less than zero for a layer with no heat release, and increases steadily with heat release, as shown in Fig. 2. The parameter $(\rho_0-\bar\rho)/\rho_0$ represents the mean normalized density reduction in the layer due to heat release, where $\bar\rho$ is the mean density in the layer and $\rho_0=(\rho_1+\rho_2)/2$ is the average (cold) density of the freestreams. The mean density is defined as

$$\bar\rho=\rho_0\int_{y_2}^{y_1}\frac{T_0}{(T_0+\Delta\bar T)}\mathrm{d}y$$

where $y_{1,2}$ are the 1% points of the mean temperature profile on the high- and low-speed sides, respectively; T_0 the ambient temperature; and $\Delta\bar T$ the time-averaged temperature rise at each point across the layer. This calculation neglects the small changes in pressure across the layer by taking the pressure to be constant. Alternatively, the effects of heat release could be quantified by use of the parameter $\tau\equiv\langle\Delta\bar T\rangle/T_0$, which represents, at constant pressure, the additional volume created by heat addition. $\langle\Delta\bar T\rangle$ denotes the mean temperature rise in the layer, which is defined here in a similar fashion to the mean density.

The observed 1% temperature profile thickness at zero pressure gradient is plotted vs the mean density in the layer in Fig. 3. It may be worth noting that the actual shear-layer thickness, in spite of large heat release and large density changes, does *not* increase with heat release and, in fact, shows a slight decrease, even though the displacement thickness (Fig. 2) increases with heat release. This effect was noted by Wallace[17] and was observed in the present set of experiments in which the maximum mean flow temperature increase was about three times greater than in Ref. 17. Since it was difficult to hold the speed ratio at exactly 0.40 from run to run and also because the density ratio of the freestreams was slightly different from unity for some runs, each data point in Fig. 3 has been corrected by normalization with the expected growth rate for a cold layer with the identical speed and density ratio, using the formula derived in Ref. 18.

$$\frac{\delta}{x}=\epsilon\left(\frac{1-r}{1+s^{1/2}r}\right)\left(1+s^{1/2}-\frac{1-s^{1/2}}{1+2.9[(1+r)/(1-r)]}\right)$$

where $s=\rho_2/\rho_1$, $r=U_2/U_1$, and ϵ is a constant. A linear least-squares fit to the data in Fig. 3 suggests that the layer thinning, for a mean density reduction of 40% may be as high as 15%. The largest mean density reduction presented in this work, $(\rho_0-\bar\rho)/\rho_0=0.38$, corresponds to a run with an adiabatic flame temperature rise of $\Delta T_f=940$ K and a mean temperature rise in the layer of $\langle\Delta\bar T\rangle=248$ K. No dependence of the thinning trend on stoichiometric mixture ratio was observed.

The slight reduction in layer thickness with increasing heat release is also confirmed by the mean velocity data. Sample velocity profiles, at different heat release but identical speed and density ratios, are presented in Fig. 4. It can be seen that the hotter layer is noticeably steeper in maximum slope, in agreement with Ref. 17. Normalization of this maximum slope by the freestream velocity difference gives the vorticity thickness δ_ω of the layer,

$$\frac{1}{\delta_\omega}=\frac{1}{\Delta U}\left(\frac{\mathrm{d}U}{\mathrm{d}y}\right)_{\max}$$

A plot of the vorticity thickness variation with heat release, again corrected for variations in speed ratio and density

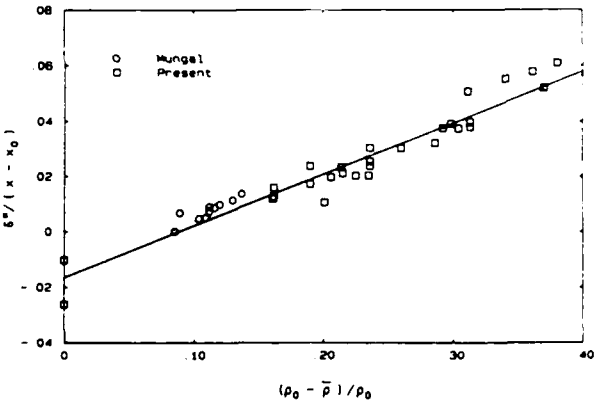

Fig. 2 Layer displacement vs heat release.

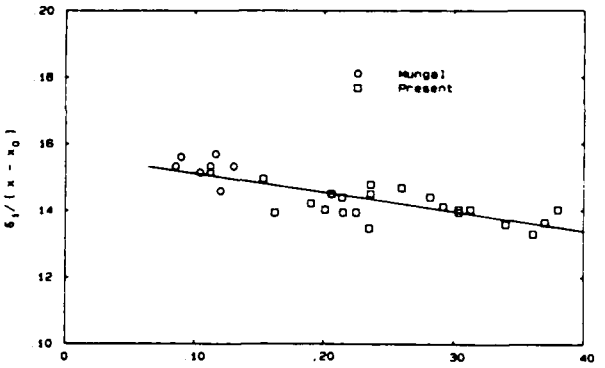

Fig. 3 Temperature profile thickness growth rate vs heat release: ○ —$\Delta T_f=0$, $(\rho_0-\bar\rho)/\rho_0=0$; □ —$\Delta T_f=457$ K, $(\rho_0-\bar\rho)/\rho_0=0.286$.

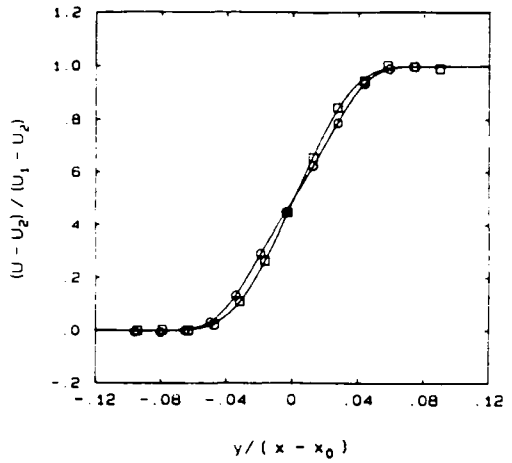

Fig. 4 Mean velocity profile comparison, nonreacting and at high heat release.

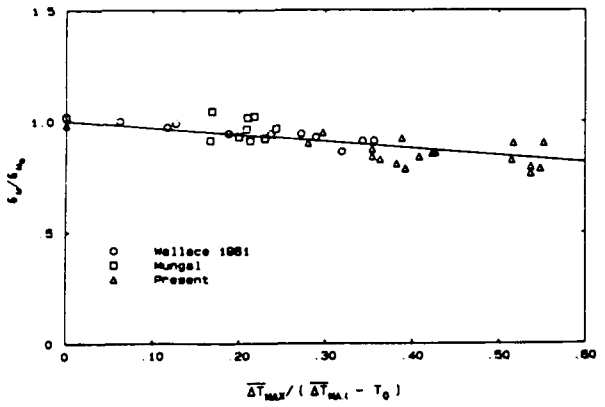

Fig. 5 Normalized vorticity thickness comparison with Ref. 17.

ratio, is shown in Fig. 5. Each point is normalized by a representative value for the vorticity thickness at zero heat release. The portion of the present results at moderate heat release, including some unpublished data of Mungal, are seen to be in good agreement with Ref. 17. Since the data of Ref. 17 were originally given in terms of $\Delta\bar{T}_{max}/T_0$, the maximum time-averaged temperature rise over the ambient temperature, it was necessary to use the quantity $\Delta\bar{T}_{max}/(\Delta\bar{T}_{max}+T_0)$ for the abscissa parameter of Fig. 5. This quantity is slightly different than $(\rho_0-\bar{\rho})/\rho_0$ because the density is not a linear function of the temperature rise, but nonetheless yields a comparable thinning effect to Fig. 3.

Direct numerical simulations of a reacting mixing layer performed by McMurtry et al.[19] also suggest a decrease in layer thickness when exothermic reactions occur, in qualitative agreement with the present results. Those simulations indicate both a decrease in the width of the calculated product concentration profile as well as a steepening in the mean velocity profile with increasing heat release.

Experiments performed at higher temperatures than those in this work by Pitz and Daily[20] in a combusting mixing layer formed downstream of a rearward-facing step indicated that the vorticity thickness did not appear to change between their cold runs and high heat-release runs. However, Keller and Daily[21] report that, in a reacting mixing layer between a cold premixed reactant stream and a preheated combustion product stream, the vorticity thickness increases significantly with increasing temperature. The reasons for the discrepancy between those results and the ones reported here are not clear at this writing. However, two important differences exist between the experimental conditions of those investigations and the present work. First, Pitz and Daily[20] and Keller and Daily[21] studied shear layers formed between unequal density fluids, unlike the present study with matched freestream densities. Second, those experiments, in contrast to the present investigation, were performed in a constant area duct in which a pressure gradient was allowed to develop.

A complicating factor in any discussion of growth rate is the location of the virtual origin x_0, since the relevant similarity downstream coordinate is in fact $y/(x-x_0)$. The trends in layer thinning reported here do allow the possibility that some of the effects could be accounted for by a shift in the virtual origin with heat release. The location of the virtual origin x_0 was determined visually from the intersection of the apparent layer edges as revealed by spark schlieren photographs (see Sec. IV. B). These results did not, however, suggest any systematic change in the location of the virtual origin with heat release, and a representative value of $x_0=-3.2$ cm was used for all normalizations in this investigation.[4] Initial conditions can have a significant effect on layer growth as has been shown, for example, by Browand and Latigo;[22] see also Batt,[23] Bradshaw,[24] and the discussion in the review paper by Ho and Huerre.[25]

One implication of the fact that the layer width does not increase with increasing temperature is that, since the density in the layer is substantially reduced but the layer does not grow faster, the total volumetric entrainment of freestream fluid into the layer must also be reduced greatly by heat release. The amount of entrainment into the layer can be calculated from the mean velocity and density (i.e., temperature) profiles as follows:

$$\frac{\dot{V}}{U_1(x-x_0)}=\int_{\eta_2}^{\eta_1}\frac{\rho U}{\rho_0 U_1}\mathrm{d}\eta$$

where $\dot{V}$ is the volume flux into the layer per unit span, $x-x_0$ the downstream coordinate, and $\eta=y/(x-x_0)$ the shear-layer similarity coordinate. This expression assumes that the layer is self-similar at the station at which the integral is performed. The quantity ρU was computed as $\bar{\rho}\bar{U}$, which was used here as an approximation for the density-velocity correlation $\overline{\rho U}$.

Results from Mungal et al.[3] suggest that there is a Reynolds number dependence on product formation. Since the growth rate does appear to be a function of the product formation (i.e., heat release), strictly speaking, the flow would not be expected to be exactly self-similar. An alternate method,[18,26] which approximates the overall entrainment, is to use the geometry of the layer as shown in Fig. 1 to derive

$$\frac{\dot{V}}{U_1(x-x_0)}=\eta_1-r(\eta_2+\tan\beta)$$

where $r=U_2/U_1$, $\eta_{1,2}$ are the similarity coordinate edges of the shear layer, and β is the deflection angle of the low-speed sidewall. A common difficulty of both methods is that of selecting values for η_1 and η_2. One reasonable choice is the pair of points corresponding to the 1% edges of the temperature profile. Resulting calculations for choices of 1 and 10% points in the temperature profiles, for both the integral and geometric methods, are plotted in Fig. 6. It can be seen that, regardless of the choice of edge reference points, the inference is that the entrainment into the layer is strongly reduced as a function of heat release, amounting to about 50% for a mean density in the layer of 40% below its nominal cold value. The decrease in entrainment with heat release is greater than that suggested by considering only the increase in volume and taking the entrainment to be proportional to $1/(\tau+1)$. That the entrainment reduction is in ex-

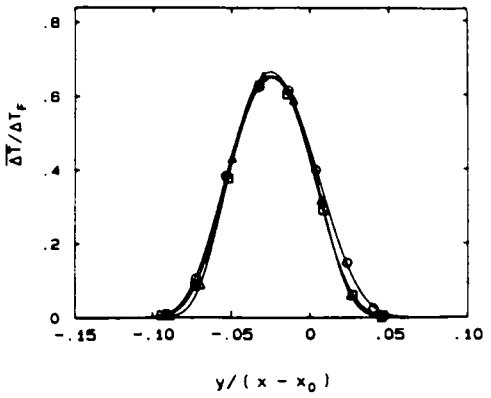

Fig. 9 Pressure gradient effect on mean temperature profile, 6% F_2:6%H_2. ○ —$dp/dx = 0$; □ —$\Delta dp/dx < 0$).

significant change in either the maximum time-averaged temperature or in the total amount of product formed, which is related to the area under the mean temperature profile normalized by the layer thickness.[2,4] Temperature profiles at lower temperatures also show no systematic changes in the total amount of product resulting from pressure gradient, at least to within the estimated reproducibility and accuracy of the data (3-5%).

VI. Conclusions

The results of this investigation suggest that the growth rate of a chemically reacting shear layer with heat release does not increase and, in fact, decreases slightly with increasing heat release. In the presence of an increase in the shear-layer displacement thickness as a result of heat release, one might expect a commensurate increase in shear layer thickness. The implication is that the decrease in the entrainment flux due to volume expansion must more than compensate for the displacement effect.

The imposition of a favorable pressure gradient is found to not have any noticeable effect on the amount of mixing and chemical production in the layer.

Acknowledgments

The assistance of C. E. Frieler as well as the expert help of Mr. Earl E. Dahl in running the experiments reported here is greatly appreciated. The authors would also like to acknowledge many helpful discussions with Dr. J. E. Broadwell. This work was sponsored by the Air Force Office of Scientific Research under Contract F49620-79-C-0159 and Grant 83-0213.

References

[1]Mungal, M. G., Dimotakis, P. E., and Broadwell, J. E., "Turbulent Mixing and Combustion in a Reacting Shear Layer," *AIAA Journal*, Vol. 22, June 1984, pp. 797-800.

[2]Mungal, M. G. and Dimotakis, P. E., "Mixing and Combustion with Low Heat Release in a Turbulent Shear Layer," *Journal of Fluid Mechanics*, Vol. 148, 1984, pp. 349-382.

[3]Mungal, M. G., Hermanson, J. C., and Dimotakis, P. E., "Reynolds Number Effects on Mixing and Combustion in a Reacting Shear Layer," *AIAA Journal*, Vol. 23, Sept. 1985, pp. 1418-1423.

[4]Hermanson, J. C., "Heat Release Effects in a Turbulent, Reacting Shear Layer," Ph.D. Thesis, California Institute of Technology, Pasadena, CA, 1985.

[5]Koochesfahani, M. M. and Dimotakis, P. E., "Mixing and Chemical Reactions in a Turbulent Liquid Mixing Layer," *Journal of Fluid Mechanics*, Vol. 170, 1986, pp. 83-112.

[6]Brown, G. L. and Roshko, A., "On Density Effects and Large Structure in Turbulent Mixing Layers," *Journal of Fluid Mechanics*, Vol. 64, No. 4, 1974, pp. 775-816.

[7]Bernal, L. P., Breidenthal, R. E., Brown, G. L., Konrad, J. H., and Roshko, A., "On the Development of Three-Dimensional Small Scales in Turbulent Mixing Layers," *Turbulent Shear Flows 2, Second Symposium on Turbulent Shear Flows*, July 1979, Springer-Verlag, Berlin, pp. 305-313.

[8]Breidenthal, R. E., "Structure in Turbulent Mixing Layers and Wakes Using a Chemical Reaction," *Journal of Fluid Mechanics*, Vol. 109, 1981, pp. 1-24.

[9]Konrad, J. H., "An Experimental Investigation of Mixing in Two-Dimensional Turbulent Shear Flows with Application to Diffusion-Limited Chemical Reactions," Ph.D. Thesis, California Institute of Technology, Pasadena, CA, 1976; also, Project SQUID Tech. Rept. CIT-8-PU, 1976.

[10]Caldwell, F. R., "Thermocouple Materials," National Bureau of Standards Monograph 40, U.S. Department of Commerce, National Bureau of Standards, 1962.

[11]Scadron, M. D. and Warshawsky, I., "Experimental Determination of Time Constants and Nusselt Numbers for Bare-Wire Thermocouples in High-Velocity Air Streams and Analytic Approximation of Conduction and Radiation Errors," NACA Tech. Note 2599, 1952.

[12]Rebollo, M. R., "Analytical and Experimental Investigation of a Turbulent Mixing Layer of Different Gases in a Pressure Gradient," Ph.D. Thesis, California Institute of Technology, Pasadena, CA, 1973.

[13]Kee, R. J., Miller, J. A., and Jefferson, T. H., "CHEMKIN: A General Purpose, Problem Independent, Transportable, Fortran Chemical Kinetics Code Package," Sandia Labs., Livermore, CA, Rept. SAND80-8003, 1980.

[14]Cohen, N. and Bott, J. F., "Review of Rate Data for Reactions of Interest in HF and DF Lasers," The Aerospace Corporation, CA, Rept. SD-TR-82-86, 1982.

[15]Baulch, D. L., Duxbury, J., Grant, S. J., and Montague, D. C., "Evaluated Kinetic Data for High Temperature Reactions," *Journal of Physical Chemistry*, Vol. 4, 1981; Reference data in Vol. 10, Suppl. 1, 1981.

[16]Mungal, M. G. and Frieler, C. E., "The Effects of Damköhler Number on a Turbulent Shear Layer—Experimental Results," GALCIT, California Institute of Technology, Pasadena, CA, Rept. FM85-01, 1985.

[17]Wallace, A. K., "Experimental Investigation of the Effects of Chemical Heat Release in the Reacting Turbulent Plane Shear Layer," Ph.D. Thesis, University of Adelaide, 1981; also AFOSR Report AFOSR-TR-84-0650.

[18]Dimotakis, P. E., "Entrainment into a Fully Developed, Two-Dimensional Shear Layer," *AIAA Journal*, Vol. 24, Sept. 1986, pp. 1791-1796.

[19]McMurtry, P. A., Jou, W-H., Riley, J. J., and Metcalfe, R. W., "Direct Numerical Simulations of a Reacting Mixing Layer with Chemical Heat Release," *AIAA Journal*, Vol. 24, June 1986, pp. 962-970.

[20]Pitz, R. W. and Daily, J. W., "Combustion in a Turbulent Mixing Layer Formed at a Rearward-Facing Step," *AIAA Journal*, Vol. 21, Nov. 1983, pp. 1565-1570.

[21]Keller, J. O. and Daily, J. W., "The Effect of Large Heat Release on a Two Dimensional Mixing Layer," AIAA Paper 83-0472, 1983.

[22]Browand, F. K. and Latigo, B. O., "Growth of the Two-Dimensional Mixing Layer from a Turbulent and Non-Turbulent Boundary Layer, *The Physics of Fluids*, Vol. 22, No. 6, June 1979, pp. 1011-1019.

[23]Batt, R. G., "Some Measurements on the Effect of Tripping the Two-Dimensional Shear Layer," *AIAA Journal*, Vol. 13, Feb. 1975, pp. 245-247.

[24]Bradshaw, P., "The Effect of Initial Conditions on the Development of a Free Shear Layer," *Journal of Fluid Mechanics*, Vol. 26, No. 2, 1966, pp. 225-236.

[25]Ho, C. M. and Huerre, P., "Perturbed Free Shear Layers," *Annual Review of Fluid Mechanics*, Vol. 16, 1984, pp. 365-424.

[26]Brown, J. L., "Heterogeneous Turbulent Mixing Layer Investigations Utilizing a 2-D 2-Color Laser Doppler Anemometer and Using a Concentration Probe," Ph.D. Thesis, University of Missouri, Columbia, MO, 1978.

[27]Ganji, A. T. and Sawyer, R. F., "Experimental Study of the Flowfield of a Two-Dimensional Premixed Turbulent Flame," *AIAA Journal*, Vol. 18, July 1980, pp. 817-824.

[28]Libby, P. A. and Bray, K. N. C., "Countergradient Diffusion in Premixed Turbulent Flames," *AIAA Journal*, Vol. 19, Feb. 1981, pp. 205-213.

[29]Spalding, D. B., "The Two-Fluid Model of Turbulence Applied to Combustion Phenomena, *AIAA Journal*, Vol. 24, June 1986, pp. 876-884.

Appendix B

FRIELER, C. E. and DIMOTAKIS, P. E. [1988] "Mixing and Reaction at Low Heat Release in the Non-Homogeneous Shear Layer", *First National Fluid Dynamics Congress*, 24-28 July 1988 (Cincinatti, Ohio), AIAA Paper 88-3626.

AIAA/ASME/SIAM/APS AIAA-88-3626
1st National Fluid Dynamics Congress
25-28 July 1988, Cincinnati, Ohio

Mixing and Reaction at Low Heat Release in the Non-Homogeneous Shear Layer

C. E. Frieler† and P. E. Dimotakis*

June 1988

Graduate Aeronautical Laboratories
California Institute of Technology

Abstract

The effects of freestream density ratio on the mixing and combustion in a high Reynolds number, subsonic, gas-phase, non-buoyant, two-dimensional turbulent mixing layer, have been investigated. Measurements of temperature rise (heat release) have been made which enable us to examine the effect of freestream density ratio on several aspects of the mixed fluid state within the turbulent combustion region. In experiments with very high and very low stoichiometric mixture ratios ("flip" experiments), the heat release from an exothermic reaction serves as a quantitative label for the lean reactant freestream fluid that becomes molecularly mixed. Properly normalized, the sum of the mean temperature rise profiles of the two flip experiments represent the probability of fluid molecularly mixed at any composition. The mole fraction distribution and number density profile of the mixed fluid can also be inferred from such measurements. Although the density ratio in these experiments was varied by a factor of thirty, profiles of these quantities show little variation, with integrals varying by less than 10%. This insensitivity differs from that of the *composition* of molecularly mixed fluid, which is very sensitive to the density ratio. While the profiles of composition exhibit some similarity of shape, the average composition of mixed fluid in the layer varies from nearly 1:2 to over 2:1 as the density ratio is increased. A comparison of data and available theory for this offset or average composition is discussed.

Introduction

The two-dimensional turbulent shear layer has been the subject of investigation for many years, particularly the gas phase layer with uniform freestream densities. This flow represents one of the simplest in which turbulent mixing occurs between two separate streams. Relatively simple boundary conditions and strong similarity properties combine to make this one of the more attractive flows to experimentalists, theorists and modelers.

Although it has been the subject of study in the past, there are several reasons why the present work focuses on the effects of freestream density ratio on the shear layer. As noted by Brown & Roshko (1974), this knowledge is a necessary precursor to the study of compressibility effects. The renewed interest in supersonic mixing and combustion, combined with the experimental difficulties of producing density matched supersonic shear flows has given a new impetus to the search for an understanding of the effects of the density ratio in these flows. However, this is not to imply that the only interest rests in the connection to compressible flows. In many important engineering applications the shear layer geometry is used to mix reactants or to ignite premixed streams which release large amounts of heat. Optimization of combustion systems used in propulsion and energy "production" roles requires knowledge of the physical mechanisms involved. Again, a study of turbulent combustion with large heat release and therefore large density differences, is aided by an understanding of density ratio effects.

Several investigations in the past have dealt directly with this issue. Brown & Roshko (1971, 1974) performed a series of experiments in subsonic non-homogeneous layers and concluded, contrary to proposals entertained at the time, that the large reductions in spreading rate found in compressible layers could not be attributed to density ratio effects. Based on directly measured concentration fields in shear layers at two freestream density ratios, Konrad (1976) concluded that the composition of the mixed fluid was strongly affected by the density ratio of the freestreams but that for each case it did not vary within the mixing region as expected based on conventional gradient transport modeling. Wallace (1981) investigated the product formed due to mixing and reaction for both density ratios studied by Konrad. By measuring the temperature rise for several values of the freestream reactant concentration, he found the mean composition of the mixed fluid to be in good agreement with Konrad for the uniform density case, but was unable to use the technique for the non-uniform density case.

---

† Graduate Student, Aeronautics

* Professor of Applied Physics and Aeronautics

Although it did not deal specifically with non-homogeneous flows, there is another study which helped lay the ground work for the present investigation. Koochesfahani & Dimotakis (1986) measured the amount of reaction product in a liquid shear layer at flow conditions comparable to the uniform density case of Konrad. They concluded that the amount of mixed fluid was much less than that found in gas phase shear layers and argued that this difference indicated the importance of the Schmidt number as a parameter. This dependence countered fundamental assumptions in classical analyses of high Reynolds number flow, where the molecular transport coefficients are several orders of magnitude smaller than the effective turbulent transport coefficients.

Of particular interest to this work, they also demonstrated how several quantities could be determined from reacting flow measurements as if directly measured with the requisite resolution. This is one of the motivations for the present work. Breidenthal (1981) noted that in all techniques which attempt to directly measure the composition field, any failure to resolve fully all the features of the flow field leads to an over-estimate for the amount of mixed fluid. As demonstrated by Koochesfahani & Dimotakis, by using the molecular nature of chemical reactions and measuring only the mean value of the product concentration, an estimate can be derived which is conservative.

In 1982 a new facility was completed which permits the investigation of reacting, gas-phase shear flows. This study follows in the wake of the low heat release study (Mungal & Dimotakis 1984), the study of heat release effects (Hermanson 1985, Hermanson *et al.* 1987), the study of Reynolds number effects (Mungal *et al.* 1985) and the investigation of Damkohler number effects (Mungal & Frieler 1988). Using the same facility, the present study has extended the range of topics to include the effects of freestream density ratio.

Experiments

The facility consists of a blowdown tunnel described in detail in Mungal & Dimotakis (1984) and Hermanson (1985). Gases are loaded by a partial pressure technique into high pressure reactant tanks. Driven by a large (nearly) constant pressure source, these gases flow during a run through sonic metering valves and into the apparatus test section. In the present experiments, the high-speed flow issues from a 6:1 contraction through a 5×20 cm^2 exit at a velocity of $U_1 = 22$ m/s. The low-speed flow emerges from a 7.5×20 cm^2 exit after a 4:1 contraction at a velocity of $U_2 = 8.5$ m/s. These streams enter the test section as shown in Fig. 1.

Experiments involving chemical reaction between mixtures of hydrogen and inert gases in the high-speed stream and fluorine and inert gases in the low-speed stream have been performed. Table 1 contains the detailed composition of each stream for all experiments for which results are presented here. The apparatus allows the use of precise mixtures of gases which have significant density differences, keeping most other relevant quantities constant. The choices of diluent gases allowed

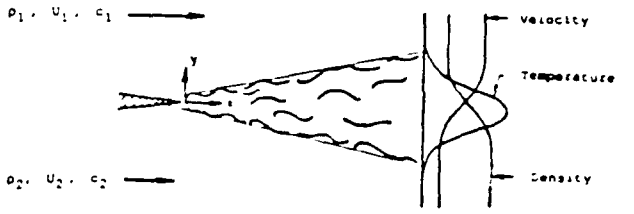

Figure 1. Turbulent Shear Layer Geometry

experiments to be carried out for the range of freestream density ratios $1/8 < \rho_2/\rho_1 < 8$, with the heat capacity of the mixtures carefully matched. Unfortunately, results for $\rho_2/\rho_1 > 4$, which could be directly compared to the $\rho_2/\rho_1 = 7$ case of Konrad, are not included. We suspect that a new mode of instability, details of which were discussed in Koochesfahani & Frieler (1987), becomes important for large values of the density ratio. Although results for $\rho_2/\rho_1 = 4$ show only a hint of the effects, results for higher density ratios were sufficiently different that comparison with "normal" shear layers would be outside the scope of present work. The data presented here cover the range of density ratios $0.136 < \rho_2/\rho_1 < 4$, which corresponds to a factor of 30 for that parameter.

			Composition (%)					
ρ_2/ρ_1	ϕ		HZ	FZ	NZ	Ar	He	NO
.136	1/8	HSS	4.		.9	95.		.1
		LSS		.5	4.5		95.	
	8	HSS	.5		3.5	96.		.01
		LSS		4.			96	
.25	1/8	HSS	4.		17.	79.		.1
		LSS		.5	20.5		79.	
	8	HSS	.5		20.1	79.4		.01
		LSS		4.	16.6		79.4	
.5	1/8	HSS	4.		47.4	48.6		.1
		LSS		.5	50.9		48.6	
	8	HSS	.5		51.3	48.2		.01
		LSS		4.	47.8		48.2	
1.	1/8	HSS	4.		93.	3.		.1
		LSS		.5	96.5		3.	
	8	HSS	.5		98.	1.5		.01
		LSS		4.	94.5		1.5	
2.	1/8	HSS	4.		52.9		43.1	.1
		LSS		.5	56.4	43.1		
	8	HSS	.5		53.9		45.6	.01
		LSS		4.	50.4	45.6		
4.	1/8	HSS	4.		22.1		73.9	.1
		LSS		.5	25.6	73.9		
	8	HSS	.5		22.6		76.9	.01
		LSS		4.	19.1	76.9		

Table 1. Composition details for each experiment.

Based on an estimation technique described in Mungal & Frieler (1988) and refined in Dimotakis & Hall (1987), kinetic rates for these experiments were established to be more than a factor of two higher than the rates at which product formation may be assumed to be mixing-limited. The HF chemical system may be regarded as a fast and hypergolic reaction system, even at low concentrations of reactants and at extreme stoichiometric ratios. This allowed experiments to be performed with the heat release maintained below the threshold suggested by Wallace (1981) and confirmed by Hermanson (1985) and Hermanson *et al.* (1987), beyond which density changes resulting from heat release begin to affect the fluid mechanics of the turbulent shear layer. At the downstream location where our measurements were made ($x = 46$ cm) the Reynolds number for these experiments, based on properties of the nitrogen diluent and the velocity difference between the two freestreams, was $Re = \Delta U\,\delta/\nu = 6.7\times10^4$. Here the length δ is the reference length scale used throughout the present work and is defined as the distance between the 1% points of the mixed fluid probability profiles, $p_m(y)$ in Fig. 4. This width has been found to correspond closely to the visual thickness of the mixing region. Measurements of temperature rise were made using a rake of eight resistance wire (2.5 μm) thermometers, as described in Mungal & Dimotakis (1984). Run times were 6 seconds with 1.5 second start-up and 4 seconds of data acquisition. Probes were sampled at an aggregate rate of 240 kHz for a total of $\sim 10^6$ data points for each run.

In the limit of low heat release, temperature rise measures the number density of product molecules. As a result of the finite heat release in these experiments, however, the number density of molecules is not constant. Because of the careful matching of specific heats, we can still relate the measurements to the amount of product formed in the present experiments. In particular,

$$\frac{n_p}{n} \propto \Delta T$$

where ΔT, n_p and n are respectively the temperature rise above ambient, the number density of product molecules and the total number density. Assuming isobaric conditions, the quantities n_p and n can be inferred separately from the temperature rise and the perfect gas law, i.e.

$$\frac{n_p}{n_\infty} \propto \frac{\Delta T}{T_0 + \Delta T}\,, \qquad \text{and} \qquad \frac{n}{n_\infty} = \frac{T_0}{T_0 + \Delta T}\,,$$

where T_0 is the ambient temperature (~ 300 K) and n_∞ is the number density of molecules in the freestreams at T_0. Fortunately, as argued by Mungal & Dimotakis (1984), the probes used in these experiments produce very accurate measurements of the *mean* temperatures. Therefore the mean of the ratio n_p/n can be reliably determined, although averages of n_p and n separately will suffer to some degree from inadequate probe resolution.

A sample of the results of a single experiment is shown in Fig. 2. Measured mean temperatures at each of the eight probe locations are indicated by the circles (ΔT_{gage}). Fitted profiles are also shown for the mean temperature, mean number density of product (n_p/n_∞) and mean number density (n/n_∞) .

These curves are of the form

$$\overline{\Delta T}(\eta) = e^{-(c_0 + c_1\eta + c_2\eta^2 + c_3\eta^3 + c_4\eta^4)}$$

where $\eta = y/(x-x_0)$.

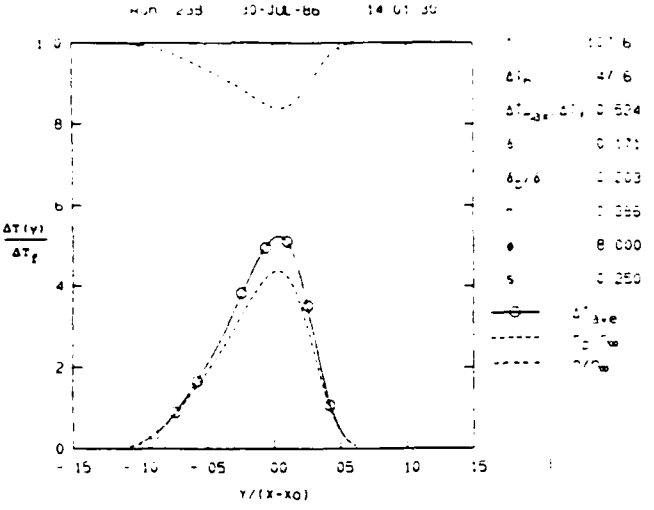

Figure 2. Data for the case $\rho_2/\rho_1 = .25$, $c_2/c_1 = 8$.

Analysis

The major concepts involved in the analysis of the data were derived for the laser induced fluorescence (LIF) technique in liquids by Koochesfahani & Dimotakis (1986). Some differences exist, however, which will be described here.

Starting with two distinguishable fluids, we will label the pure fluid from the low speed side as $\xi = 0$, and pure fluid from the high speed side as $\xi = 1$. We define ξ as the (conserved scalar) composition, with intermediate values, $0 < \xi < 1$, corresponding to the fraction of high speed fluid in the mixture. If we were able to make measurements with perfect resolution in both time and space, a properly normalized histogram of composition sampled at discrete times would approximate the probability density function (PDF) of composition, $P(\xi)$. Although laboratory measurements of sufficient resolution can not currently be made in high Reynolds number flows, for the present discussion it is only necessary to accept the existence of the PDF. A conceptual model of the PDF of composition appears in Fig. 3.

Next we apply the change of variables from composition to temperature shown in Fig. 4. This temperature dependence, $\Delta T(\xi)$, represents the temperature rise above ambient which results from a fast, irreversible exothermic reaction occuring between two fluids containing reactants mixed at a composition ξ (eg. Bilger 1980). For the chemical system used here, the stoichiometric mixture ratio is equal to the ratio of the freestream reactant concentrations, $\phi = c_2/c_1$.

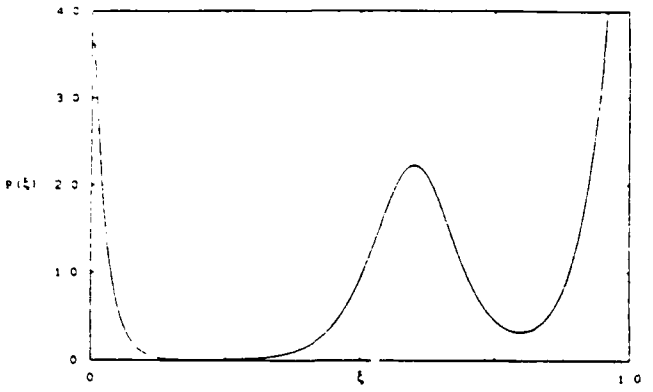

Figure 3. Conceptual Model for the PDF of Composition

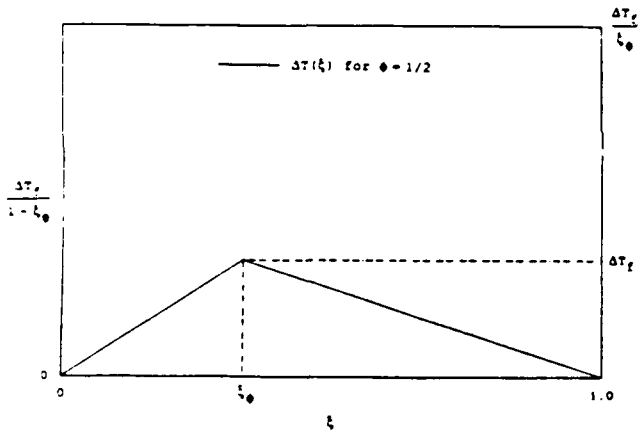

Figure 4. Transform between Composition and Temperature Rise

The value

$$\xi_\phi = \frac{\phi}{1+\phi}$$

is the stoichiometric composition and the temperature rise at this composition is the adiabatic flame temperature rise (ΔT_f). The PDF of temperature rise, $P_T(\Delta T)$, is given by

$$P_T(\Delta T) = \frac{1}{\Delta T_f}\left\{\xi_\phi P\left[\xi_\phi \frac{\Delta T}{\Delta T_f}\right] + (1-\xi_\phi) P\left[1-(1-\xi_\phi)\frac{\Delta T}{\Delta T_f}\right]\right\}.$$

Normalization of P_T is guaranteed by this transform, if P is properly normalized.

If we then relate the mean temperature, at a specific value of ϕ, to P we obtain

$$\frac{\overline{\Delta T}}{\Delta T_f} = \int_0^{\Delta T_f} \frac{\Delta T}{\Delta T_f} P_T(\Delta T)\, d(\Delta T)$$

$$= \int_0^{\xi_\phi} \frac{\xi}{\xi_\phi} P(\xi)\, d\xi + \int_{\xi_\phi}^{1} \frac{1-\xi}{1-\xi_\phi} P(\xi)\, d\xi .$$

The second form results from a change of variables from ΔT back to ξ.

There are two interesting limits immediately apparent from this expression. These are the "flip" experiments described in Koochesfahani, Dimotakis & Broadwell (1985). If we let the stoichiometric composition $\xi_\phi \to 1$, then the second integral vanishes and we are left with

$$\frac{\overline{\Delta T}}{\Delta T_f} \to \int_0^1 \xi P(\xi)\, d\xi = \overline{\xi} .$$

Here $\overline{\xi}$ is the mean composition and also represents the mean high speed fluid mixture fraction. If we let $\xi_\phi \to 0$, the first integral vanishes and we are left with

$$\frac{\overline{\Delta T}}{\Delta T_f} \to \int_0^1 (1-\xi) P(\xi)\, d\xi = 1 - \overline{\xi} .$$

Here the roles of $\xi = 0$ and $\xi = 1$ have been reversed (ie. $\phi \to 1/\phi$) and therefore $\overline{\xi} \to 1 - \overline{\xi}$, which represents the low speed fluid mixture fraction.

It is necessary to consider an aspect of the data which affects this analysis. Previous experimental work (Konrad 1976, Koochesfahani & Dimotakis 1984) demonstrated that there is a finite probability of observing pure fluid from each of the freestreams in the interior of the layer. Consequently, we must admit integrable singularities (delta functions) in $P(\xi)$ at the values $\xi = 0$ and $\xi = 1$. The process of taking the limit in each case above relied on the integrand being finite at these points, though delta functions at any other value of ξ would not pose a problem. Note that measurements of temperature cannot distinguish between pure high-speed or pure low-speed fluid since $\Delta T(0) = \Delta T(1) = 0$. Because the transform introduces an ambiguity at points where the PDF is singular, the connection between mean temperature and mean composition cannot be made. However, since this ambiguity arises from the probability of seeing *pure* fluid from the lean reactant freestream, it can be avoided if we restrict our attention to the molecularly mixed fluid (compositions $\xi \neq 0, 1$).

We have examined how the mean temperature rise is related to the mean composition. Another useful, though perhaps less precise, interpretation is that in these limits $\overline{\Delta T}/\Delta T_f$ measures the *amount* of fluid originating in the lean reactant freestream.

Building on this idea, we can define two reduced temperature profiles as

$$\theta_1(y) = \frac{\xi_0}{\Delta T_f}\,\Delta\bar{T}(y) \le \int_0^{1-\varepsilon} \xi\, P(\xi,y)\, d\xi ,$$

and

$$\theta_2(y) = \frac{1-\xi_0}{\Delta T_f}\,\Delta\bar{T}(y) \le \int_{\varepsilon}^{1} (1-\xi)\, P(\xi,y)\, d\xi .$$

An arbitrary small number, ε, has been introduced in the limits of integration solely to indicate that contributions from the pure fluid originating from either stream have been excluded. Note the dependence on the spatial coordinate, y, which appears in these expressions. This dependence was left implicit to the present but will be explicitly included for the remainder of this discussion.

The limits discussed above may now be reexamined. As ξ_0 approaches 1, the equality in the first expression is realized and θ_1 becomes equal to the amount of high speed fluid which is molecularly mixed. Similarly, in the limit of $\xi_0 \to 0$, θ_2 measures the amount of low speed fluid which is molecularly mixed. As shown in Fig. 4, the normalization has been chosen such that for any other stoichiometric composition, $\theta_1(y)$ and $\theta_2(y)$ provide conservative estimates for the profile of mixed fluid which originated from the respective freestream.

We can now estimate the probability of mixed fluid at any composition, $P_m(y)$. In particular, if we add the reduced temperatures we obtain

$$\theta_1(y) + \theta_2(y) \le \int_{\varepsilon}^{1-\varepsilon} (1-\xi)\, P(\xi,y)\, d\xi + \int_{\varepsilon}^{1-\varepsilon} \xi\, P(\xi,y)\, d\xi$$

$$= \int_{\varepsilon}^{1-\varepsilon} P(\xi,y)\, d\xi = P_m(y)$$

where this is again a conservative estimate for this quantity. This particular result was introduced in a previous discussion (Dimotakis 1987) in a somewhat more direct fashion. There, the mixed fluid function, $\theta_m(\xi)$, was defined to be the normalized sum of the temperature rises for the "flip" experiments, i.e.

$$\theta_m(\xi) = (1-\xi_0)\left(\frac{\Delta T(\xi;\xi_0)}{\Delta T_f(\xi_0)} + \frac{\Delta T(\xi;1-\xi_0)}{\Delta T_f(1-\xi_0)}\right) .$$

This transform provides an estimate for the amount of mixed fluid through the relation

$$P_m(y) \ge \int_0^1 \theta_m(\xi)\, P(\xi,y)\, d\xi .$$

As shown in Fig. 5, this estimate will be quite good for small values of ξ_0. Note that the figure corresponds to the stoichiometry $\xi_0 = \xi_\Phi$ at which these experiments were performed. These two approaches are clearly equivalent.

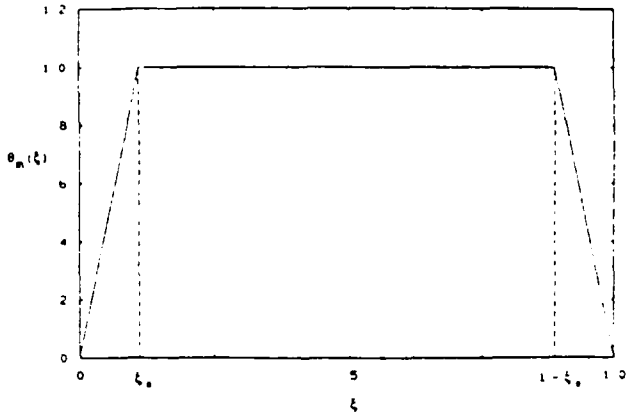

Figure 5. Mixed Fluid Function for $\xi_0 = 1/9$ ($\Phi_0 = 1/8$).

Having an estimate for the amount of mixed fluid originating from each stream separately, we can also estimate the average composition profile of the mixed fluid, i.e.

$$\xi_m(y) = \frac{\int_{\varepsilon}^{1-\varepsilon} \xi\, P(\xi,y)\, d\xi}{\int_{\varepsilon}^{1-\varepsilon} P(\xi,y)\, d\xi} = \frac{\theta_1(y)}{\theta_1(y) + \theta_2(y)} .$$

Note that this expression differs from that for the mixed fluid probability in one important respect. Here the quantity $\xi_m(y)$ is expressed as the quotient of two approximations and cannot *a priori* be said to represent a bound of the actual value.

Results

Fig. 6 shows the result of adding the reduced temperatures from the flip experiments for six density ratios. Shown is the mixed fluid probability, $P_m(y)$, versus position within the mixing region normalized by the width δ. Also shown in the column at far right is the integral of each profile in these coordinates, P_m. This quantity represents the integral probability of mixed fluid and can also be thought of as the mean volume (or mean mole) fraction occupied by mixed fluid within the boundaries of the layer.

Konrad used the probability of mixed fluid as a measure of the intermittency. In agreement with his measurements, we find that for all density ratios the probability of finding unmixed fluid in the center of the layer is low. This is contrary to the liquid shear layer result (Koochesfahani & Dimotakis 1984) where this probability was found to be as high as 0.45. When normalized in the same manner, our measurements of the mixed fluid probability distribution are in good agreement with Konrad's intermittency profiles. This includes the uniform density case in each study and a comparison of the present $\rho_2/\rho_1 = 4$ case with Konrad's $\rho_2/\rho_1 = 7$ case.

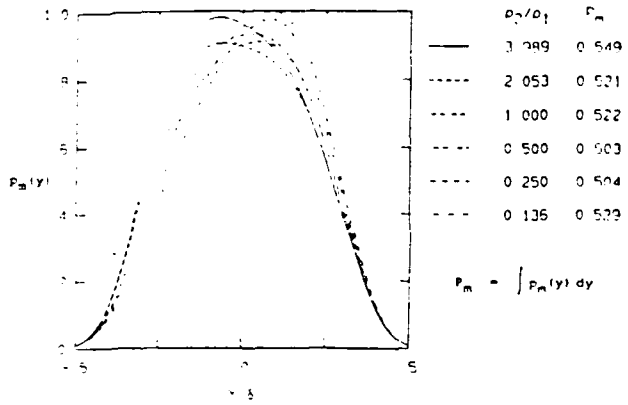

Figure 6. Mixed Fluid Probability Distributions.

The small systematic differences displayed by these distributions are interesting. They could be a manifestation of the weak effects of finite heat release in these experiments. Note that the density decrease owing to heat release is different for each experiment of the 'flip'. This could rearrange the distribution of the mixed fluid probability slightly for each case and thereby cause the sum of the reduced temperatures to be skewed toward one side. Since this heat release effect is partitioned within each of the flip pairs in a fashion which depends on the density ratio, this could result in the observed systematic trend. It is important to note that although this would reflect on the accuracy of the local distributions, it would not affect their integral values, e.g. P_m. Whether this trend in the profiles is a result of density ratio or the effect of the slight heat release will have to be determined by subsequent experiments.

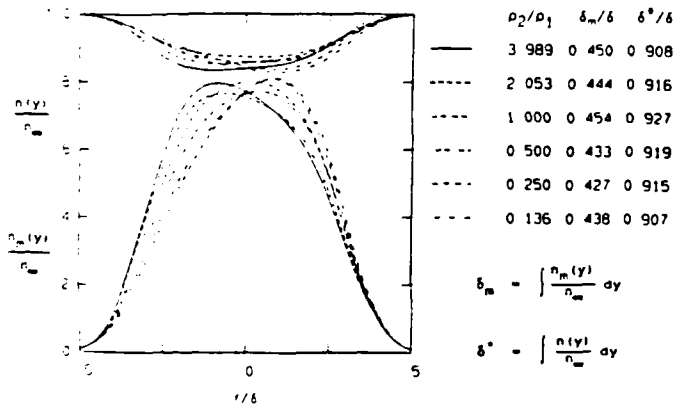

Figure 7. Mixed Fluid Number Density and Total Number Density Profiles.

The mean number density of product and mean molecular number density were also determined for each experiment. The results of adding the number density of product for the flip experiments are the bell shaped profiles shown in Fig. 7. These distributions represent the mean number density of mixed fluid, $n_m(y)$, within the shear layer. Note the similarity of these distributions despite a variation in the density ratio of a factor of thirty. Their integrals (δ_m) shown in the far right column, represent the total amount of mixed fluid expressed as a thickness. The lack of variation with density ratio shown by this quantity is particularly noteworthy, with the mixed fluid fraction, δ_m/δ, changing by less than 6%. Also shown in Fig. 7 are the profiles of mean number density for each case. The integrals of molecular number density, δ^*, can be used to estimate the dilatation resulting from heat release. In each case, $1 - \delta^*/\delta$ is below 0.1, indicating that the average number density in the layer has been reduced by less than 10%. Using the same approximations, the mean number density of mixed fluid can be divided by the mean number density to estimate the profiles of mixed fluid mole fraction. These profiles are shown in Fig. 8. In the far right column is the integral mole fraction of mixed fluid (δ_m) determined using this approach.

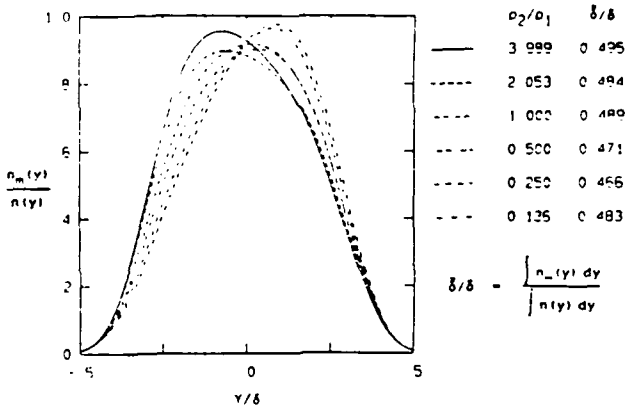

Figure 8. Mixed Fluid Mole Fraction Profiles.

Note the close similarity in the data in Figs. 6 and 8. The mole fraction profile, $n_m(y)/n(y)$, differs from the mixed fluid probability profile, $P_m(y)$, only because we have taken the quotient of time averages, rather that the time average of a quotient. The relative insensitivity of these profiles to this averaging process indicates that the statistics are not too pathological. This suggests that possible resolution inadequacies in this work are not serious in this context, and provides support for the approximations used to produce Figs. 7 and 8. Remember that, in the limit of zero heat release, Figs. 6, 7 and 8 would be identical. All four of the integral quantities, P_m, δ_m, $\tilde{\delta}_m$ and δ^* are plotted in Fig. 9 versus the freestream density ratio. Note the insensitivity of these quantities to the factor of thirty change in density ratio.

Using the approximations detailed in the analysis section, the mean composition profiles of the mixed fluid, $\xi_m(y)$, were also estimated. Shown in Fig. 10 are the composition profiles for each of the density ratios investigated. With the exception of an offset or average composition which

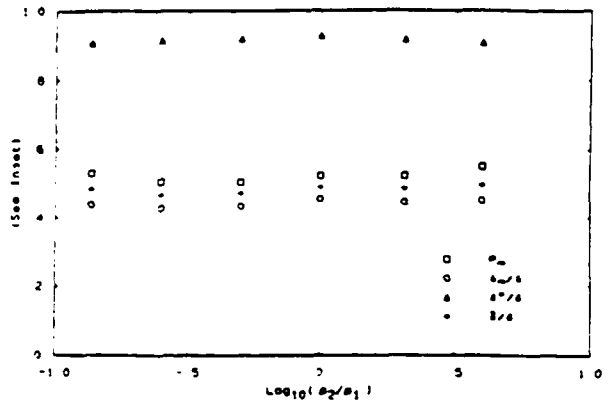

Figure 9. Normalized Mixing Layer Thicknesses for each Density Ratio.

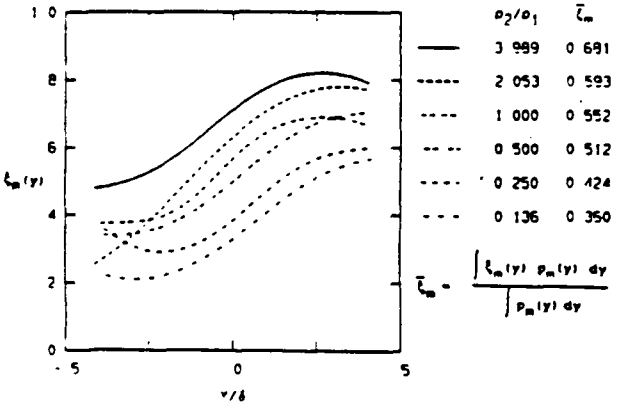

Figure 10. Mixed Fluid Composition Profiles.

is dependent upon density ratio, the similarity between composition curves is noteworthy. As noted by Konrad, the mean composition of the *mixed* fluid does not extend to the two limits, $\xi = 0, 1$. Nevertheless, the variation is not small, with important implications for models which approximate the mixing in the gas phase layer as independent of the transverse coordinate. No strong conclusions should be drawn, however, owing to the approximations used to arrive at these profiles and the possibility that some details of these distributions might be the result of the small heat release.

Dimotakis (1986) has proposed a theory for the entrainment into the mixing layer based on consideration of the large structure dynamics. For a velocity ratio $r = U_2/U_1$ and a density ratio $s = \rho_2/\rho_1$, he proposed an estimate of the entrainment ratio into the mixing layer given by

$$E_v(r,s) = s^{1/2}\left(1 + 0.68\,\frac{1-r}{1+r}\right) .$$

In his conceptual model of mixing and entrainment, the evolution of a "typical" vortex as viewed in its rest frame, Dimotakis envisions E_v as being the volume flux ratio of fluid entering the large scale structure from the freestreams. This ratio is related to both the flux ratio and the composition ratio, and as such, cannot be related rigorously to a function of the field quantities. However, since some models (e.g. Broadwell Breidental 1982, Dimotakis 1987) treat the mixing process as being independent of the transverse coordinate and it is precisely in this case that the distinction between flux and composition ratios vanish, a comparison is in order. If we proceed under this assumption and further assume that the fluids mix at the ratio they are entrained, we arrive at a prediction for the average mixed fluid composition, for the present velocity ratio, of

$$\bar{\xi}_m = \frac{E_v(r,s)}{1 + E_v(r,s)} = \frac{1.3\, s^{1/2}}{1 + 1.3\, s^{1/2}}$$

Shown in the far right column of Fig. 10 are the average mixed fluid composition for each density ratio. A comparison between our inferred experimental values and the theoretical estimate for the average composition versus density ratio, is shown in Fig. 11. It is important to note that, analogous to the integrals of mixed fluid probability, these values are not affected by the heat release as are the distributions. However, the small systematic variation between data and theory could stem from several sources. Most obviously, one could question the basic premise which led to the comparison, that the distinction between flux and composition ratios is negligible. Secondly, there is some evidence based on flow visualization that the fluids may not mix at the same ratio as they exist within the mean boundary of the turbulent region. Still Schlieren photographs indicate that regions within the mixing layer of unmixed fluid increase in size on the light fluid side as density differences increase. Finally, the determination of mixing by chemical reaction implicitly assumes that diffusivities of all the species involved are equal. This is clearly not the case when H_2 is one of the reactants. The extent to which these considerations may affect the inferences drawn from these measurements is being investigated.

Conclusions

Based on the similarity of the profiles in Figs. 6, 7 and 8 we conclude that the distribution of mixed fluid within the two-dimensional shear layer is relatively insensitive to freestream density differences. This is reinforced by the invariance of the integral amounts (Fig. 9) which differ by only 10% for all density ratios investigated. This is not the case for the *composition* of mixed fluid, which is quite sensitive to the density ratio. The average composition of mixed fluid in the layer varies from nearly 1:2 to over 2:1 as density ratio increases. Small differences notwithstanding, the agreement between theory based on the large structure dynamics and experimental results is compelling evidence for the central role of the large structures in the mixing process.

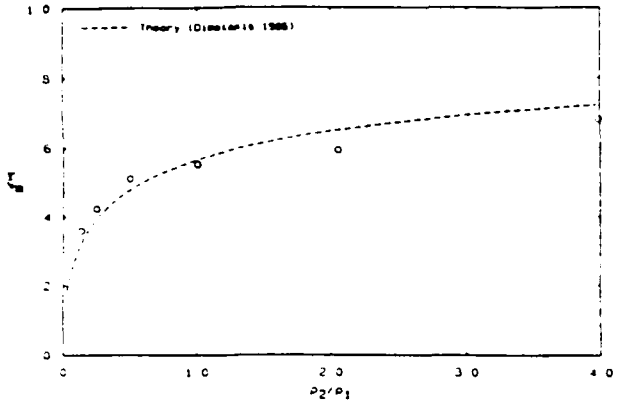

Figure 11. Average Mixed Fluid Composition versus Density Ratio.

Our results indicate that simple models can represent several aspects of mixing in a turbulent non-homogeneous shear layer. When normalized by the local width of the mixing region, the distribution of mixed fluid could be modeled as a function of the position in the layer only. Also the composition of the mixed fluid could be represented by an average composition which is qualitatively predicted by theory, multiplied by a function of position only.

References

BILGER, R. W. [1980] "Turbulent Flows with Nonpremixed Reactants", Turbulent Reacting Flows (Springer-Verlag, Topics in Applied Physics 44, 1980, Ed. P. A. Libby, F. A. Williams), 65-113.

BREIDENTHAL, R. E. [1981] "Structure in Turbulent Mixing Layers and Wakes Using a Chemical Reaction", J. Fluid Mech. 109, 1-24.

BROADWELL, J. E. and BREIDENTHAL, R. E. [1982] "A Simple Model of Mixing and Chemical Reaction in a Turbulent Shear Layer", J. Fluid Mech. 125, 397-410.

BROWN, G. L. and ROSHKO, A. [1971] "The Effect of Density Difference on the Turbulent Mixing Layer", Turbulent Shear Flows, AGARD-CP-93, 23.1-12.

BROWN, G. L. and ROSHKO A. [1974] "On Density Effects and Large Structure in Turbulent Mixing Layers", J. Fluid Mech. 64, 775-816.

DIMOTAKIS, P. E. [1986] "Two-Dimensional Shear-Layer Entrainment", AIAA J. 24(11), 1791-1796.

DIMOTAKIS, P. E. [1987] "Turbulent Shear Layer Mixing with Fast Chemical Reactions", invited lecture, US-France Workshop on Turbulent Reactive Flows, 7-10 July 1987 (Rouen, France), (GALCIT Report FM87-01).

DIMOTAKIS, P. E. and HALL, J. L. [1987] "A simple model for finite chemical kinetics analysis of supersonic turbulent shear layer combustion", AIAA/SAE/ASME/ASEE Joint Propulsion Conference Colloquium on Supersonic Combustion, 29 June - 2 July 1987 (San Diego, California), AIAA Paper 87-1879.

HERMANSON, J. C. [1985] Heat Release Effects in a Turbulent, Reacting Shear Layer, California Institute of Technology, Ph. D. thesis.

HERMANSON, J. C., MUNGAL, M. G. and DIMOTAKIS, P. E. [1987] "Heat Release Effects on Shear Layer Growth and Entrainment", AIAA J. 25(4), 578-583 (AIAA Paper 85-0142).

KONRAD, J. H. [1976] "An Experimental Investigation of Mixing in Two-dimensional Turbulent Shear Flows with Applications to Diffusion-limited Chemical Reactions" Ph.D. Thesis, California Institute of Technology, also Project SQUID Technical Report CIT-8-PU.

KOOCHESFAHANI, M. M. , DIMOTAKIS, P. E. and BROADWELL, J. E. [1985] "A 'Flip' Experiment in a Chemically Reacting Turbulent Mixing Layer", AIAA J. 23, 1191-1194.

KOOCHESFAHANI, M. M. and DIMOTAKIS, P. E. [1986] "Mixing and Chemical Reactions in a Turbulent Liquid Mixing Layer", J. Fluid Mech. 170, 83-112.

KOOCHESFAHANI, M. M. and FRIELER, C. E. [1987] "Inviscid Instability Characteristics of Free Shear Layers with Non-Uniform Density", AIAA-87-0047.

MUNGAL, M. G. and DIMOTAKIS, P. E. [1984] "Mixing and Combustion with Low Heat Release in a Turbulent Mixing Layer", J. Fluid Mech. 148, 349-382.

MUNGAL, M. G, HERMANSON, J. C. and DIMOTAKIS, P. E. [1985] "Reynolds Number Effects on Mixing and Combustion in a Reacting Shear Layer", AIAA J. 23(9), 1418-1423.

MUNGAL, M. G. and FRIELER, C. E. [1988] "The Effects of Damköhler Number in a Turbulent Shear Layer", Comb. & Flame 71, 23-34.

WALLACE, A. K. [1981] "Experimental Investigation of the Effects of Chemical Heat Release in a Turbulent Shear Flow" Ph.D. Thesis, University of Adelaide, Australia, AFOSR-TR-84-0650.

Appendix C

DIMOTAKIS, P. E. [1987] "Turbulent shear layer mixing with fast chemical reactions", US-France Workshop on Turbulent Reactive Flows (Rouen, France), 7–10 July 1987. *Turbulent Reactive Flows*, (eds.) R. Borghi and S. N. B. Murthy *Lecture Notes in Engineering* **40** (Springer-Verlag, New York, 1989), 417–485.

TURBULENT SHEAR LAYER MIXING WITH FAST CHEMICAL REACTIONS

by,

Paul E. DIMOTAKIS

Graduate Aeronautical Laboratories
California Institute of Technology
Pasadena, California 91125

ABSTRACT

A model is proposed for calculating molecular mixing and chemical reactions in fully developed turbulent shear layers, in the limit of infinitely fast chemical kinetics and negligible heat release. The model is based on the assumption that the topology of the interface between the two entrained reactants in the layer, as well as the strain field associated with it, can be described by the similarity laws of the Kolmogorov cascade. The calculation estimates the integrated volume fraction across the layer occupied by the chemical product, as a function of the stoichiometric mixture ratio of the reactants carried by the free streams, the velocity ratio of the shear layer, the local Reynolds number, and the Schmidt number of the flow. The results are in good agreement with measurements of the volume fraction occupied by the molecularly mixed fluid in a turbulent shear layer and the amount of chemical product, in both gas phase and liquid phase chemically reacting shear layers.

1.0 INTRODUCTION

Understanding chemically reacting, turbulent free shear flows is important not only for the obvious technical reasons associated with the engineering of a variety of reacting and combusting devices but also for reasons of fundamental importance to fluid mechanics and our perception of turbulence.

From a theoretical point of view, chemically reacting flows provide important tests of turbulence theories by adding to the dimensionality of the questions that can be asked of turbulence models. To compute chemical reactions in turbulent flow, the physics of reactant species turbulent transport and mixing need to be described correctly down to the diffusion scale level. This is a much more stringent specification than needs be imposed on momentum transport turbulence models.

From an experimental point of view, a fast chemical reaction provides a probe with an effective spatial and temporal resolution and sensitivity that is usually unattainable by conventional direct flow field measurement techniques in high Reynolds number turbulent

flows. Chemically reacting turbulent flow experiments are therefore to be regarded as a complementary means of interrogation; a valuable adjunct to the more conventional probing of the behavior of turbulent flow.

A broad class of current efforts to understand chemically reacting turbulent flows is based on classical turbulence formulations founded on the Reynolds-averaged Navier-Stokes equations. In such formulations, species transport is conventionally modeled as proportional to the gradient of the corresponding mean species concentration, with an effective diffusivity that is prescribed to be some function of the flow. See Tennekes & Lumley (1972) for an introduction. Estimates of mixing at the molecular scale must be modeled separately, in these formulations, in a manner that unfortunately cannot be addressed without additional assumptions, that are essentially ad hoc. See Sreenivasan, Tavoularis & Corrsin (1981), the introduction in Broadwell & Breidenthal (1982) and the discussion in Broadwell & Dimotakis (1986) for a discussion of these issues.

A different approach is taken by modeling efforts based on attempts to write transport equations for the probability density functions (PDF) of the conserved scalars, or joint PDFs for scalars, and/or the (vector) velocity field and pressure. See Pope (1985) and related work by Kollmann & Janicka (1982) and Kollmann (1984), for example. These efforts, which are in principle capable of addressing the issues of transport and mixing in a unified manner, must nevertheless resort to essentially equally ad hoc assumptions to close the problem. In other words, while having the correct fluctuation statistics through the relevant PDFs, and conditional statistics through one-time joint PDFs, would undoubtedly permit the molecular mixing and resulting chemical product formation to be computed correctly, it would appear that those PDFs are no easier to obtain than the ab initio solution of the original problem.

Finally, a model was recently proposed by Broadwell & Breidenthal (1982) which is not based on gradient transport concepts. This model will be discussed below in the context of recent data on chemically reacting shear layers in both gas phase and liquid phase shear layers.

1.1 Recent experimental results

The aspirating probe (Brown & Rebollo 1972) measurements of Brown & Roshko (1974), and the measurements of Konrad (1976) of the probability density function of the high speed fluid fraction in a non-reacting, gas phase shear layer suggested that the mixed fluid composition does not vary appreciably across the width of the layer, even as the mean high speed fluid fraction varies smoothly from unity on the high speed side, to zero on the low speed side. Additionally, as Konrad recognized, the most likely values of the mixed fluid high speed fluid fraction seem to be clustered around a value dictated by the shear layer entrainment ratio. In the light of these results, the smooth variation of the

mean is then to be understood as the variation of the local probability of finding:

a. pure high speed fluid,

b. mixed fluid,

and,

c. pure low speed fluid,

as we traverse the width of the layer.

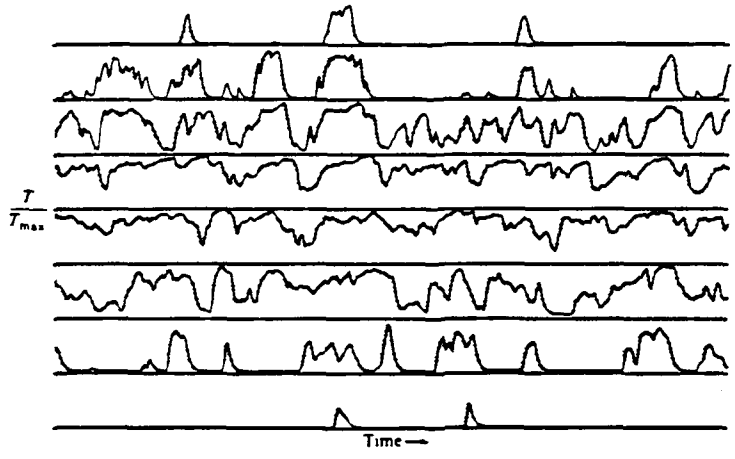

FIGURE 1. Temperature vs. time time traces for $\phi = 1$ ($\Delta T_{flm} = 93$ K). High speed ($U_1 = 22$ m/s) fluid (1% F_2 + 99% N_2) on top trace. Low speed ($U_2 = 8.8$ m/s) fluid (1% H_2 + 99% N_2) on bottom. Probe positions at $y/x = 0.076, 0.057, 0.036, 0.015, -0.008, -0.028, -0.049, -0.070$. Partial record of 51.2 ms time span ($\Delta T_{max} = 81$ K). From Mungal & Dimotakis (1984, figure 4b).

The near uniformity in the mixed fluid composition, apparent in Konrad's passive scalar non-reacting shear layer experiments, can be seen to have an important counterpart in the gas-phase, chemically reacting shear layer experiments (e.g. Mungal & Dimotakis 1984). Measuring the temperature field in the reaction zone of a mixing layer bringing together H_2 and F_2 reactants carried in a N_2 diluent, it is found that within the discernible regions that can be associated with the interior of the large scale structures the temperature was nearly uniform. See figure 1. The resulting mean temperature (chemical product) profile that peaks in the interior of the reaction zone is more a consequence of the variation of the fraction of the time a given fixed point is visited by the hot large scale cores (duty cycle), rather than the variation of the temperature field within a core. See figure 2.

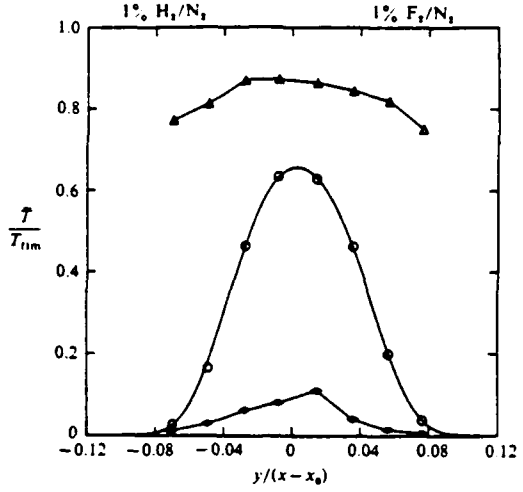

FIGURE 2. Peak, mean and minimum temperature rise observed for total data record at each station. Experimental parameters as in figure 1. Smooth curve least squares fitted through mean data points. From Mungal & Dimotakis (1984, figure 4c).

These results and conclusions are in good agreement with the results of Fiedler (1975), who measured the temperature with a fair temporal/spatial resolution at several points across a shear layer, one free stream of which was marked by a small temperature difference serving as a label for the passive conserved scalar. Measurements in both reacting and non-reacting liquid phase shear layers of the PDF of the high speed fluid fraction also corroborate these findings. See figure 3.

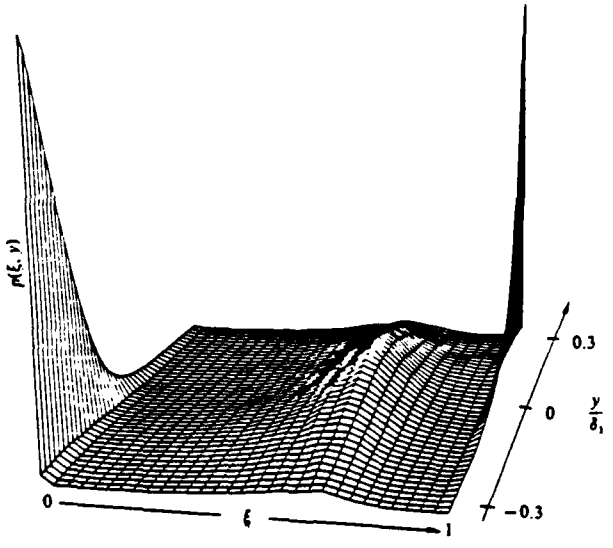

FIGURE 3. Probability density function of the high speed fluid mixture fraction in a liquid layer ($U_2/U_1 = 0.38$, $Re = 2.3\times10^4$). $\xi = 0$ corresponds to low speed fluid, $\xi = 1$ corresponds to high speed fluid. From Koochesfahani & Dimotakis (1986, figure 10).

An important conclusion can be drawn from these data, which is also consistent with the results of the flow visualization studies and the earlier pilot, liquid phase, chemically reacting experiments in Dimotakis & Brown (1976), as well as the study of liquid phase reacting layers by Breidenthal (1981), namely that the large scale motion within the cores of the shear layer vortical structures is capable of transporting a small fluid element from one edge of the layer to the other, before any significant change in its internal composition can occur. During this transport phase, initially unmixed fluid within the fluid element will mix to contribute to the amount of molecularly mixed fluid, but will do so to produce a range of compositions clustered around the value corresponding to the relative amounts of unmixed fluid originally within the small fluid element. This is the reason why the mixed fluid composition cannot exhibit a substantial systematic variation across the layer and, in particular, need not be centered about the value of the local mean. This observation represents an important simplification to the problem, as it suggests that it may be justified to treat the composition field in a uniform manner across the shear layer width.

In the gas phase, hydrogen-fluorine experiments of Mungal & Dimotakis (1984), the stoichiometric mixture ratio ϕ, defined by

$$\phi = \frac{c_{02}/c_{01}}{(c_{02}/c_{01})_s} , \tag{1.1}$$

was varied, where c_{02} and c_{01} are the low and high speed free stream reactant concentrations respectively, and the subscript "s" in the denominator denotes the corresponding chemical reaction stoichiometric ratio (unity for the $H_2 + F_2$ reaction). The quantity ϕ can be viewed as representing the mass of high speed fluid required (to be mixed and react) to exactly consume a unit mass of low speed fluid. For uniform density, chemically reacting shear layers (low heat release), ϕ can also be interpreted in terms of the requisite volumes of the free stream fluids for complete reaction.

For a given value of ϕ, the total amount of chemical product in the mixing layer can be expressed in terms of the integral product thickness

$$\delta_{P1} = \frac{1}{c_{01}} \int_{-\infty}^{\infty} c_P(y,\phi)\, dy , \tag{1.2}$$

where the subscript 1 in δ_{P1} denotes that c_{01}, the high speed stream reactant concentration, was used to normalize the mean chemical product concentration profile $c_P(y,\phi)$. Using the mean temperature rise $\Delta T(y,\phi)$ as the measure of product concentration, and normalizing the transverse coordinate y by the total width of the layer δ, we can also write

$$\frac{\delta_{P1}}{\delta} = \frac{1}{\delta} \int_{-\infty}^{\infty} \frac{\Delta T(y,\phi)}{\Delta T_{flm(\infty)}}\, dy . \tag{1.3}$$

If we keep c_{01} fixed and vary ϕ by, say, increasing c_{02}, also keeping the heat capacities for the free stream fluids matched, we find that the dependence of the adiabatic flame temperature rise on ϕ is given by

$$\Delta T_{flm}(\phi) = \frac{2\phi}{\phi + 1} \Delta T_{flm}(1) , \qquad (1.4)$$

where $\Delta T_{flm}(1)$ is the adiabatic flame temperature rise corresponding to a stoichiometric reactant concentration ratio. Note that, for a fixed high speed stream reactant concentration c_{01}, the normalizing temperature in equation 1.3 is given by $\Delta T_{flm}(\infty) = 2\,\Delta T_{flm}(1)$. The experimental values for the product thickness δ_{p1}/δ, in such an experiment, are plotted in figure 4.

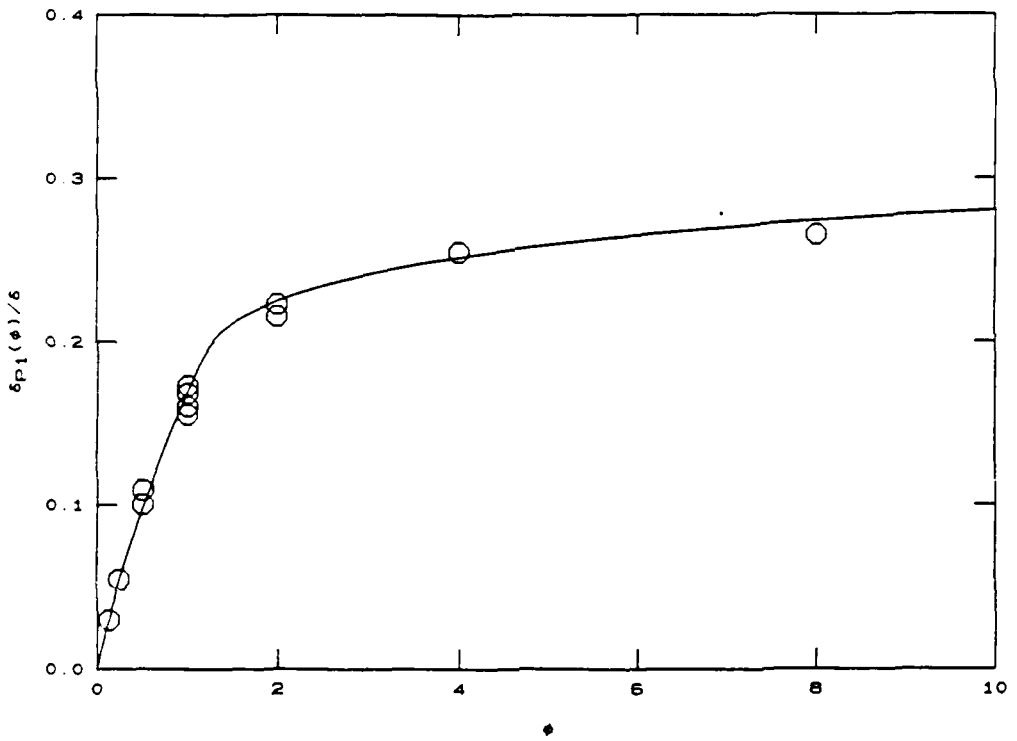

FIGURE 4. Normalized δ_{p1}/δ HF gas phase chemical product thickness data vs. stoichiometric mixture ratio ϕ (Mungal & Dimotakis 1984). $U_2/U_1 = 0.38$, $Re = 6.6\times10^4$. Smooth curve drawn to aid the eye.

In the data in figure 4, the width of the layer δ was estimated by δ_1, which is defined as the extent across the layer where the product concentration (mean temperature rise) has fallen to 1% of its peak mean value. To remove the small differences in the values of δ_1 computed from the temperature profiles measured for each ϕ (see Mungal & Dimotakis 1984, Table I), a fixed (average) value for δ/x ($= 0.165$) was used in

normalizing the data in figure 4. We note that the 1% width δ_1, in both the gas phase reacting layer data and the liquid phase measurements of Koochesfahani & Dimotakis (1986), was found to be very close to the visual shear layer width δ_{vis} of Brown & Roshko (1974). As can be seen in the data in figure 4, as ϕ is increased from small values, the amount of chemical product at first increases rapidly. Beyond a certain value, however, a further increase in ϕ (increase of the low speed stream reactant concentration) does not result in a commensurate increase in the total chemical product, as the fluid in the shear layer is low speed reactant rich and much of the entrained high speed stream reactant has already been consumed. The smooth curve in figure 4 was drawn to aid the eye.

A slightly different definition of product thickness, which avoids the asymmetric choice of using one stream or the other as a reference, is to use the adiabatic flame temperature $\Delta T_{flm}(\phi)$ to normalize the temperature profile, corresponding to each value of ϕ. This yields a new normalized product thickness δ_p/δ, given by

$$\frac{\delta_P}{\delta} = \frac{1}{\delta}\int_{-\infty}^{\infty}\frac{\Delta T(y,\phi)}{\Delta T_{flm}(\phi)}\,dy\ , \tag{1.5}$$

which represents the volume fraction occupied by chemical product. Note that the integrand is in the units of the normalized mean temperature rise profile, as plotted in figure 2, and that $\delta_p/\delta = (\delta_{p_1}/\delta)/\xi_\phi$, where

$$\xi_\phi = \frac{\phi}{\phi+1}\ . \tag{1.6}$$

For equal density free streams, negligible heat release, and a given free stream reactant stoichiometric mixture ratio ϕ, the quantity ξ_ϕ represents the high speed fluid volume fraction, in the mixed fluid, required for complete consumption of both reactants. A volume fraction $\xi > \xi_\phi$ in the molecularly mixed fluid, for example, corresponds to an excess of high speed fluid, relative to that required by the stoichiometry of the reaction, and would result in complete consumption of the low speed reactant in the mixture, and a remainder of unreacted high speed fluid. A plot of the experimental values of δ_p/δ for the hydrogen-fluorine gas phase data, versus ξ_ϕ, appears in figure 5. The smooth curve through the gas phase data of Mungal & Dimotakis (1984) denoted by circles is the same curve that appears in figure 4, transformed to the coordinates of figure 5. The data point denoted by the triangle corresponds to the similarly defined chemical product volume fraction in a liquid phase two dimensional shear layer, as measured by Koochesfahani & Dimotakis (1986) at the same free stream speed ratio and comparable Reynolds number.

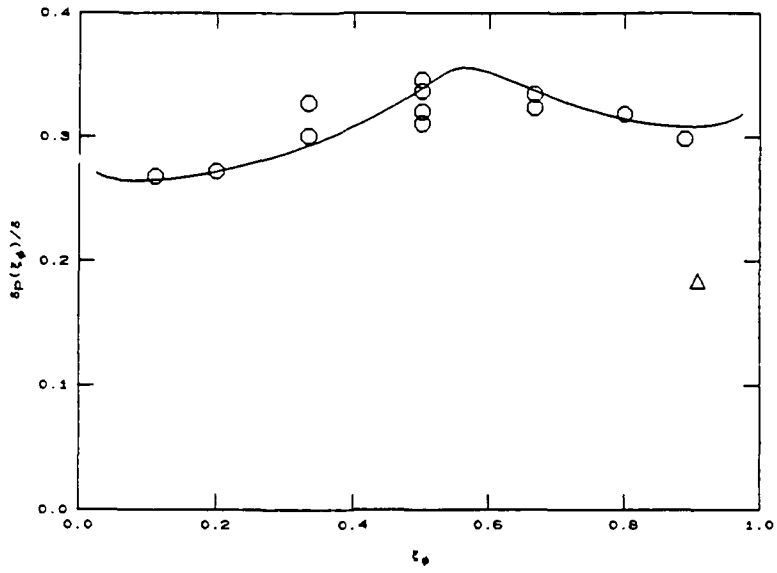

FIGURE 5. Chemical product δ_p/δ volume fraction data vs. stoichiometric mixture fraction ξ_ϕ. Circles from gas phase Mungal & Dimotakis (1984) data (see figure 4). Triangle from liquid phase Koochesfahani & Dimotakis (1986) data ($U_2/U_1 = 0.4$, $Re = 7.8\times10^4$). Smooth curve transformed from that of figure 4.

Since (for equal species and heat diffusivities) $\Delta T_{flm}(\phi)$ is the highest temperature that can be achieved in the reaction zone, the ratio δ_p/δ represents the volume fraction occupied by the chemical product within the mixing zone and is a measure of the shear layer turbulent mixing and chemical reactor "efficiency". If the two reactants were entrained from the two free streams in such a way as to produce molecularly mixed fluid everywhere within the layer at a single-valued composition corresponding to a mixture fraction ξ_ϕ, then the resulting temperature profile would be a top-hat of height $\Delta T_{flm}(\phi)$ and width δ, resulting in a value of δ_p/δ of unity. This clearly represents the highest possible total chemical product that can be formed within the confines of the shear layer turbulent region. If, on the other hand, the mean temperature rise profile was a triangle whose base was equal to δ and which reached $\Delta T_{flm}(\phi)$ at the apex somewhere within the layer, then δ_p/δ would be equal to 1/2. It is interesting that, in these units, the gas phase data (circles) in figure 5, for all the values of the stoichiometric mixture ratio investigated, are in the relatively narrow range of $\delta_p/\delta = 0.31 \pm 0.03$.

Comparison of the total amount of chemical product measured in gas phase reacting layers (Mungal & Dimotakis 1984), and liquid phase reacting layers (Breidenthal 1981,

length

Koochesfahani & Dimotakis 1986), points out another important feature of these data; at comparable flow conditions, the amount of chemical product formed at high Reynolds numbers is a function of the (molecular) Schmidt number $Sc = \nu/D$ of the fluid, where ν is the kinematic viscosity and D is the relevant species diffusivity. In particular, roughly twice as much product is formed in a gas phase chemically reacting shear layer ($Sc = 0.8$) as in a liquid phase layer ($Sc = 600$).

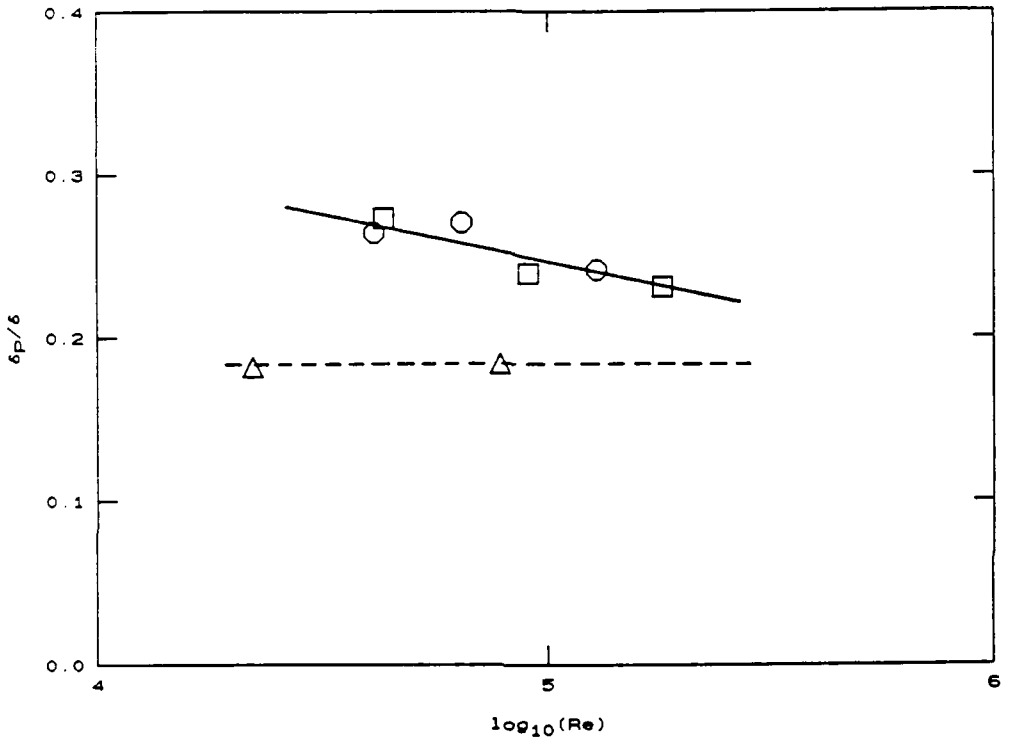

FIGURE 6. Chemical product δ_P/δ volume fraction versus Reynolds number. Circles and squares are for gas phase data (Mungal et al 1985) at $\phi = 1/8$. Circles are for initially laminar splitter plate boundary layers, squares for turbulent boundary layers. Triangles for liquid phase data from Koochesfahani & Dimotakis (1986), at $\phi = 10$.

Finally, in a further investigation in gas phase reacting shear layers, the Reynolds number was varied over a range of almost an order of magnitude, keeping all other conditions as constant as was feasible (Mungal et al 1985). The resulting data for δ_P/δ, for a fixed stoichiometric mixture ratio of $\phi = 1/8$, are plotted in figure 6. It can be seen that there is a modest but unmistakeable decrease in the total amount of product in the layer as the Reynolds number is increased. The authors estimate that, at the operating conditions for those experiments, a factor of 2 increase in the Reynolds number results in approximately a 6% reduction in δ_P/δ, the chemical product volume fraction. Also included in the same plot, for comparison purposes, are the reacting liquid layer

data of Koochesfahani & Dimotakis (1986) at a stoichiometric mixture ratio of $\phi = 10$. As can be seen, the data indicate a much weaker Reynolds number dependence of the liquid phase product volume fraction $\delta_{P/\delta}$. We note, however, that the lower Reynolds number liquid data point may be at a value of the Reynolds number that is too close to the shear layer mixing transition (Konrad 1976, Bernal et al 1979, Breidenthal 1981) and the flow may not have attained fully turbulent behavior.

1.2 Entrainment ratio for a spatially growing shear layer

An important conclusion drawn by Konrad (1976) was that a spatially growing shear layer entrains fluid from each of the two free streams in an asymmetric way, even for equal free stream densities. In particular, for equal free stream densities ($\rho_2/\rho_1 = 1$) and a free stream speed ratio of $U_2/U_1 = 0.38$, Konrad estimated the volume flux entrainment ratio E to be 1.3. For a free stream density ratio of $\rho_2/\rho_1 = 7$ (helium high speed fluid and nitrogen low speed fluid), and the same velocity ratio, he estimated an entrainment ratio of $E = 3.4$.

This behavior can be understood in terms of the upstream/downstream asymmetry that a given large scale vortical structure sees in a spatially growing shear layer. Simple arguments suggest that the volume flux entrainment ratio can be estimated and is given by

$$E = \left(\frac{\rho_2}{\rho_1} \right)^{1/2} (1 + \ell/x) , \qquad (1.7a)$$

where ℓ/x is the large structure spacing to position ratio. See Dimotakis (1986) for the arguments leading to this result.

Konrad's data support the hypothesis that $\langle \ell/x \rangle$, the ensemble averaged value of ℓ/x, is independent of the free stream density ratio ρ_2/ρ_1. Fitting available data for ℓ/x, one finds that the relation

$$\langle \ell/x \rangle = 0.68 \, \frac{1 - r}{1 + r} , \qquad (1.7b)$$

where $r = U_2/U_1$ is the free stream speed ratio, is a good representation for this quantity. It can be verified that equations 1.7 produce estimates for E that are in good agreement with Konrad's measurements. Finally, we note that to the extent that ℓ/x is a fluctuating quantity, we would expect, on the basis of equation 1.7a, that the entrainment ratio E should exhibit corresponding fluctuations. We will develop this idea in the discussions to follow and incorporate its consequences in the proposed model calculations.

In the context of chemically reacting flows, it is important to recognize that fluid homogenized at the entrainment ratio E produces a (high speed fluid) mixture fraction ξ_E given by,

$$\xi_E = \frac{E}{E+1} \quad . \tag{1.8}$$

For $E > 1$, as is always the case for matched density free streams, this corresponds to a value for ξ_E that is greater than 1/2. The resulting mixture fraction ξ_E has a special significance in the shear layer, as Konrad recognized, and helps explain the large differences in the composition fluctuations between his equal free stream density data and his helium/nitrogen free stream data. See sketch and discussion on page 27 in Konrad (1976).

This picture suggests a zeroth order model for mixing in a two-dimensional shear layer in which the reactants are entrained at the ratio E, as dictated by the large scale dynamics, and eventually mixed to a (nearly) homogeneous composition in which the distribution of values ξ of the resulting mixed fluid mixture fraction is clustered around ξ_E by the efficient action of the turbulence. A useful cartoon is that of a bucket filled by two faucets with unequal flow rates, as a laboratory stirring device mixes the effluents. For all the complexity of the ensuing turbulent motion, we would expect to find a distribution of mixed fluid compositions in the bucket clustered around the value of the mixture fraction given by equation 1.8, where E, in our cartoon, would correspond to the ratio of the flux from each of the two faucets. In fact, as the the faucet flow rate is decreased relative to the mixing rate, the mixed fluid composition probability density function is tightened around the value ξ_E, with $p(\xi)\,d\xi \rightarrow \delta(\xi - \xi_E)\,d\xi$ in the limit.

The asymmetric entrainment ratio also helps explain the outcome of the chemically reacting "flip" experiments, as they have been coined. In particular, it is known that if the concentration of the reactants carried by the two free streams corresponds to a stoichiometric mixture ratio $\phi = 1$, then one obtains more or less total chemical product, depending on whether or not the lean reactant is carried by the free stream fluid that is preferentially entrained. This can be seen in the gas phase reacting shear layer data pairs for $\phi = (1/4, 4)$ and $\phi = (1/8, 8)$, which correspond to "flipping" the side on which the lean reactant is carried. Compare the coresponding pairs of values for δ_p/δ in the data in figure 5. See figures 9 and 17, and related discussions in Mungal & Dimotakis (1984), and also the liquid phase "flip" experiments documented in Koochesfahani et al (1983), and in Koochesfahani & Dimotakis (1986) for additional information and discussions.

1.3 The Broadwell-Breidenthal model

In the Broadwell-Breidenthal (1982) mixing model for the two-dimensional shear layer, tne entrained fluid is described as existing in one of three states:

1. recently entrained, as yet unmixed fluid from each of the two free streams,

2. homogeneously mixed fluid at a composition ξ_E corresponding to the entrainment ratio E (equation 1.8),

and,

3. fluid mixed at strained laminar interfaces (flame sheets).

In this picture, the total chemical product is computed as the sum of the contributions corresponding to the homogeneously mixed fluid, and the contribution from the flame sheets.

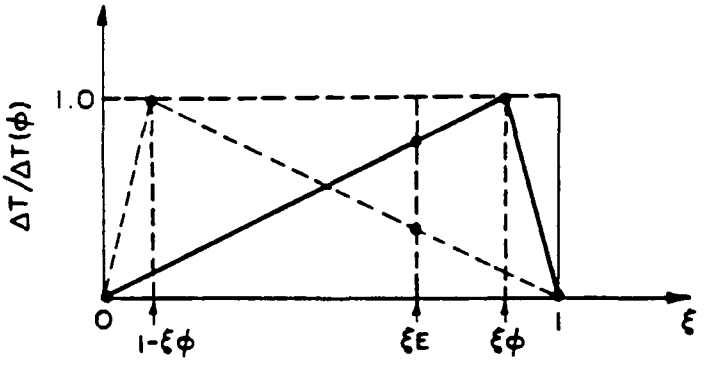

FIGURE 7. Normalized temperature rise for free stream fluids at a stoichiometric mixture fraction $\xi_\phi = \phi/(\phi+1)$, as a function of the high speed mixture fraction ξ. Dashed triangle indicates correspondding function for a "flip" experiment and the resulting temperature rise for a mixture at the entrainment mixture fraction $\xi_E = E/(E+1)$.

The volume fraction in the reaction zone, corresponding to the homogeneously mixed fluid at $\xi = \xi_E$, has experienced a temperature rise (product concentration) $\Delta T_H(\xi_E, \xi_\phi)$,

$$\Delta T_H(\xi_E, \xi_\phi) = \Theta_H(\xi_E, \xi_\phi) \times \Delta T_{flm}(\phi) \ , \qquad (1.9a)$$

where, for a fixed low speed stream reactant concentration, $\Delta T_{flm}(\phi)$ is given by equation

1.4. $\Theta_H(\xi_E,\xi_\phi)$ is the dimensionless temperature rise, normalized by the adiabatic flame temperature rise, that results when the two fluid elements at a stoichiometric mixture ratio ϕ are homogenized to form a mixture fraction equal to the entrainment mixture fraction ξ_E. This is given by

$$\Theta_H(\xi_E,\xi_\phi) = \begin{cases} \dfrac{\xi_E}{\xi_\phi}, & \text{for } \xi_E \le \xi_\phi \\ \dfrac{1-\xi_E}{1-\xi_\phi}, & \text{for } \xi_E > \xi_\phi, \end{cases} \tag{1.9b}$$

corresponding to the complete consumption of the lean reactant as a function of the resulting composition ξ_E. See figure 7.

The heat released (amount of product) in the strained laminar interfaces (flame sheets), for equal species and heat diffusivities, is found proportional to

$$(Sc \cdot Re)^{-1/2} F(\xi_\phi)\, \Delta T_{flm}(\phi), \tag{1.10}$$

where $F(\xi_\phi)$ is the Marble flame sheet function (Marble & Broadwell 1977), and given by

$$F(\xi_\phi) = \frac{e^{-z_\phi^2}}{\sqrt{\pi}\,\xi_\phi\,(1-\xi_\phi)}. \tag{1.11a}$$

In this expression, z_ϕ is implicitly defined by the relation

$$\mathrm{erf}(z_\phi) = \frac{2}{\sqrt{\pi}} \int_0^{z_\phi} e^{-\zeta^2}\, d\zeta = \frac{\phi-1}{\phi+1}, \tag{1.11b}$$

where erf(z) is the error function. The flame sheet function $F(\xi_\phi)$ is plotted in figure 8. We note here that in the original discussion (Broadwell & Breidenthal 1982), the exponent for the Reynolds number dependence could be taken as $-1/2$ or $-3/4$, depending on whether the appropriate flame sheet strain rate was estimated from the large scales of the flow or the small (Kolmogorov) scales, respectively. The Reynolds number exponent is taken here (equation 1.10) as $-1/2$, corresponding to the large scale strain rate, following the recommendation in the revised discussion of this model in Broadwell & Mungal (1986).

The contributions from the homogeneously mixed fluid and the mixed fluid on the flame sheets should be added. Normalizing the total amount of product with $\Delta T_{flm}(\phi)$, as in equation 1.5, we obtain the Broadwell-Breidenthal expression for the product volume fraction, i.e.

$$\frac{\delta_P}{\delta} = c_H \Theta_H(\xi_E, \xi_\phi) + c_F \left(Sc \cdot Re\right)^{-1/2} F(\xi_\phi) \ , \qquad (1.12)$$

where c_H and c_F are dimensionless constants to be determined by fitting the data.

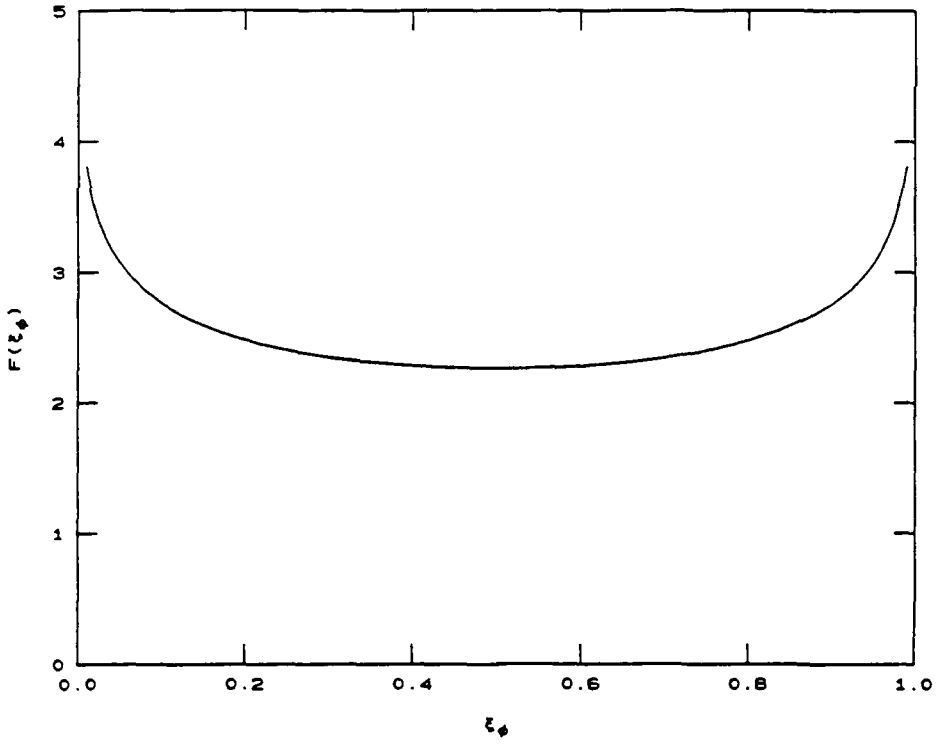

FIGURE 8. Marble (Marble & Broadwell 1977) flame sheet function $F(\xi_\phi)$.

In the more recent discussion of this model, Broadwell & Mungal (1986) recommend that the coefficients c_H and c_F in equation 1.12 should be determined by fitting the experimental value for δ_P/δ at $\phi = 1/8$, $Sc = 0.8$ and $Re = 6.6 \times 10^4$, derived from the gas phase data of Mungal & Dimotakis (1984), and the experimental value for δ_P/δ at $\phi = 1/10$, $Sc = 600$ and $Re = 2.2 \times 10^4$ derived from the liquid phase data of Koochesfahani & Dimotakis (1986). It should be mentioned, however, that in the latter discussion (which also models finite chemical kinetic rate effects in two-dimensional shear layers using the Broadwell-Breidenthal model) Broadwell & Mungal concluded, on the basis of their model calculations, that the gas phase data of Mungal & Dimotakis (1984) and Mungal et al (1985) were not quite in the fast chemistry limit. In fitting the two coefficients to the data, however, we will ignore such effects for the purposes of the discussion, noting that the differences in the resulting estimates for the model coefficients are not large. In the notation of equation 1.12, we then obtain

$$c_H = 0.27 , \quad c_F = 11.5 , \tag{1.13}$$

for the Broadwell-Breidenthal model constants.

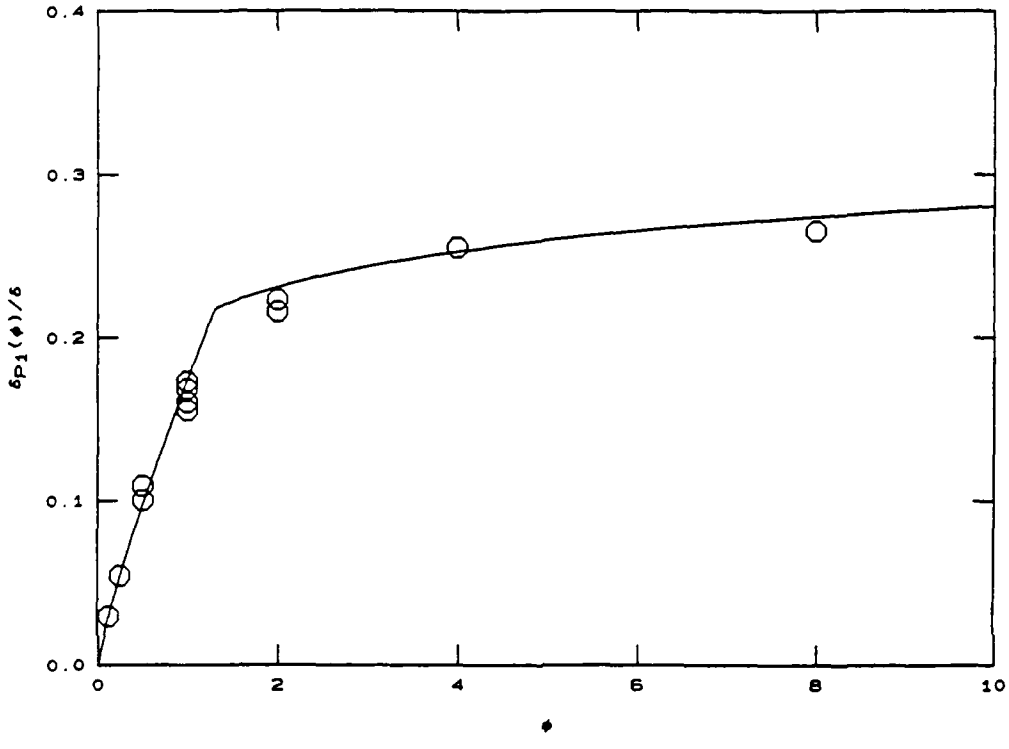

FIGURE 9. Broadwell-Breidenthal model predictions for the δ_{P1}/δ gas phase product thickness data of Mungal & Dimotakis (1984) at Sc = 0.8 and Re = 6.6×10^4.

The curve in figure 9 represents the resulting model predictions for the gas phase product thickness $\delta_{P1}(\phi)/\delta$ data that were plotted in figure 4. The $\delta p/\delta$ product volume fraction data and the corresponding Broadwell-Breidenthal model curves are plotted in figure 10 versus ξ_ϕ. The top solid curve in figure 10 is computed for the gas phase data (circles; Sc = 0.8, Re = 6.6×10^4). The dashed curve is computed for the lower Reynolds number $\phi = 1/10$ and $\phi = 10$ (inverted triangles; Re = 2.3×10^4), while the dot-dashed curve is computed for the higher Reynolds number experimental value at $\phi = 10$ (upright triangle; Re = 7.8×10^4) of the liquid phase data (Sc = 600) of Koochesfahani & Dimotakis (1986).

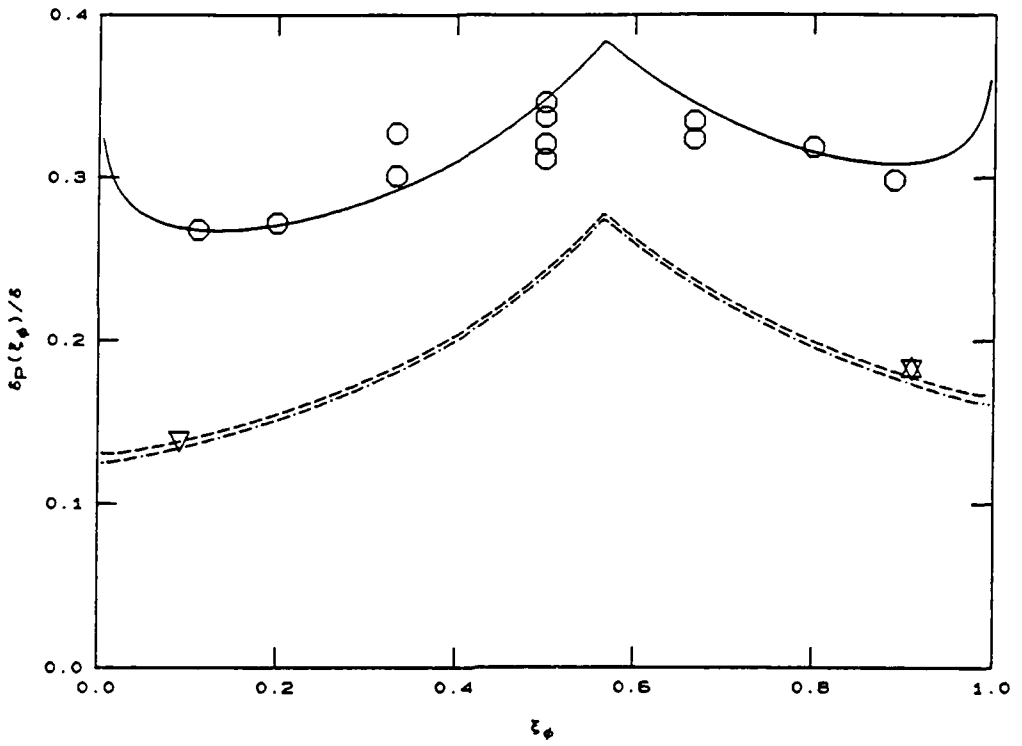

FIGURE 10. Broadwell-Breidenthal model predictions for $\delta p/\delta$ vs. ξ_ϕ data. Solid line for gas phase data (circles; Sc = 0.8, Re = 6.6×10^4; Mungal & Dimotakis 1984). Dashed line for liquid phase (Sc = 600, Koochesfahani & Dimotakis 1986) data (inverted triangles; Re = 2.3×10^4). Dot-dashed line for higher Reynolds number point (upright triangle; Re = 7.8×10^4).

It can be seen that several features of the reacting shear layer data can be accounted for by this model. For a given Reynolds number, the $1/\sqrt{Sc}$ Schmidt number dependence of the flame sheet part renders its contribution in a liquid (Sc ~ 600) negligible (~ 25 times smaller) as compared to that in a gas (Sc ~ 1). Secondly, we can see that even though the flame sheet contribution is symmetric with respect to a change from ϕ to $1/\phi$, i.e. $F(\xi_\phi) = F(1-\xi_\phi)$, the homogeneous mixture contribution is not, since $\Theta_H(\xi_E,1-\xi_\phi) = \Theta_H(\xi_E,\xi_\phi)/E$ (compare the solid triangle function with the dashed triangle function in figure 7). This allows the outcome of the "flip" experiments to be accommodated. We note here that, for values of the stoichiometric mixture ratio ϕ close to the entrainment ratio E, the model predicts a relatively smaller difference for the product volume fraction between gases and liquids, than for small (or high) values of ϕ. Unfortunately, no relevant chemically reacting liquid phase data are available at present to provide a direct assessment of Schmidt number effects in this regime.

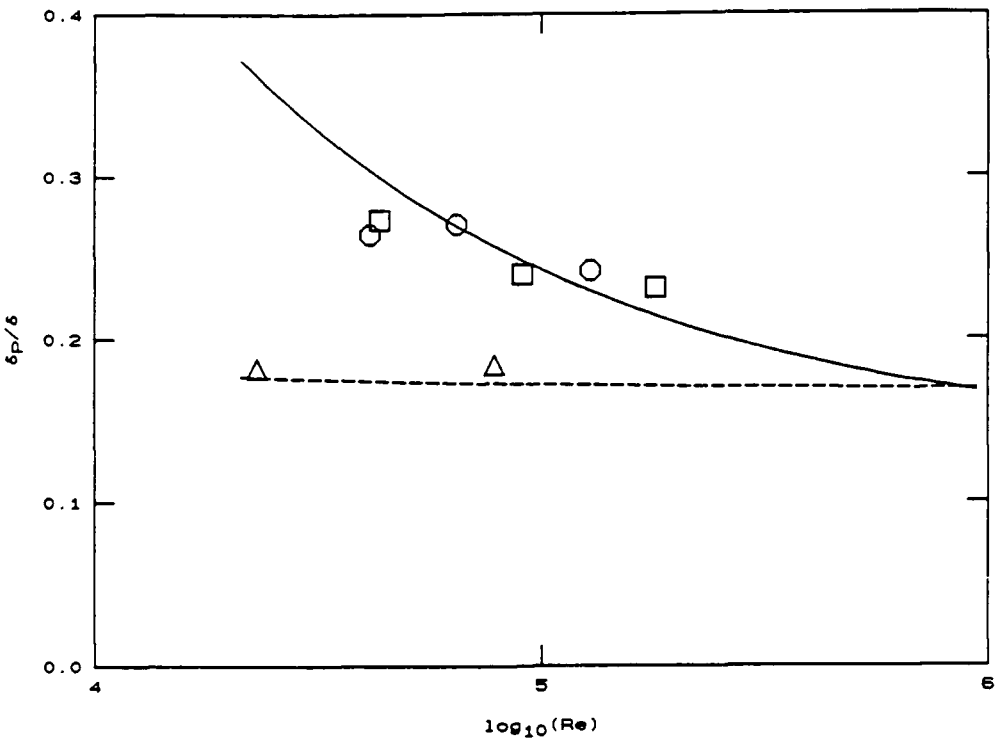

FIGURE 11. Broadwell-Breidenthal model predictions for δ_p/δ dependence on Reynolds number. Solid curve for gas phase data (Mungal et al 1985) at $\phi = 1/8$. Dashed curve for liquid phase data (Koochesfahani & Dimotakis 1986) at $\phi = 10$. Note that curves cross as a result of the larger homogeneously mixed fluid contribution for the liquid phase data at large ϕ.

Plots of the Broadwell-Breidenthal model predictions for the product volume fraction versus Reynolds number are depicted in figure 11 along with the corresponding gas phase data at $\phi = 1/8$ of Mungal et al (1985) and the liquid phase data at $\phi = 10$ of Koochesfahani & Dimotakis (1986). The predicted curves start at a Reynolds number of 2×10^4, based on the velocity difference and the local visual width of the layer, estimated to be the minimum Reynolds number for the quasi-asymptotic behavior to have been attained, following the shear layer mixing transition (Konrad 1976, Bernal et al 1979, Breidenthal 1981). The solid line is the model prediction for the gas phase data. The dashed line corresponds to the model prediction for the liquid phase data. Note that the predicted curves for the gas and the liquid phase product thickness curves are computed for the values of the stoichiometric mixture ratio corresponding to the one used in the experiments ($\phi = 1/8$ and $\phi = 10$ respectively) and will cross at some Reynolds number as a consequence of the larger homogeneous fluid contribution for the ($\phi = 10$) liquid data. There would, of course, be no crossing of the model predictions at the same ϕ, as the gas phase product volume fraction would always be larger than the corresponding liquid phase estimate for each value of the Reynolds number.

It can be seen that an additional important feature of the data is well represented by the model. Namely, the Reynolds number dependence of the product thickness for the gas phase data is predicted to be stronger than that for the liquid data. In fact, the model prediction is that at a Schmidt number of 600 the liquid product thickness will be almost independent of the Reynolds number. On the other hand, it would appear that the Broadwell-Breidenthal model predicts a Reynolds number dependence for the gas phase product thickness that may be too strong (algebraic), when compared to the dependence of the experimental data for the product thickness versus Reynolds number of Mungal et al (1985), which suggest a dependence on Reynolds number that may be closer to logarithmic (recall that those authors suggest a 6% drop in δ_P/δ, per factor of two in Reynolds number, for the range of Reynolds numbers investigated). It may be interesting to note, as was pointed out by these authors, that the model dependence on Schmidt number and Reynolds number is through the product Sc×Re (Peclet number) considered as a single variable. Lastly, in the limit of infinite Reynolds number, the model prediction is that gas phase shear layers should behave like liquids, with an asymptotic value of δ_P/δ, the chemical product volume fraction, given by $c_H\,\Theta_H(\xi_E,\xi_\phi)$.

From a theoretical vantage point, the Broadwell/Breidenthal model considers the mixed fluid as residing in strained flame sheets, as would be appropriate for interfaces separated from each other by distances large enough such that the composition ξ (mixture fraction) swings from 0 to 1 across them, and as homogeneously mixed fluid, as would perhaps be appropriate at scales of the order of the (scalar) diffusion scale λ_D, after the diffusion process has homogenized adjacent layers of the entrained fluids. This partition of the mixed fluid states is an idealization, as the actual dynamics of this process would be expected to result in a smooth transition from one regime to the other. The authors argue that the Lagrangian time associated with that transition is short and, therefore, intermediate states can be neglected. It can also be argued, however, that the volume fraction associated with the molecularly mixed fluid in this intermediate state is not small, increasing rapidly as the diffusion scales are approached by the force of the same arguments, and is consequently not necessarily negligible.

Another related difficulty of the Broadwell/Breidenthal model, in my opinion, is the assignment of the volume fraction given to the homogeneously mixed fluid at $\xi = \xi_E$, i.e. the value of the coefficient c_H in equation 1.12. According to the model, c_H is a constant that, in particular, is independent of both Schmidt number and Reynolds number. It is reasonable to expect, however, that the fraction of the mixed fluid generated at the scalar diffusion scales of the flow will be a function of the ratio λ_D/δ, i.e. of the scalar diffusion scale λ_D to the overall transverse extent of the flow δ.

We shall return to these issues in the discussion of the model proposed in this paper and the comparison of its predictions with those of the Broadwell-Breidenthal model.

2.0 THE PROPOSED MODEL

The approach that is adopted in the model proposed here is that of viewing an Eulerian slice of the spatially growing shear layer, at a downstream station in the neighborhood of x, and imagining the instantaneous interface between the two interdiffusing and chemically reacting fluids as well as the associated strain field imposed on that interface. It is recognized that both the Eulerian state and the local behavior of that interface are the consequence of the Lagrangian shear layer dynamics from all relevant points upstream of the station of interest at x. It is assumed, however, that this upstream history acts in such a manner as to produce a self-similar state at x, whose statistics can be described in terms of the local parameters of the flow. In particular, it is assumed that a Kolmogorov cascade process has been the appropriately adequate description of the upstream dynamics, leading to the local Eulerian spectrum of scales and associated strain rate field at x.

The justification for this approach is that while the large scale dynamics are all important in determining such things as the growth rate and entrainment ratio into the spatially growing shear layer, the predominant fraction of the interfacial area is associated with the smallest spatial scales of the flow, which can perhaps be adequately dealt with in terms of universal similarity laws. The large scales, therefore, are to be viewed as the faucets in our cartoon, feeding the reactants that are entrained at some upstream station into the smaller scale turbulence at the appropriate rate. These reactants subsequently get processed by the evolution of the cascade processes upstream to produce the local spectrum of scales at x (see discussion in Broadwell & Dimotakis 1986). This conceptual basis is also aided by the notion of a conserved scalar, according to which the state of diffusion and the progress of an associated chemical reaction, in the limit of fast (diffusion-limited) chemical kinetics, is completely determinable by the local (Eulerian) state of the conserved scalar. See, for example, Bilger (1980) for a more complete description of this notion.

An important part of the proposed procedure is the normalization that will have to be imposed on the statistical weight (contribution) of each scale λ to the total amount of molecularly mixed fluid and associated chemical product. This is done via the expected interfacial surface per unit volume ratio that must be assigned to each scale λ. When totalled over all scales, these statistical weights must add up to unity.

The results are first obtained conditional on a uniform value of the dissipation rate ϵ. An attempt to incorporate and assess the effects of the fluctuations in the local dissipation rate $\epsilon(\underline{x},t)$ will be made by folding the conditional results over a probability density function for ϵ.

In a similar vein, a refinement of the entrainment ratio idea is proposed, as noted earlier, in which it is recognized that the large scale spacing ℓ/x is a random variable and that therefore, by the force of equation 1.7a, the entrainment ratio is itself a

random variable of the flow. Accordingly, the results will be obtained conditional on a given value of the entrainment ratio E, and will subsequently be folded over the expected distribution of values of E about its average value $\bar{E}$.

In the calculations that follow, it is assumed that the molecular diffusivities for all relevant species are equal to each other, but not necessarily equal to the kinematic viscosity. Heat release effects and temperature dependence effects of the molecular transport coefficients are also ignored. This is appropriate for the liquid phase measurements of Koochesfahani & Dimotakis (1986), and may be adequate for the description of the gas phase measurements of Mungal & Dimotakis (1984) and the Reynolds number study of Mungal et al (1985). The issue of heat release effects on the flow was specifically addressed elsewhere (see Hermanson et al 1987). In computing the temperature corresponding to the heat released in the reaction, equal heat capacities are also assumed for the two fluids brought together within the mixing zone. While some of these assumptions are not necessary for the proposed formulation outlined below, they allow calculations to be performed in closed form permitting, in turn, the examination of the dependence of the results on the various dimensionless parameters of the problem.

The proposed procedure assumes that the relevant statistics of the velocity field are known (or can be estimated) and computes the behavior of the passive scalar process in response to that velocity field. Finally, the procedure is "closed" in that it yields the (absolute) chemical product volume fraction δ_P/δ in the shear layer at x, with no adjustable parameters.

2.1 Turbulent diffusion of an entrained conserved scalar

Consider the shear layer as it entrains fluid from each of the two free streams and is interlaced with the resulting interfaces formed between the interdiffusing free stream fluids into a "vanilla-chocolate cake jelly roll" like structure. In describing the ensuing interdiffusion process it is useful to consider the scalar concentration field of, say, the high speed fluid mixture fraction $\xi(\underline{x},t)$, where $\xi = 0$ represents pure low speed fluid and $\xi = 1$ represents pure high speed fluid. A space curve intersecting the interface of the two interdiffusing fluids everywhere normal to this interface, i.e. in the direction of the local gradient of $\xi(\underline{x},t)$, would see at an instant in time a concentration field $\xi(s,t)$, where s is the arc length along the space curve. See figure 12. Note that, for an entrainment ratio E of high speed fluid relative to low speed fluid which is greater than unity, we would expect that the intervals along the space curve for which $\xi \sim 1$, labeled "a" in figure 12, would be longer, on average, than the intervals labeled "b", for which $\xi \sim 0$. In fact, the ratio of the expected $\xi > \xi_E$ time "a" to total time "a + b" for adjacent layers would be given by

$$\frac{\langle a \rangle}{\langle a+b \rangle} = \frac{E}{E+1} \quad . \tag{2.1}$$

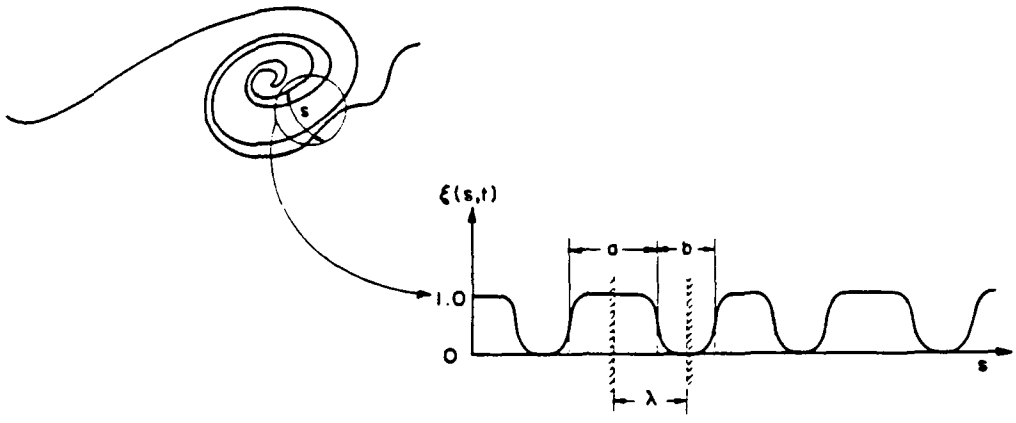

FIGURE 12. Shear layer mixing interface. Inset curve depicts values of the conserved scalar $\xi(s,t)$ at fixed time, as a function of the arc length s on a line in the direction of $\nabla\xi$.

Correspondingly, for portions of the segment that may have captured "jelly-roll" layers, which have been diffusing into each other for some time, we would expect that the high speed fluid fraction, in the resulting molecularly mixed fluid, would tend to homogenize to a local composition value ξ_E determined by the entrainment ratio E, i.e.

$$\xi \rightarrow \xi_E = \frac{\langle a \rangle}{\langle a+b \rangle} = \frac{E}{E+1} \quad . \tag{2.2}$$

In this context, ξ_E is equal to the long term (local) value of the scalar ξ, resulting from the interdiffusion of several successive $\xi = 1$ and $\xi = 0$ layers into each other, in a manner that preserves the (conserved) scalar ξ. This special role of the value of the scalar $\xi = \xi_E$ allows us to be more precise with the definition of the interfacial surface between the two entrained fluids, which we will define below as the three dimensional surface on which $\xi(\underline{x},t) = \xi_E$.

The evolution of the composition $\xi(s,t)$ from the initial stages, which bring together adjacent layers of newly entrained high speed fluid ($\xi = 1$) and low speed fluid ($\xi = 0$), to the (local) completion of the molecular mixing ($\xi \rightarrow \xi_E$), is an unsteady diffusion problem that proceeds under the important influence of the straining field, imposed on the diffusion process by the turbulent velocity field. For the purposes of the present discussion, we will idealize this unsteady diffusion process as taking place in cells of

length

$$\lambda = \frac{a+b}{2} , \tag{2.3}$$

extending from the zero $\nabla\xi$ point in the $\xi = 1$ ("a") interval on one side of the interface to the zero $\nabla\xi$ point in the $\xi = 0$ ("b") interval on the other. See figure 12.

Using the scale λ, it is convenient to define a dimensionless space variable $\eta = s/\lambda$, for each cell of extent λ, where

$$0 \leq \eta \leq 1 , \tag{2.4}$$

and a dimensionless time $\tau(\lambda)$, corresponding to the cell scale λ, given by

$$\tau(\lambda) = \frac{D\,t}{\lambda^2} , \tag{2.5}$$

where D is the scalar species molecular diffusivity. The initial conditions for this problem are given by

$$\xi(\eta,0) = \begin{cases} 1 , & \text{for } 0 \leq \eta < \dfrac{E}{E+1} \\ 0 , & \text{for } \dfrac{E}{E+1} < \eta \leq 1 , \end{cases} \tag{2.6a}$$

with adiabatic boundary conditions at the edges, i.e.

$$\frac{\partial}{\partial\eta}\xi(\eta,t) = 0 , \quad \text{at } \eta = 0,\ 1 . \tag{2.6b}$$

2.2 Strain-balanced diffusion

It is important to appreciate the role of the strain imposed on the interface, in the vicinity of some Lagrangian point of interest, in this unsteady diffusion process.

Imagine a point on the $\xi(\underline{x},t) = \xi_E$ surface associated with an arc interval λ between the two zero gradient points on either side of the interface. Imagine also a Taylor expansion of the velocity field component in the direction of the local $\nabla\xi$, in a frame convecting with that point. If we denote by s the arc length measured from the $\xi(\underline{x},t) = \xi_E$ surface and along the space curve in the direction of $\nabla\xi$, we expect the local

Gas-like : $x_H = \lambda_H/\lambda_C = G^{3/2}(\xi_\phi) > 1$

expression

$$\underline{u} \cdot \frac{\partial \xi}{\partial \underline{x}} = u_s \frac{\partial \xi}{\partial s} = -\sigma(\lambda)\, s \frac{\partial \xi}{\partial s} ,$$

to be an adequate approximation for this scalar product, over the transverse extent of the diffusing layer on either side of the interface. The quantity $\sigma(\lambda)$ represents the expected value of the local strain rate, which we should be able to approximate as

$$\sigma(\lambda) = -\frac{1}{\lambda} \frac{d\lambda}{dt} . \qquad (2.7)$$

We note that $\sigma(\lambda)$ is not necessarily identified here with $-\sigma_3$, the local maximum contraction strain rate eigenvalue, where $\sigma_1 \geq \sigma_2 \geq \sigma_3$ are the local strain rate tensor eigenvalues and where $\sigma_1 + \sigma_2 + \sigma_3 = \nabla \cdot \underline{u} = 0$. We do expect that identification to represent an improving approximation as the viscous scales are approached, however, in as much as we expect the scalar interfaces to orient themselves normal to the direction of the local maximum contraction strain rate eigenvector in the limit of small scales, and the approximate relation of equation 2.7 to become exact in that limit. This was assumed by Batchelor (1959) in his discussion of the scalar spectrum at high wavenumbers, and recently corroborated by the analysis by Ashurst et al (1987) of the Rogers et al (1986) shear flow direct turbulence simulation data.

Returning to the unsteady diffusion problem, if the initial/boundary value problem has been proceeding in the cell of extent λ for a time $t(\lambda)$ that is large compared to the reciprocal of the imposed (contraction) strain rate $\sigma(\lambda)$ then the solution to the diffusion problem becomes independent of the time $t(\lambda)$ and a function of the strain rate $\sigma(\lambda)$ only. See figure 13. Specifically, for $\sigma(\lambda) \gg 1/t(\lambda)$, the appropriate dimensionless "time" for the problem is given by substituting $1/\sigma(\lambda)$ for t, in equation 2.5, or

$$\tau(\lambda) \rightarrow \frac{D}{\lambda^2 \sigma(\lambda)} , \quad \text{as } t \rightarrow \infty . \qquad (2.8)$$

This can be seen directly from the form of the diffusion equation, i.e.

$$\frac{\partial \xi}{\partial t} + \underline{u} \cdot \frac{\partial \xi}{\partial \underline{x}} = D \nabla^2 \xi ,$$

which can approximately be expressed in the local Lagrangian frame as

$$\frac{\partial \xi}{\partial t} - \sigma s \frac{\partial \xi}{\partial s} = D \frac{\partial^2 \xi}{\partial s^2} . \qquad (2.9)$$

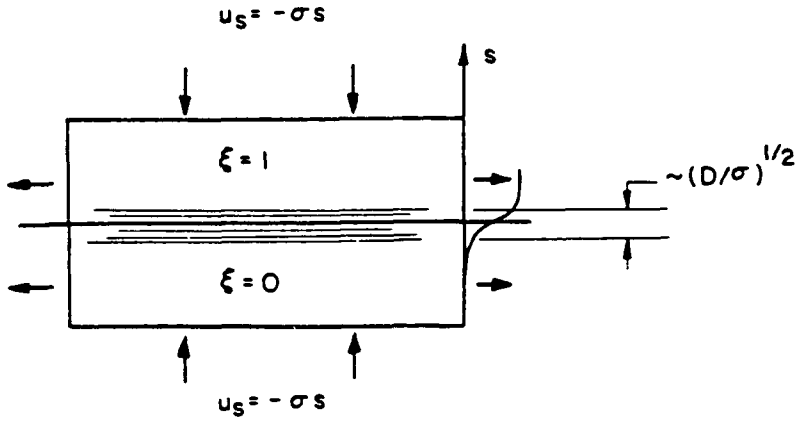

FIGURE 13. Strain-balanced diffusion process. Shaded region indicates thickness of equilibrium diffusion layer.

Physically, as the aspect ratio of the volume containing the strained interface changes, we can see that for long times the dominant species transport mechanism towards the interface becomes the convection owing to the strain field velocity normal to the interface. At equilibrium, the diffusive thickening of the mixed fluid layer is balanced by the steepening caused by the strain field, in a manner that tends to a time-independent concentration gradient and diffusive flux per unit area of interface. It can be ascertained, by solving the diffusion equation 2.9 for $\partial/\partial t \to 0$, that the resulting equilibrium flux corresponds to its value for the unsteady, time-dependent, zero strain problem, at the time $t = 1/\sigma(\lambda)$, hence, equation 2.8. It can be argued that, for $\lambda \ll \delta$, which will prove to be the important regime for the problem, the Lagrangian cascade time $t(\lambda)$ required to reach the scale λ is long compared to $1/\sigma(\lambda)$, the reciprocal of the strain rate we will associate with the scale λ. Consequently, we are encouraged to consider the additional simplification of the diffusion process, as it proceeds down the turbulent cascade of scales, as evolving in quasi-equilibrium with the associated strain rate $\sigma(\lambda)$, corresponding to the scale λ.

The unsteady diffusion problem in the normalized unit cell can be handled numerically in a straightforward manner. Nevertheless, it is worth noting that, for small $\tau(\lambda)$, the thickness of the diffusion layer will be small compared to its distance from either of the two cell edges. Consequently, the composition field can be approximated by the infinite domain solution to the problem, i.e.

$$\xi(z) = \frac{1}{2}\left[1 - \mathrm{erf}(z)\right], \qquad (2.10a)$$

where, corresponding to the boundary conditions of the problem (equation 2.6a),

$$z = \frac{1}{2\sqrt{\tau}} \left(\eta - \frac{E}{E+1} \right) , \qquad (2.10b)$$

and erf(z) is the error function (equation 1.11b). This result should be valid for times τ that are short such that ξ is not appreciably different from 1 and 0 at the boundaries $\eta = 0, 1$ respectively, in which case the approximation that the imposition of the boundary conditions at a finite distance from the interface has not been felt as yet in the interior of the cell is a good one.

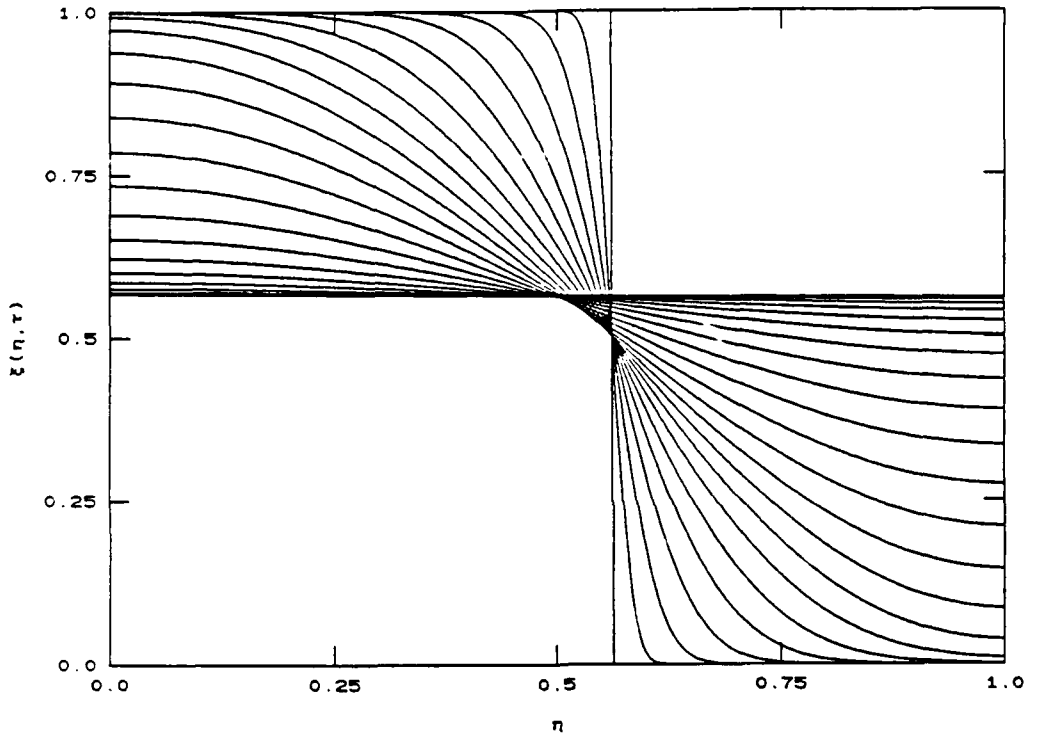

FIGURE 14. Numerical solution sequence $\xi(\eta,\tau)$ for unsteady diffusion of the conserved scalar in an adiabatic cell, corresponding to $\xi_E = E/(E+1)$ for $E = 1.3$. Curves computed for dimensionless times $\tau_{n+1} = \tau_n + n^2 \tau_0$, where $\tau_0 = 1.6 \times 10^{-4}$.

All this can, of course, be verified by the exact numerical solution to the problem. In particular, a numerical solution sequence, for a value of $E = 1.3$, is depicted in figure 14, for a sequence of values of the dimensionless time τ given by

$$\tau_{n+1} = \tau_n + n^2 \tau_0, \quad n = 1, 2, \ldots$$

where $\tau_0 = 1.6 \times 10^{-4}$. Note that, consistent with the area-preserving diffusion process, guaranteed in this case by the adiabatic boundary conditions, the composition field in the

cell tends, for long times, to the value $\xi_E = E/(E+1)$, corresponding to the conserved value of

$$\langle \xi(\eta,\tau) \rangle = \int_0^1 \xi(\eta,\tau)\, d\eta = \xi_E \tag{2.11}$$

(recall also equation 1.8 and the related discussion).

2.3 Diffusion of chemically reacting species

Consider now a fast chemical reaction, with negligible heat release, between the two interdiffusing species. By fast here we mean that the thickness of the overlap region required to sustain a reaction rate, per unit area of interface, that can consume the diffusive flux of reactant towards the interface, is small compared to the diffusion layer thickness. In this fast reaction regime, commonly referred to as a "diffusion-limited" chemical reaction regime, the rate of production is dictated by the diffusive flux per unit area towards the interface and not by the reaction kinetics. More importantly, however, as a result of the inter-diffusion process, wherever the conserved scalar ξ is different from 0 or 1, the amount of chemical product formed will be equal to that corresponding to the complete local consumption of the lean reactant in the mixed fluid.

As noted earlier, we can use temperature rise (heat release) as a means of labeling the formation of cheemical product. In that case, the fast chemistry assumption allows us to compute the amount of product (temperature rise) as a function of ξ, by assuming complete consumption of the lean reactant. Specifically, as was argued in the case of equation 1.9b,

$$\theta(\xi,\xi_\phi) = \frac{\Delta T(\xi,\phi)}{\Delta T_{flm}(\phi)} = \begin{cases} \dfrac{\xi}{\xi_\phi}, & \text{for } 0 \le \xi \le \xi_\phi \\ \dfrac{1-\xi}{1-\xi_\phi}, & \text{for } \xi_\phi \le \xi \le 1, \end{cases} \tag{2.12a}$$

where ξ_ϕ is given by equation 1.6, i.e. $\xi_\phi = \phi/(\phi+1)$, and where

$$\Delta T_{flm}(\phi) = \frac{2\phi}{\phi+1}\, \Delta T_{flm}(1) = 2\,\xi_\phi\, \Delta T_{flm}(1) \tag{2.12b}$$

is the adiabatic flame temperature rise corresponding to the stoichiometric mixture ratio ϕ. See figure 15 and discussion following equation 1.4.

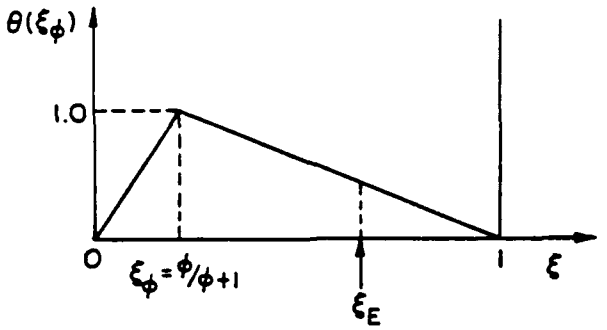

FIGURE 15. Normalized product function (temperature rise) as a function of the stoichiometric mixture fraction ξ, for a given free stream stoichiometric mixture fraction $\xi_\phi = \phi/(\phi+1)$.

Using equation 2.12 and the solution sequence depicted in figure 14 we can compute the amount of chemical product, or temperature (heat release) along η as a function of τ. Again, it is useful to consider the result for small "times" τ. In particular, we have for the total normalized temperature rise (chemical product) in the cell,

$$\theta(\xi_\phi,\tau) = \langle \theta[\xi(\eta,\tau),\xi_\phi] \rangle = \frac{1}{z_2 - z_1} \int_{z_1}^{z_2} \theta[\xi(z),\xi_\phi]\, dz \ , \qquad (2.13a)$$

where z_1 and z_2 are the values of the similarity coordinate (equation 2.10b) at the cell edges (at "time" τ), i.e.

$$z_1 = -\frac{1}{2\sqrt{\tau}}\left(\frac{E}{E+1}\right) , \quad z_2 = \frac{1}{2\sqrt{\tau}}\left(\frac{1}{E+1}\right) . \qquad (2.13b)$$

Note that

$$z_2 - z_1 = \frac{1}{2\sqrt{\tau}} \qquad (2.14)$$

(independently of E), and therefore, for small τ,

$$\theta(\xi_\phi,\tau) = \sqrt{\tau}\left\{\frac{1}{\xi_\phi}\int_{-\infty}^{z_\phi}[1-\mathrm{erf}(z)]\,dz + \frac{1}{1-\xi_\phi}\int_{z_\phi}^{\infty}[1+\mathrm{erf}(z)]\,dz\right\} \qquad (2.15a)$$

where z_ϕ is the value of the similarity coordinate z at which the stoichiometric composition is attained, i.e.

$$\mathrm{erf}(z_\phi) = 2\xi_\phi - 1 = \frac{\phi-1}{\phi+1} \ . \qquad (2.15b)$$

Note also that, consistently with the small τ (boundary layer) approximation, the limits of integration have been taken to infinity. The indefinite integrals in equation 2.15 can be computed in closed form and we have, after a little algebra,

$$\theta(\xi_\phi,\tau) \approx \sqrt{\tau}\, F(\xi_\phi) \ , \qquad (2.16)$$

where $F(\xi_\phi)$ is the Marble strained flame sheet function (Marble & Broadwell 1977) plotted in figure 8, obtained here by different arguments. We note that the (weak) divergence of $F(\xi_\phi)$, as $\xi_\phi \to 0$ and $\xi_\phi \to 1$, is traceable to the "boundary layer" approximation and the additional approximation of taking z_1 and z_2 in the integral limits of equation 2.13a to infinity and can be lifted by folding the numerical solution sequence in equation 2.13 instead of the approximate closed form solution of equation 2.10 .

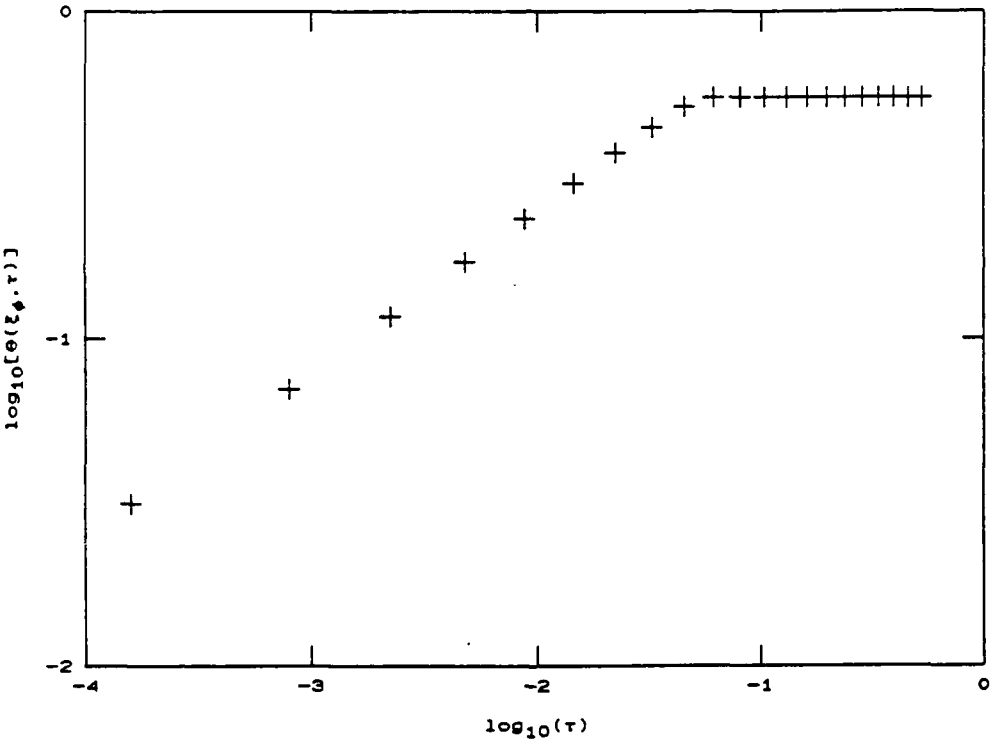

Figure 16(a)

Recall now that the $\sqrt{\tau}$ increase in the average temperature in the cell with "time", as indicated in equation 2.16, is expected to be valid for small τ only. For large τ, we know that the average temperature in the cell cannot exceed the temperature (total chemical product) resulting from the complete consumption of the lean reactant. Equivalently, if we <u>first</u> homogenize the reactants in the cell, to produce a composition

ξ_E, and <u>then</u> allow them to react, we will reach an average (total) temperature rise $\theta_H(\xi_\phi)$ that cannot be exceeded by the transient diffusion problem. In other words,

$$\theta(\xi_\phi,\tau) \rightarrow \theta_H(\xi_\phi) = \theta(\xi_E,\xi_\phi) \ , \quad \text{as } \tau \rightarrow \infty \ , \tag{2.17}$$

where $\theta(\xi,\xi_\phi)$ is given by equation 2.12. See also equation 1.9b and related discussion.

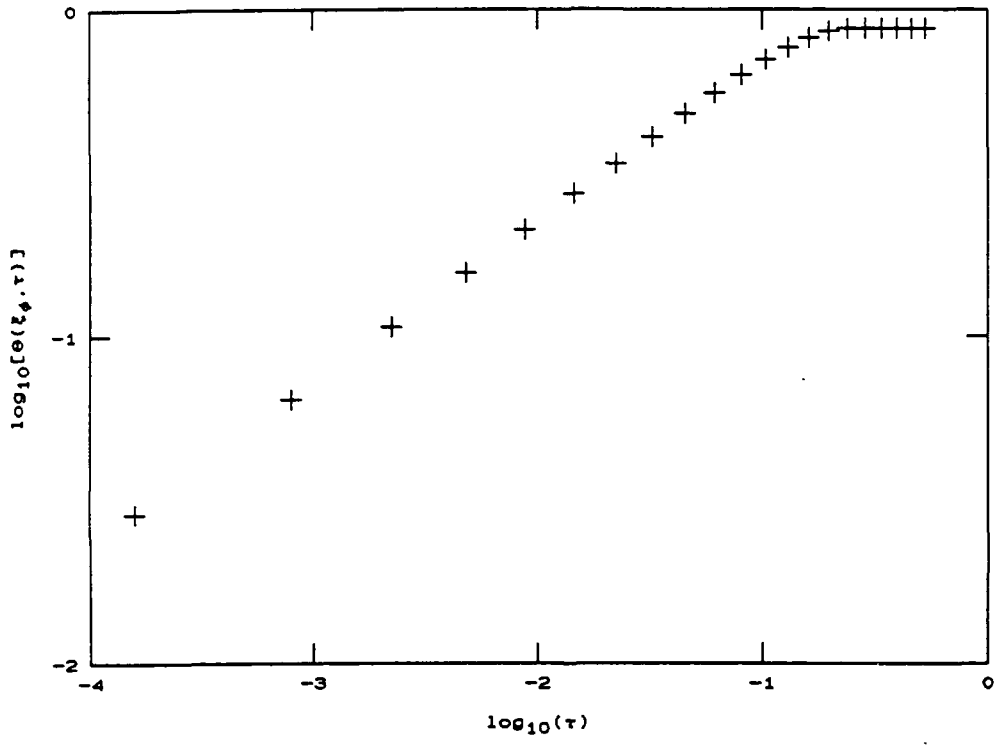

(b)

FIGURE 16. Normalized total chemical product (temperature rise) in λ-cell as a function of the (dimensionless) time τ, computed from exact numerical solution sequence in figure 14. (a) $\xi_\phi = 0.2$ ($\phi = 1/4$). (b) $\xi_\phi = 0.5$ ($\phi = 1$).

Sample exact numerical calculations of the solution to the original problem (without recourse to the "boundary layer" approximation) are plotted in figure 16 for E = 1.3 and for two values of ξ_ϕ, using the computed diffusion equation solutions depicted in figure 14. The results suggest that the "boundary layer" approximation can be used almost until the "time" τ the homogeneous composition temperature is attained, i.e.

$$\theta(\xi_\phi,\tau) = \begin{cases} \sqrt{\tau}\, F(\xi_\phi) , & \text{for } \tau < \tau_H \\ \theta_H(\xi_\phi) , & \text{for } \tau \geq \tau_H . \end{cases} \tag{2.18a}$$

τ_H, in this approximation, is the dimensionless "time" when the homogeneous mixture total temperature rise (completion of the reaction) is attained by the boundary layer solution. In particular, matching the two regimes at $\tau = \tau_H$, we have

$$\sqrt{\tau_H} = \frac{\theta_H(\xi_\phi)}{F(\xi_\phi)} . \tag{2.18b}$$

See figure 17.

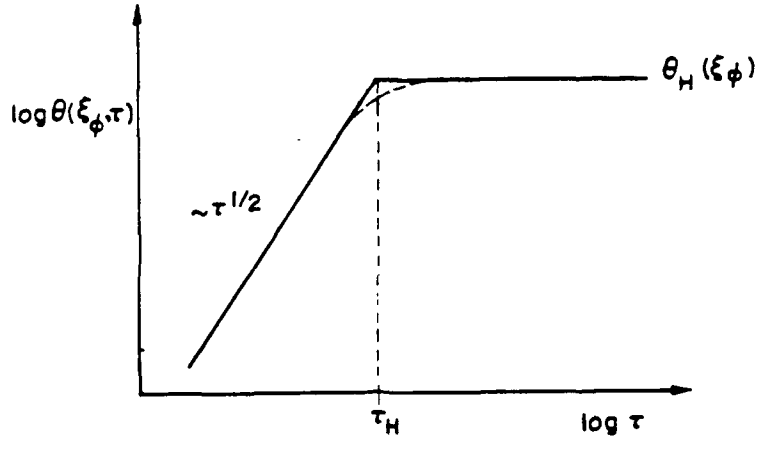

FIGURE 17. Proposed model scaled chemical product (temperature rise) function dependence on dimensionless time τ.

2.4 The scale diffusion "time" $\tau(\lambda)$

To proceed further, we need an estimate for $\sigma(\lambda)$, the strain rate associated with the scale λ. In particular, if $u(\lambda)$ is the expected velocity difference across a scale λ, we have the Kolmogorov (1941) relation for the self-similar inviscid inertial range,

$$u^2(\lambda) \sim \varepsilon^{2/3} \lambda^{2/3} , \tag{2.19}$$

where ε is the local dissipation rate. Consequently, for diffusion interfaces spaced by distances λ in the inertial range, the associated strain rate $\sigma(\lambda)$ imposed on these interfaces should be scaled by

$$\sigma(\lambda) \sim \frac{u(\lambda)}{\lambda} \sim \varepsilon^{1/3} \lambda^{-2/3} . \tag{2.20}$$

We note that the highest strain rates are associated with the smallest scales.

These power laws should hold for scales λ smaller than δ, where δ is identified here with the transverse extent of the vorticity-bearing region (δ_{vis} of Brown & Roshko 1974), but larger than the viscous dissipation (Kolmogorov 1941) scale λ_K, given by

$$\lambda_K = (\nu^3/\varepsilon)^{1/4} , \tag{2.21}$$

where ε is the kinetic energy dissipation rate (per unit mass) in the shear layer turbulent region. Accepting ε as an integral quantity averaged over the extent δ of the turbulent region, and scaling with the outer flow variables, we can write

$$\varepsilon = \alpha \frac{(\Delta U)^3}{\delta} , \tag{2.22}$$

where α is a dimensionless factor. This yields a relationship between λ_K and the outer variables given by

$$\frac{\lambda_K}{\delta} = \left(\alpha^{1/3} \mathrm{Re} \right)^{-3/4} = \alpha^{-1/4} \mathrm{Re}^{-3/4} . \tag{2.23}$$

where,

$$\mathrm{Re} = \frac{\Delta U \, \delta}{\nu} \tag{2.24}$$

is the local Reynolds number for the shear layer. We note here that the dependence of λ_K / δ on the scaled dissipation rate α is weak.

In the opposite limit of small scales, corresponding to the viscous flow $\lambda \leq \lambda_K$ regime, the associated velocity gradients are imposed onto the small scales λ by the aggregate effect of the larger scales in the flow. In this case,

$$u(\lambda) \sim \lambda , \quad \text{for } \lambda \leq \lambda_K ,$$

and therefore,

$$\sigma(\lambda) = \text{constant} = \sigma_c , \quad \text{for } \lambda \leq \lambda_K ,$$

where σ_c is the expected contraction strain rate in the viscous regime. Consequently, we see that, in the inertial range, the strain rate increases as λ decreases, in accord with equation 2.20 , until a maximum value is reached, corresponding to a scale λ_c . Below this scale, the associated expected strain rate can be taken to be a constant.

The assumption of a scale-independent expected strain in the viscous range was first proposed by Townsend (1951), who suggested (to quote Batchelor 1959), that "the action of the whole flow field on small-scale variations of any quantity ... is primarily to impose a uniform persistent straining motion". This idea was used by Batchelor (1959) to derive the k^{-1} conserved temperature fluctuation spectrum in a high Prandlt number ($Pr = \nu/\kappa$) fluid.

Gibson (1968) has argued that the estimate for σ_c can be bracketed by the inequality

$$\sqrt{3} < \frac{1}{\sigma_c t_K} \leq 2\sqrt{3} , \tag{2.25a}$$

where $t_K = \sqrt{\nu/\varepsilon}$ is the Kolmogorov dissipation time scale, but notes that if fluctuations in the local dissipation rate ε are taken into account these bounds must be increased (see also Novikov 1961 and discussion in Monin & Yaglom II 1975, end of section 22.3). Defining

$$\beta = \frac{1}{\sigma_c t_K} \tag{2.25b}$$

and in view of the bounds in the inequality 2.25a we shall accept an estimate for β of 3 . Gibson's caveat, with respect to the effect of fluctuations in ε , will be dealt with below, as the effect of fluctuations in the local dissipation rate ε will be considered explicitly.

Matching to the $\lambda^{-2/3}$ behavior of $\sigma(\lambda)$ in the inertial range (equation 2.20), we now have for the expected value of $\sigma(\lambda)$, over the complete range of scales,

$$\sigma(\lambda) = \begin{cases} \sigma_c \left(\frac{\lambda_c}{\lambda}\right)^{2/3}, & \text{for } \lambda > \lambda_c \\ \sigma_c, & \text{for } \lambda < \lambda_c, \end{cases} \tag{2.26a}$$

where λ_c is a cut-off scale where the two regimes match. In other words,

$$\lambda_c = \beta^{3/2} \lambda_K \quad \rightarrow \quad \lambda_c = 5.2\, \lambda_K, \quad \text{for } \beta = 3. \tag{2.26b}$$

This yields for the maximum expected contraction strain rate,

$$\sigma_c = \frac{\nu}{\beta \lambda_K^2} = \frac{\beta^2 \nu}{\lambda_c^2} = \frac{9\nu}{\lambda_c^2}, \tag{2.26c}$$

and where the numerical estimate is again for $\beta = 3$. A sketch of $\sigma(\lambda)$, versus λ, is depicted in figure 18.

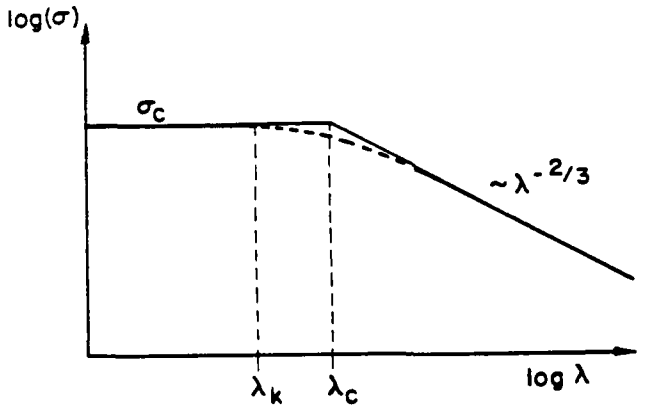

FIGURE 18. Proposed model contraction strain rate dependence on scale λ.

Using these relations for the strain rate $\sigma(\lambda)$ associated with the scale λ, we can now, in turn, associate the "time" $\tau(\lambda)$ to the scale λ, as required by the proposed approximate solution to the transient diffusion problem. In particular, combining equations 2.8 for $\tau(\lambda)$ and 2.23 for $\sigma(\lambda)$, we have

$$\tau(\lambda) = \begin{cases} \dfrac{1}{\beta^2\, Sc} \left(\dfrac{\lambda}{\lambda_c}\right)^{-4/3}, & \text{for } \lambda > \lambda_c \\ \dfrac{1}{\beta^2\, Sc} \left(\dfrac{\lambda}{\lambda_c}\right)^{-2}, & \text{for } \lambda < \lambda_c \,, \end{cases} \tag{2.27}$$

where $Sc = \nu/D$ is the Schmidt number. See figure 19.

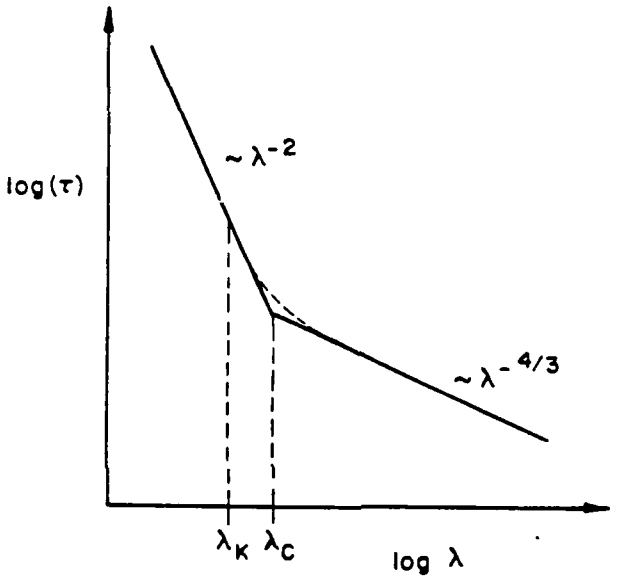

FIGURE 19. Proposed dimensionless "time" τ dependence on scale λ.

The implicit picture here is one in which the energy dissipation is more or less uniform in intermediate sized regions in the flow, of extent smaller that the outer scale δ of the flow but larger than the molecular diffusion scales. In the spirit of the earlier similarity hypotheses of Kolmogorov and Oboukhov, we would expect that the dynamics within these regions would be described in terms of their now local dissipation rate ε, which must be allowed to vary from one region to another, however, as formulated, for example, in the revised similarity hypotheses put forth by Kolmogorov (1962) and Oboukhov (1962). In the context of the model, the progress of the unsteady diffusion process is computed separately for each of these regions, conditional on their local value of the dissipation rate ε, and the total mixing is subsequently estimated as an ensemble average over regions whose dissipation rate can be treated as a random variable.

2.5 The reaction completion scale

The idealizations permitting the association of the unsteady diffusion "time" τ with a definite scale λ, through equation 2.27, and the "time" τ_H at which the homogeneous mixture temperature $\Theta_H(\xi_\phi)$ is attained (equation 2.18b), allow us to define, in turn, a reaction completion scale λ_H, at which the lean reactant in the cell has been consumed and the homogeneous temperature has been reached. Substituting in these equations, we find that the ratio λ_H/λ_C is determined, in turn, by the function

$$G(\xi_\phi) = \frac{F(\xi_\phi)}{\beta \sqrt{Sc}\, \Theta_H(\xi_\phi)} , \tag{2.28}$$

where $F(\xi_\phi)$ is the flame sheet function of equation 2.16b. In particular, we have

$$\frac{\lambda_H}{\lambda_C} = \begin{cases} [G(\xi_\phi)]^{3/2} , & \text{for } G(\xi_\phi) > 1 \\ \\ G(\xi_\phi) , & \text{for } G(\xi_\phi) < 1 . \end{cases} \tag{2.29}$$

We note here that the controlling function $G(\xi_\phi)$ can be made large or small, other things held constant, by manipulating the value of the Schmidt number. Accordingly, corresponding to the two cases of equation 2.29 dictated by the magnitude of $G(\xi_\phi)$, we will recognize two reacting flow regimes:

1. gas-like, for which the reaction is completed before λ_C is reached, i.e. $\lambda_H > \lambda_C$ [$G(\xi_\phi) > 1$, low Sc fluid],

and

2. liquid-like, for which the reaction is completed at scales smaller than λ_C, i.e. $\lambda_H < \lambda_C$ [$G(\xi_\phi) < 1$, large Sc fluid].

Combining these results with the expressions for the chemical product associated with a particular diffusion "time" $\tau(\lambda)$, see equations 2.18 and 2.27, we obtain for these two diffusion-reaction regimes,

Gas-like : $x_H = \lambda_H/\lambda_c = G^{3/2}(\xi_\phi) > 1$

$$\frac{\theta(x)}{\theta_H} = \begin{cases} 1 , & x < 1 < x_H \\ 1 , & 1 < x < x_H \\ \dfrac{G}{x^{2/3}} , & 1 < x_H < x , \end{cases} \tag{2.30a}$$

and

Liquid-like : $x_H = \lambda_H/\lambda_c = G(\xi_\phi) < 1$

$$\frac{\theta(x)}{\theta_H} = \begin{cases} 1 , & x < x_H < 1 \\ \dfrac{G}{x} , & x_H < x < 1 \\ \dfrac{G}{x^{2/3}} , & x_H < 1 < x , \end{cases} \tag{2.30b}$$

where

$$x = \frac{\lambda}{\lambda_c} \tag{2.30c}$$

is the dimensionless interface scale λ, normalized by the strain rate cross-over scale λ_c.

2.6 The statistical weight of interface scales. Normalization.

The preceding approximations yield an estimate for the contribution to the total chemical product in the shear layer associated with each scale λ of the reactant interface, per unit surface area associated with λ. To compute the total product per unit volume of shear layer fluid, however, we need to estimate the statistical weight $W(\lambda)$ for the scale λ, in the range $d\lambda$, as the expected surface per unit volume of interface associated with the scale λ. Evidently, the resulting statistical weight (associated expected total surface-to-volume ratio) over the range of scales λ must be normalizable to the unit volume, i.e.

$$\int_0^\delta W(\lambda)\, d\lambda = 1 . \tag{2.31}$$

Recall that, for every differential surface element dS of the $\xi(\underline{x},t) = \xi_E$ interface, the associated scale λ was defined as the arc length along $\nabla\xi$ between the two points on either

2.9 The effect of entrainment ratio fluctuations

side of the interface where $\nabla\xi$ has decreased to zero, or, operationally, to some nominally small fraction γ (say, $\gamma \approx 10^{-3}$) of its value at $\xi = \xi_E$. This operation is to be imagined as performed for every element dS on the interface, with $W(\lambda)$ the resulting probability density function of λ.

It will be convenient to first consider the interface that would be formed between the two entrained fluids in the absence of any scalar diffusion, i.e. in the limit of $Sc \to \infty$, or surface tension. It will also be convenient for the discussion below to factor $W(\lambda)$ into the surface to volume ratio of a scale λ and the probability $p(\lambda)$ of finding that scale λ in our Eulerian slice. This yields the relation

$$W(\lambda)\, d\lambda \sim \frac{1}{\lambda}\, p(\lambda)\, d\lambda = \tilde{p}[\ln(\lambda)]\, d\ln(\lambda), \tag{2.32}$$

within a normalization constant.

If we may regard the self-similar inertial range ($\lambda_c \ll \lambda \ll \delta$) as not possessing an intrinsic characteristic scale, we must accept that the (dimensionless) product $W(\lambda)\, d\lambda$ can only depend on the scale λ itself. Accordingly, again within a normalization constant, we must have

$$W(\lambda)\, d\lambda \sim \frac{d\lambda}{\lambda}, \tag{2.33}$$

as the only dimensionless, scale-invariant group that can be formed between $d\lambda$ and λ. It can be seen that, in this range of scales, $\tilde{p}[\ln(\lambda)]$, and therefore also $p(\lambda)$, must be uniform (independent of λ), as perhaps one might have argued a priori.

It is reasonable to assume that interface scales below the strain rate cross-over scale λ_c are primarily generated within regions of extent λ_c or smaller. We can imagine a Taylor expansion of the velocity field about the center of one such sub-λ_c region and a (non-inertial) frame of reference that convects with the velocity field at the point of expansion, rotating about the local vorticity axis at a rate that cancels the local value of the (nearly uniform) vorticity in that region. It has been a common assumption to regard the direction of the principal strain rate axes as also fixed in that frame (Townsend 1951, Batchelor 1959, Novikov 1961), at least for a time interval of the order of $t_K = (\nu/\varepsilon)^{1/2}$. We shall accept this same approximation here, and also assume that within each of these sub-λ_c regions the local normal to the scalar interface has already been aligned with the principal contraction axis. As mentioned earlier, this latter was also assumed by Batchelor (1959) and recently corroborated for shear flows by the analysis of Ashurst et al (1987). We should note, however, that the time that the axes need to stay fixed in the rotating frame is scaled by the time t_{DK} to diffuse across λ_K, which at

high Schmidt numbers can be longer than t_K[†].

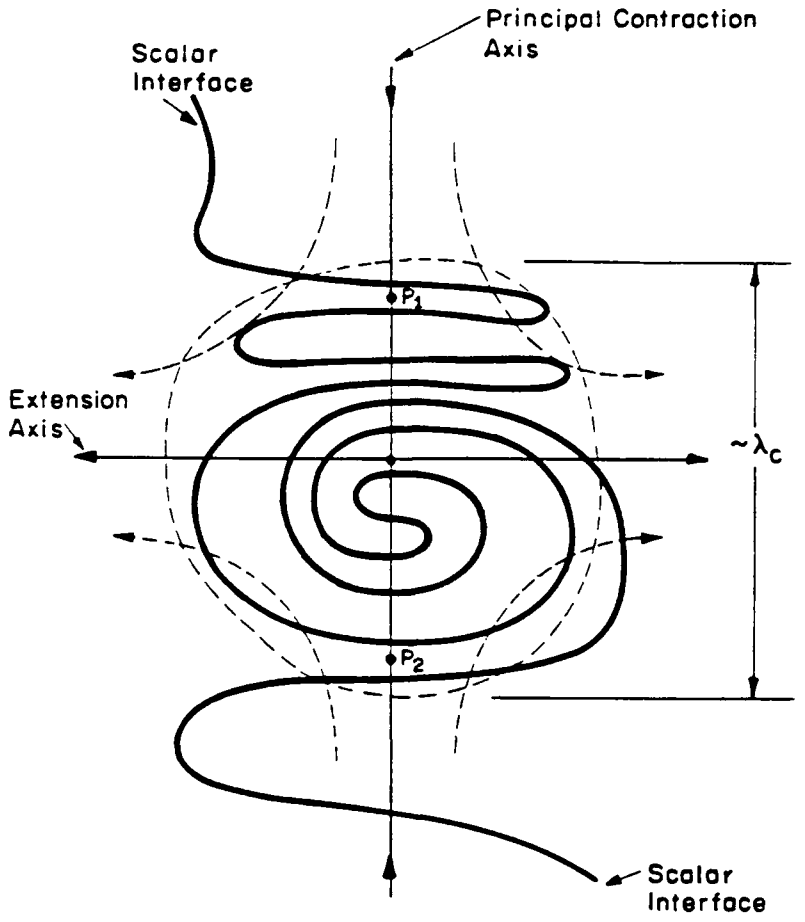

FIGURE 20. Schematic of scalar interface in the interior of a fluid element of extent λ_c.

Imagine now any two points P_1 and P_2 that remain on the principal contraction axis in this frame and, in view of our assumptions, can be regarded as moving with the fluid. It can be seen that the number of intersections of the interface and the principal

[†] Considering the diffusion geometry in figure 13 for $\lambda \approx \lambda_K$ and $Sc > 1$, this time can be estimated to be of the order of $t_{DK} \approx t_K \ln(\sqrt{Sc})$. Batchelor (1959) was aware of this time scaling, but the issue is ignored in the implicit assumption made about the contraction axis alignment during the diffusion process. We should also note, however, that if the diffusion geometry is one of sheets rolled up around vortex filaments, as assumed by Lundgren (1982,1985), then the vorticity axis is normal to the maximum contraction axis and the scalar gradient, and the assumption (and the k^{-1} spectrum) remains valid. In that case, however, the scalar gradient would be at 45° to the maximum contraction axis (corroborated for the Kerr 1985 isotropic flow data analysis by Ashurst et al 1987) and not aligned with it, as appears to be the case in the Rogers et al (1986) shear flow data (Ashurst et al 1987) and as assumed here.

contraction axis between the points P_1 and P_2 will be constant, as the interface geometry is strained continuously reducing the normal spacings λ of the intersections of the interface with the principal contraction axis. This conclusion is the same regardless of whether the interface crosses the principal contraction axis with a zig-zag sheet topology, or as a rolled-up sheet, or a combination of these two possibilities. See figure 20. Moreover, the subsequent reduction of the normal spacings λ of these crossings along the contraction axis will proceed in accord with equation 2.7, which we may accept as exact for this flow regime and which we shall rewrite as

$$\frac{d}{dt} \ln(\lambda) = -\sigma_c \ . \tag{2.34}$$

Imagine now that we are tracking a group of crossing spacings on the $\ln(\lambda)$ axis as they evolve, transformed in time by the strain field within the sub-λ_c region, initially between the limits, say, $\lambda_1 < \lambda < \lambda_2 < \lambda_c$, and described by a probability density function $\tilde{p}[\ln(\lambda) - \ln(\lambda_1)] = \tilde{p}[\ln(\lambda/\lambda_1)]$. Since they all "move" in Lagrangian time as a packet with a common (and constant) group velocity along the $\ln(\lambda)$ axis, we would find that their probability density function $\tilde{p}[\ln(\lambda/\lambda_1)]$ will be preserved, even as the spacings $\lambda(t)$ and $\lambda_1(t)$ themselves decrease (exponentially) with time, as dictated by equation 2.34. See figure 21.

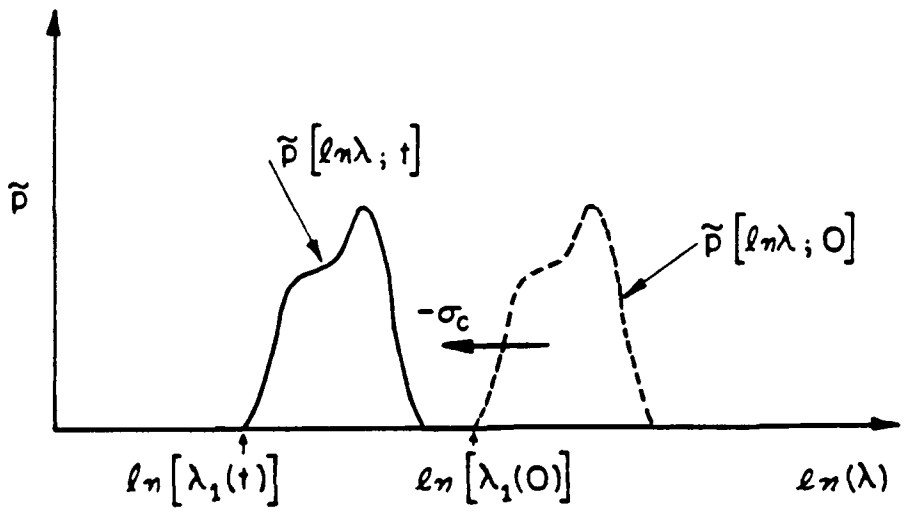

FIGURE 21. Scale packet evolution in the direction of the $-\ln(\lambda)$ axis under the action of a uniform and constant contraction strain rate σ_c.

We conclude that, in this sense, the straining field in the sub-λ_c regions does not alter the probability density function $\tilde{p}[\ln(\lambda)]$ of the larger scales that cascade to these regions from the inertial range.

These arguments suggest that $\tilde{p}[\ln(\lambda)]$, and therefore also $p(\lambda)$, must be constant not only within the inertial range but also in the viscous range and therefore throughout the spectrum of the interface scales. Consequently, for a self-similar surface, equation 2.33 may be accepted as a uniformly valid description of the expected surface to volume ratio of the interface as a function of λ, in the limit of $Sc \to \infty$.

To investigate the effect of a finite Schmidt number on the associated expected surface to volume ratio of a scale λ, we first consider the following model problem. Imagine that we are sliding the center of a ball of diameter d_b on the $Sc \to \infty$ interface and we wish to estimate the volume swept by this ball, per unit volume of flow, as its center scans the whole surface. It can be seen that for portions of the curve for which the local scale λ is large compared with the ball radius, the volume swept will be well approximated by the product of the ball diameter and the associated interface surface to volume ratio. Consequently, the volume swept by the ball as the interface scale decreases, per unit volume of fluid, will continue to increase in accord with equation 2.33, until we reach the scale $\lambda \sim d_b$, below which the contributions per unit interface surface area can be no larger that those at the scale $\lambda \sim d_b$. This picture suggests an estimate for the statistical weight of a scale λ, at finite values of the Schmidt number, given by

$$W(\lambda)\,d\lambda = \frac{1}{N(Sc,Re)} \begin{cases} \dfrac{d\lambda}{\lambda_D}, & \text{for } \lambda < \lambda_D \\ \dfrac{d\lambda}{\lambda}, & \text{for } \lambda > \lambda_D, \end{cases} \tag{2.35}$$

where λ_D is an appropriate diffusion scale and $N(Sc,Re)$ is the normalization function, as required by equation 2.31. In particular, integrating over the range of scales, we have

$$N = \left\{ \int_0^{\lambda_D} + \int_{\lambda_D}^{\delta} \right\} W(\lambda)\,d\lambda ,$$

or

$$N = 1 + \ln\left(\frac{\delta}{\lambda_D}\right) = 1 + \ln\left(\frac{\lambda_c}{\lambda_D}\right) + \ln\left(\frac{\delta}{\lambda_c}\right) . \tag{2.36}$$

To proceed further, we need an estimate for λ_D/λ_c, the ratio of the appropriate diffusion scale to the strain rate cut-off scale λ_c.

For high Schmidt number fluids (Sc > 1), we will base our estimate on the Batchelor (1959) scale. In particular,

$$\lambda_D = C_B \left(\frac{\beta}{Sc} \right)^{1/2} \lambda_K ,$$

where λ_K is the Kolmogorov scale, $\beta = 3$ (recall equation 2.25 and related discussion), and C_B is a dimensionless constant of order unity. To assign a numerical value to C_B, we use the Batchelor (1959) estimates for the scalar space correlation function

$$D_{\xi\xi}(r) = \langle \xi(\underline{x}) \, \xi(\underline{x}+\underline{r}) \rangle_{\underline{x}} ,$$

which he expresses in terms of a double integral over $r' < r$. He finds that for distances r small compared with the diffusion scale, $D_{\xi\xi}(r) \sim \zeta/6$ asymptotically, whereas for distances large compared to the diffusion scale, but small compared with the Kolmogorov scale, $D_{\xi\xi}(r) \sim \ln(\zeta)$, where

$$\zeta = \frac{\beta}{Sc} \left(\frac{r}{\lambda_K} \right)^2 .$$

Monin & Yaglom II (1975, section 22.4) express these results in terms of a differential equation for $D_{\xi\xi}(r)$, given by

$$4 \zeta h''(\zeta) + (6 + \zeta) h'(\zeta) = 1 , \quad h(0) = 0 ,$$

where $h = h(\zeta)$ is the scaled (dimensionless) $D_{\xi\xi}(r)$, and which can be estimated by numerical integration of the differential equation. The resulting solution transitions from the linear behavior to the logarithmic behavior rather smoothly over the interval $1 \leq \zeta \leq 4$. Accepting the mid-point $\zeta_c = 2.5$ of this interval as the cross over between the linear (diffusive) behavior and the logarithmic (convective) behavior, we obtain the estimate $C_B = \sqrt{\zeta_c} = 1.6$. Finally, expressing the diffusion scale λ_D in terms of the strain rate cross-over scale λ_c, as required by the normalization function, we have

$$\frac{\lambda_D}{\lambda_c} \sim \frac{C_B}{\beta \, Sc^{1/2}} , \quad \text{for} \quad Sc > 1 .$$

For $Sc < 1$, Batchelor, Howells & Townsend (1959) find that $\lambda_D / \lambda_K \sim Sc^{-3/4}$. As we are not interested in Schmidt numbers that are much smaller than unity, and requiring continuity at $Sc = 1$, we will accept the estimate

$$x_D = \frac{\lambda_D}{\lambda_c} = \begin{cases} \dfrac{C_B}{\beta\, Sc^{1/2}}, & \text{for } Sc > 1, \\ \dfrac{C_B}{\beta\, Sc^{3/4}}, & \text{for } Sc < 1, \end{cases} \tag{2.37}$$

with $C_B = 1.6$. Substituting for δ and λ_D in equation 2.36, we then obtain the expression for the normalization function,

$$N(Sc,Re) = 1 + \ln\left(\frac{\beta\, Sc^q}{C_B}\right) + \frac{3}{4}\ln\left(\frac{\alpha^{1/3}\, Re}{\beta^2}\right), \tag{2.38}$$

where $q = 1/2$ for $Sc > 1$, $3/4$ for $Sc \leq 1$, $C_B = 1.6$, $\beta = 3$ and α is the dimensionless ratio of the dissipation rate ϵ and $(\Delta U)^3/\delta$ (recall equation 2.22 and related discussion).

These considerations suggest that the problem is characterized by <u>four</u> length scales, namely:

$\delta = (\alpha^{1/3}\, Re / \beta^2)^{3/4}\, \lambda_c$: large scale of the flow,

λ_H : reaction completion scale (equation 2.29)

λ_c : strain cross-over scale,

and,

λ_D : the species diffusion scale (equation 2.37)

All four scales have been referenced to λ_c, the strain cross-over scale, related, in turn, to the Kolmogorov scale through the constant β (see equation 2.26b). These scales define the arena in which the species diffusion and chemical reaction proceeds, bounded by δ as the large scale limit, on the one hand, and λ_D as the smallest scale at which it makes sense to attempt to track the species diffusion and chemical reaction interface.

The preceding arguments also lend credence to the conjecture that the preponderant fraction of molecularly mixed fluid, and hence chemical product, resides on interfaces associated with the smallest scales. This is owing to the fact that not only is the statistical weight of the smaller scales larger (equation 2.35) but also that the chemical product (molecularly mixed fluid) per unit surface area increases monotonically as the scale λ decreases (equation 2.30). The combination of these two effects renders the overall description of the mixed fluid and chemical product fortuitously forgiving to the treatment of the large scales in the flow.

2.7 The effect of dissipation rate fluctuations

The results thus far have been obtained conditional on a fixed value of the dissipation rate ε (corresponding to the particular station x). In particular, scaling with the outer variables of the flow we wrote for the dissipation rate per unit mass (equation 2.33),

$$\varepsilon = \alpha \frac{(\Delta U)^3}{\delta} ,$$

where α is a dimensionless factor. As Landau noted soon after Kolmogorov and Oboukhov formulated their initial similarity hypotheses, however, the local dissipation rate ε (and therefore α) cannot be treated as a constant in the turbulent region, but must be regarded as a strongly intermittent field. This objection was addressed in the revised similarity hypotheses of Kolmogorov (1962), Oboukhov (1962`, and Gurvich & Yaglom (1967), which will be adopted here as yielding an adequate description for the purposes of assessing the effects of the dissipation rate fluctuations.

We can cast the revised similarity hypothesis in our notation by normalizing the fluctuating dimensionless factor α with its mean value $\overline{\alpha}$, i.e. $\alpha' = \alpha / \overline{\alpha}$, such that $\overline{\alpha'} = 1$. This yields a log-normal distribution for the values of the (scaled) dissipation rate α', averaged over a region of extent r_ε. In particular,

$$p(\alpha')\, d\alpha' = \frac{1}{\sqrt{2\pi}\, \Sigma\, \alpha'} \exp\left\{ -\frac{1}{2} \left(\frac{\ln(\alpha')}{\Sigma} + \frac{\Sigma}{2} \right)^2 \right\} d\alpha' , \qquad (2.39a)$$

where $\Sigma^2 = \Sigma^2(r_\varepsilon)$, is the variance of the distribution, in this model given by

$$\Sigma^2(r_\varepsilon) = A + \mu \ln\left(\frac{\delta}{r_\varepsilon} \right) . \qquad (2.39b)$$

The term A in this expression may depend on the large scales of the flow and μ is taken as a constant.

Monin & Yaglom II (1975, section 25) reviewed this hypothesis, and found that it represents a good approximation to measurements of the local dissipation rate. Additionally, they concluded on the basis of comparisons with data that the constant μ should be taken in the range of $0.2 \leq \mu \leq 0.5$. More recently, Van Atta & Antonia (1980) considered the consequences of this proposal on the dependence of velocity derivative moments on Reynolds number and concluded, if r_ε is taken all the way to the Kolmogorov scale λ_K, that μ should be taken as $\mu \sim 0.25$. Ashurst et al (1987) have also estimated the value of μ on the basis of direct turbulence simulation computation data (Kerr 1985, Rogers et al 1986) and concluded that $\mu = 0.3$. Considering all the evidence, this latter value will be accepted as representative and as our estimate for μ.

Estimates for $\bar{\alpha}$, corresponding to the mean value of the dissipation $\bar{\epsilon}$, are difficult to obtain for turbulent shear layers. There is enough information, however, in the data of Wygnaski & Fiedler (1970) to permit an estimate of $\bar{\alpha} \geq 0.02$. An estimate can be made from the data of Spencer & Jones (1971), which also leads to the same value. It is difficult to assess the probable error of these estimates, not to speak of the possibility intimated by Saffman (1968) that $\bar{\alpha}$ may not necessarily be a constant, i.e. independent of the Reynolds number. Nevertheless, considering the nature of the experimental difficulties, the assumptions made about isotropy, and in view of the realizable spatial and temporal resolution relative to λ_K and λ_K / U_c, respectively, where U_c is the local flow convection velocity, we can say that this estimate is probably low, even though perhaps not by more than a factor of 2 to 3. Consequently, one would argue for a plausible range of values for $\bar{\alpha}$ of

$$0.02 \leq \bar{\alpha} \leq 0.06 . \tag{2.40}$$

In applying these results to the present discussion, we will take r_ϵ down to a (fixed) viscous scale λ_0 that is a function of the (local) Reynolds number and equal to the strain rate field cut-off scale λ_c corresponding to the mean value of the dissipation, i.e. (see equation 2.31)

$$\frac{\delta}{\lambda_0} = \left(\frac{\bar{\alpha}^{1/3} Re}{\beta^2} \right)^{3/4} . \tag{2.41}$$

This yields an expression for the variance of α given by

$$\Sigma_\alpha^2(Re) = A + \frac{3\mu}{4} \ln \left(\frac{\bar{\alpha}^{1/3} Re}{\beta^2} \right) . \tag{2.42}$$

Finally, an estimate can be made for the constant A with the aid of the following argument. As the local Reynolds number is increased from very small values, the flow is initially essentially steady with no fluctuations in the dissipation rate field. At some minimum value of the Reynolds number, however, the flow will evolve into a fluctuating field with a spatial scale of the order of δ and an associated variance in the local dissipation rate fluctuations. At that critical value of the Reynolds number we must have $\Sigma_\alpha^2(Re_{cr}) = 0$. This fixes the flow-specific constant A, and also removes the unpleasant dependence of the variance on the particular choice of the reference scale λ_0, and we have

$$\Sigma_\alpha^2(Re) = \frac{3\mu}{4} \ln \left(\frac{Re}{Re_{cr}} \right) . \tag{2.43}$$

While we recognize that, strictly speaking, a free shear layer does not possess a critical Reynolds number, one can conclude from the linear stability analysis for viscous (but parallel) flow of a hyperbolic tangent profile (Betchov & Szzewczyk 1963) that an unstable mode with a spatial extent of order δ requires a *minimum* Reynolds number of the order of $15 \lesssim Re \lesssim 50$, which we will accept as bounds for Re_{cr}. Note that Re here is based on δ, the total width of the sheared region, and not on the (smaller) hyperbolic tangent maximum slope thickness. See also discussion by Betchov (1977). It is interesting that this estimate for a critical Reynolds number is not too different from the one made by Saffman (1968), who explored the idea that the structure of the flow in the dissipation range was essentially that resulting from the Taylor-Görtler instability of curved vortex sheets.

To compute the probability density function of the ratio λ_c/λ_0, we note that since

$$\lambda_c = \lambda_0 (\alpha')^{-1/4} , \tag{2.44a}$$

we must have

$$p(y)\,dy = \frac{1}{\sqrt{2\pi}} \exp\left\{ -\frac{1}{2}\left(y - \Sigma_a/2\right)^2 \right\} dy , \tag{2.44b}$$

where

$$y = \frac{4}{\Sigma_a} \ln\left(\frac{\lambda_c}{\lambda_0}\right) . \tag{2.44c}$$

This is correct to within a (near unity) normalization constant, as we wish to restrict λ_c to the range $0 \le \lambda_c \le \delta$.

To compute the effect of the dissipation fluctuations on the expected value of the scales normalization function N(Sc,Re) discussed in the preceding section, we also note that if we assume that the <u>ratio</u> λ_c / λ_D is independent of the dissipation rate ε (a function of Sc only), we have

$$\langle N(Sc,Re) \rangle_\varepsilon = 1 + \ln\left(\frac{\lambda_c}{\lambda_D}\right) + \ln\left(\frac{\delta}{\lambda_0}\right) - \left\langle \ln\left(\frac{\lambda_c}{\lambda_0}\right) \right\rangle_\varepsilon .$$

Then since

$$\left\langle \ln\left(\frac{\lambda_c}{\lambda_0}\right) \right\rangle_\varepsilon = \frac{\Sigma_a}{4} \langle y \rangle ,$$

where

$$\langle f(y) \rangle = \frac{\int_{-\infty}^{y_\delta} f(y)\, p(y)\, dy}{\int_{-\infty}^{y_\delta} p(y)\, dy} \quad ; \qquad y_\delta = \frac{4}{\Sigma_a} \ln\left(\frac{\delta}{\lambda_0}\right) , \tag{2.46}$$

and since, in particular (at high Reynolds numbers)

$$\langle y \rangle = \frac{\Sigma_\alpha}{2} - \frac{\exp\{-\frac{1}{2}(y_\delta - \Sigma_\alpha/2)^2\}}{\sqrt{2\pi}\,[1 - \frac{1}{2}\mathrm{erfc}(\frac{y_\delta - \Sigma_\alpha/2}{\sqrt{2}})]} \approx \frac{\Sigma_\alpha}{2} , \tag{2.47}$$

we have (see equations 2.38 and 2.43)

$$\langle N(Sc,Re) \rangle_\varepsilon = 1 + \ln(\frac{\beta\, Sc^q}{C_B}) + \frac{3}{4}[\ln(\frac{\bar{\alpha}^{1/3} Re}{\beta^2}) - \frac{\mu}{8}\ln(\frac{Re}{Re_{cr}})] . \tag{2.48}$$

It is useful to rewrite this expression by defining a constant Γ through the relation

$$\Gamma = \frac{\bar{\alpha}^{1/3}}{\beta^2} Re_{cr} , \tag{2.49a}$$

and where we note, at least on the basis of our numerical estimates for these quantities, that $\Gamma \sim 1$. In terms of Γ, we then have

$$\langle N(Sc,Re) \rangle_\varepsilon = 1 + \ln(\frac{\beta\, Sc^q}{C_B}) + \frac{3}{4}[(1 - \frac{\mu}{8})\ln(\frac{Re}{Re_{cr}}) + \ln(\Gamma)] . \tag{2.49b}$$

Returning to the derivation of the quantity in the brackets and recognizing the role it plays in the normalization of the range of turbulent scales, however, we can argue that it should vanish as $Re \to Re_{cr}$ and that, therefore, we must have $\Gamma = 1$. This provides us with a consistency estimate and plausible bounds for Re_{cr} (see equation 2.49a and inequality 2.40) given by

$$23 \leq Re_{cr} = \frac{\beta^2}{\bar{\alpha}^{1/3}} \leq 33 \tag{2.49c}$$

(recall $\beta^2 \sim 9$). This we can use to rewrite the expression for the ratio δ/λ_0 (equation 2.41), i.e.

$$\frac{\delta}{\lambda_0} = (\frac{Re}{Re_{cr}})^{3/4} . \tag{2.49d}$$

Finally, for high Reynolds numbers, we may certainly ignore the $\ln(\Gamma)$ term in favor of $\ln(Re / Re_{cr})$ and we have,

$$\langle N(Sc,Re) \rangle_\varepsilon = 1 + \ln(\frac{\beta\, Sc^q}{C_B}) + \frac{3}{4}(1 - \frac{\mu}{8})\ln(\frac{Re}{Re_{cr}}) , \tag{2.50}$$

where $\beta \sim 3$, $q = 1/2$ for $Sc > 1$, and $3/4$ for $Sc \leq 1$, $C_B \sim 1.6$, $\mu \sim 0.3$ and Re_{cr} is

bounded by the limits in equation 2.49c. It may be worth noting that the resulting estimate for the normalization function is quite robust, as the various uncertainties in the constants appear as arguments of logarithms.

We conclude that the effects of the dissipation fluctuations on the expected value of tne normalization function are small, being confined to the contribution to the final result owing to a non-zero value for μ.

2.8 The total product in the mixing layer

Tne total chemical product can now be computed as the weighted average of the contribution of each scale, i.e.

$$\Theta_T = \int_0^{\delta} \theta(\lambda/\lambda_c)\, W(\lambda)\, d\lambda = \int_0^{x_\delta} \theta(x)\, w(x)\, dx \,, \tag{2.51}$$

where $x = \lambda/\lambda_c$, $x_\delta = \delta/\lambda_c$, $\theta(x)$ is given by equations 2.30, and

$$w(x)\, dx = \frac{1}{\langle N \rangle_\varepsilon} \begin{cases} \dfrac{dx}{x_D} \,, & \text{for } x < x_D \\ \dfrac{dx}{x} \,, & \text{for } x_D < x \end{cases} \tag{2.52}$$

(see equation 2.36), with $x_D = \lambda_D/\lambda_c$ (see equation 2.37). We will first perform the computations conditional on a fixed value of the dissipation rate, and therefore λ_c, and then compute the total as the expectation value over the distribution of values of λ_c.

For gas-like flow-diffusion regimes (see equation 2.30 and related discussion), we have the relation

$$x_H = \frac{\lambda_H}{\lambda_c} = G^{3/2} > 1 \,,$$

where $G = G(\xi_\phi, \xi_E, Sc)$ is given by equation 2.28, and we need to distinguish between two cases depending on the relative values of x_D and x_H. The first case corresponds to $x_D < x_H$, for which

$$\langle N \rangle_\varepsilon \frac{\Theta_T}{\Theta_H} = \frac{1}{x_D} \int_0^{x_D} dx + \int_{x_D}^{x_H} x^{-1}\, dx + G \int_{x_H}^{x_\delta} x^{-5/3}\, dx$$

or,

$$\langle N \rangle_\varepsilon \frac{\Theta_T}{\Theta_H} = \frac{5}{2} - \ln(X_D) + \frac{3}{2}\ln(G) - \frac{3}{2} G x_\delta^{-3/2} . \qquad (2.53a)$$

In the second case, we have $x_H < x_D$ and therefore

$$\langle N \rangle_\varepsilon \frac{\Theta_T}{\Theta_H} = \frac{1}{x_D}\int_0^{x_H} dx + \frac{G}{x_D}\int_{x_H}^{x_D} x^{-2/3}\,dx + G\int_{x_D}^{x_\delta} x^{-5/3}\,dx$$

or

$$\langle N \rangle_\varepsilon \frac{\Theta_T}{\Theta_H} = \frac{1}{x_D}\left(\frac{9}{2} G x_D^{1/3} - 2 G^{2/3}\right) - \frac{3}{2} G x_\delta^{-3/2} . \qquad (2.53b)$$

Of these two cases, the first [$x_D < x_H$] would typically be applicable for $Sc \lesssim 1$, if $\beta \sim 3$ and we have reasonable values for the stoichiometric mixture ratio ϕ and entrainment ratio E .

For <u>liquid-like</u> flow-diffusion regimes we have the relation

$$x_H = \frac{\lambda_H}{\lambda_c} = G < 1 ,$$

and, in principle, we need to distinguish between three cases. The first liquid-like case corresponds to the inequalities $x_D < x_H < 1$ and the integrals

$$\langle N \rangle_\varepsilon \frac{\Theta_T}{\Theta_H} = \frac{1}{x_D}\int_0^{x_D} dx + \int_{x_D}^{x_H} x^{-1}\,dx + G\int_{x_H}^{1} x^{-2}\,dx + G\int_1^{x_\delta} x^{-5/3}\,dx ,$$

which yields

$$\langle N \rangle_\varepsilon \frac{\Theta_T}{\Theta_H} = 2 - \ln(x_D) + \frac{G}{2} + \ln(G) - \frac{3}{2} G x_\delta^{-3/2} . \qquad (2.54a)$$

For the second liquid-like case, we have $x_H < x_D < 1$, and

$$\langle N \rangle_\varepsilon \frac{\Theta_T}{\Theta_H} = \frac{1}{x_D}\int_0^{x_H} dx + \frac{G}{x_D}\int_{x_H}^{x_D} x^{-1}\,dx + G\int_{x_D}^{1} x^{-2}\,dx + G\int_1^{x_\delta} x^{-5/3}\,dx ,$$

or

$$\langle N \rangle_\varepsilon \frac{\Theta_T}{\Theta_H} = G\left[\frac{1}{2} + \frac{1}{x_D}\left(2 + \ln(x_D) - \ln(G)\right)\right] - \frac{3}{2} G x_\delta^{-3/2} . \qquad (2.54b)$$

Finally, we may also have $x_H < 1 < x_D$, in which case

$$\langle N \rangle_\varepsilon \frac{\Theta_T}{\Theta_H} = \frac{1}{x_D} \int_0^{x_H} dx + \frac{G}{x_D} \left[\int_{x_H}^{1} x^{-1}\, dx + \int_1^{x_D} x^{-2/3}\, dx \right] + G \int_1^{x_\delta} x^{-5/3}\, dx ,$$

which yields

$$\langle N \rangle_\varepsilon \frac{\Theta_T}{\Theta_H} = \frac{G}{x_D} \left(\frac{9}{2} x_D^{1/3} - 2 - \ln(G) \right) - \frac{3}{2} G x_\delta^{-3/2} . \qquad (2.54c)$$

Of the three cases for the liquid-like regime, the first one [$x_D < x_H < 1$] would typically be applicable for $Sc \gg 1$.

If treating the variable β of equation 2.25 as a constant represents an adequate approximation, it can be seen that only the last term in each of these expressions will be modified by the fluctuations in the dissipation rate. With that proviso, since $x_\delta^{-2/3} = (\lambda_c/\delta)^{2/3}$, the contribution of the last term is small at large Reynolds numbers. In any event, expressing λ_c/δ in terms of the corresponding distribution variable y (equation 2.44), we find for $Re \gg Re_{cr}$

$$\langle x_\delta^{-2/3} \rangle_\varepsilon = \left(\frac{Re}{Re_{cr}} \right)^{-(1 - 7\mu/48)/2} . \qquad (2.55)$$

Substituting in the results for the two typical cases (equations 2.53a and 2.54a), for example, we obtain for the expected value of the gas-like ($G > 1$), product volume fraction in the layer,

$$\langle \Theta_T \rangle_\varepsilon = \left\{ \frac{\frac{5}{2} - \ln(x_D) + \frac{3}{2}\ln(G) - \frac{3}{2} G \langle x_\delta^{-2/3} \rangle_\varepsilon}{1 - \ln(x_D) + \frac{3}{4}\left(1 - \frac{\mu}{8}\right) \ln\left(\frac{Re}{Re_{cr}} \right)} \right\} \Theta_H , \qquad (2.56)$$

and for the typical ($Sc \gg 1$) liquid-like ($G < 1$) product fraction

$$\langle \Theta_T \rangle_\varepsilon = \left\{ \frac{2 - \ln(x_D) + \frac{G}{2} + \ln(G) - \frac{3}{2} G \langle x_\delta^{-2/3} \rangle_\varepsilon}{1 - \ln(x_D) + \frac{3}{4}\left(1 - \frac{\mu}{8}\right) \ln\left(\frac{Re}{Re_{cr}} \right)} \right\} \Theta_H , \qquad (2.57)$$

where x_D is given by equation 2.37 and $\langle x_\delta^{-2/3} \rangle_\varepsilon$ by equation 2.55.

2.9 The effect of entrainment ratio fluctuations

We should note, at this point, that in the discussions thus far we have treated the entrainment ratio E, and the resulting homogeneous mixture fraction ξ_E (equation 1.8), as single-valued. We should recognize, however, that ξ_E is a variable that we would expect to be distributed according to some probability density function $p(\xi_E)$. This can then be used to obtain the estimate for the expected product thickness, as would be measured in the laboratory, by weighting $\theta_T(\xi_\phi, \xi_E)$, for each value of ξ_E, with $p(\xi_E)$. An estimate for $p(\xi_E)$ can be obtained with the aid of a refined model for the entrainment ratio E of the layer, which is outlined below.

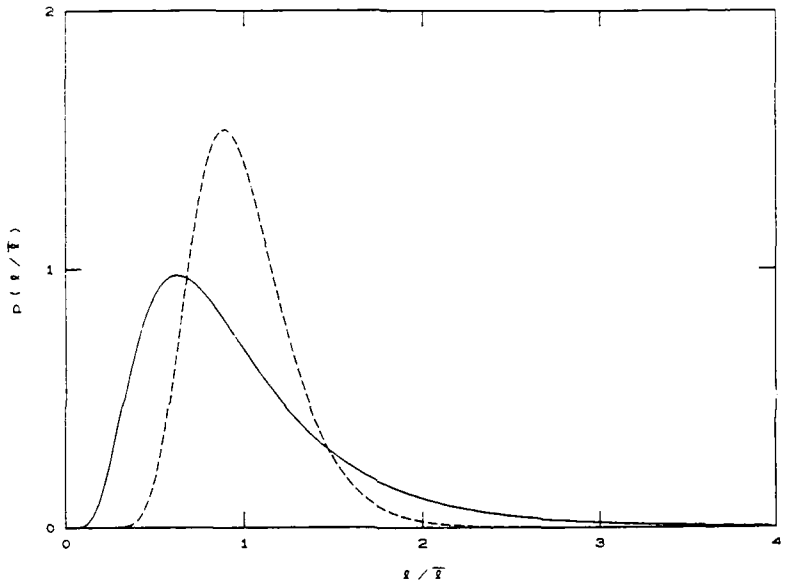

FIGURE 22. Probability density function $p(\ell/\bar{\ell})$ for normalized large scale structure spacings. Dashed curve for $\Sigma_\ell = 0.28$. Solid curve for $\Sigma_\ell = 0.56$.

If equation 1.7 can be used to estimate the entrainment ratio, then, even though the mean entrainment ratio would be given by

$$\bar{E} = \left(\frac{\rho_2}{\rho_1} \right)^{1/2} \left(1 + \bar{\ell}/x \right) , \qquad (2.58)$$

we must allow for a distribution of possible values of E about $\bar{E}$, since, experimentally,

$$E(\xi_E) = \frac{\xi_E}{1 - \xi_E} \quad . \tag{2.62b}$$

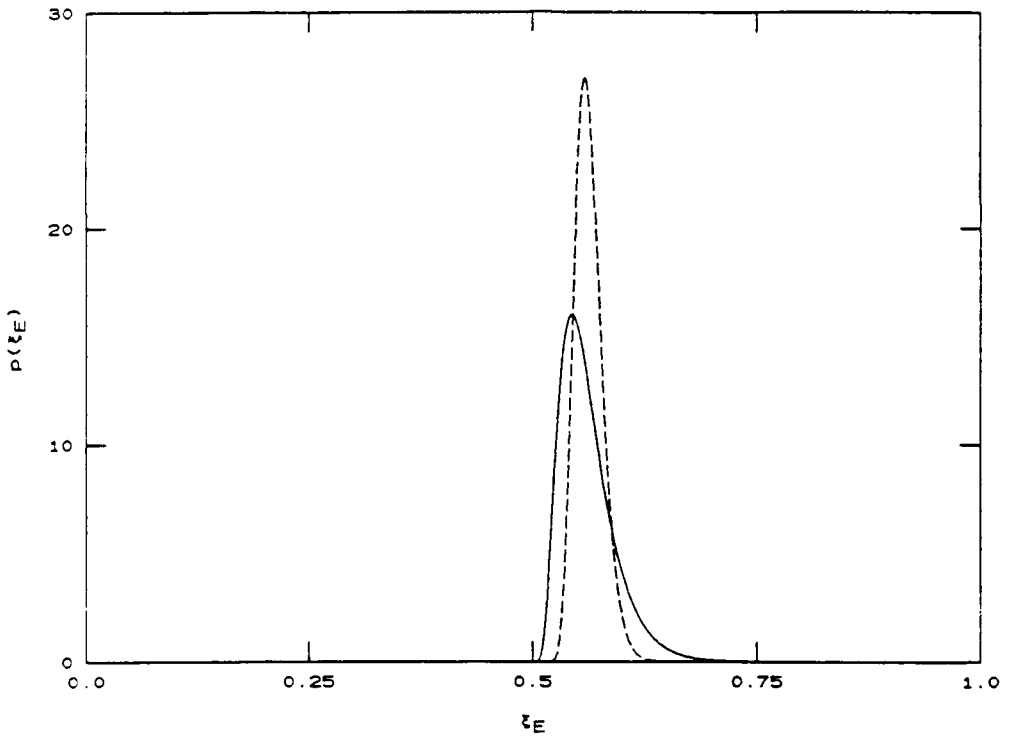

FIGURE 23. Probability density function for entrainment ratio mixture fraction $\xi_E = E/(E+1)$. Dashed curve for $\Sigma_\ell = 0.28$. Solid curve for $\Sigma_\ell = 0.56$.

The dashed line in figure 23 is the resulting probability density function $p(\xi_E)$, corresponding to equal free stream densities, a velocity ratio of $U_2/U_1 = 0.38$ and the Bernal value of $\Sigma_\ell = 0.28$. Note that, in spite of the width in the $\ell / \bar{\ell}$ distribution, the values of ξ_E are relatively narrowly distributed about the value of $\xi_{\bar{E}} = 0.567$, corresponding to a mean entrainment ratio of $\bar{E} = 1.305$, given by equation 2.36 for $\rho_2/\rho_1 = 1$ and $U_2/U_1 = 0.38$.

It should be noted that the experimental determination by Bernal (1981) of the histogram of values of $\ell / \bar{\ell}$ involved the identification of the intersection of the "braids" of each structure with the line corresponding to the trajectory of their centers. Consequently, structures in the process of tearing or coalescence, or at any other phase or configuration during which they could not be easily identified, were not included in his sample population. In other words, the distribution of spacings contributing to Bernal's experimental histogram and the resulting fit of the log-normal distribution width

one finds that the large structure spacing to position ratio ℓ/x is rather broadly distributed about its mean value $\bar{\ell}/x$. In particular, Bernal (1981) has presented data and theoretical arguments in support of a log-normal distribution, which we can write, following the notation in section 2.7, as

$$p_\ell(\ell')\, d\ell' = \frac{1}{\sqrt{2\pi}\,\Sigma_\ell} \exp\left\{ -\frac{1}{2}\left(\frac{\ell n(\ell')}{\Sigma_\ell} + \frac{\Sigma_\ell}{2} \right)^2 \right\} \frac{d\ell'}{\ell'} \,, \tag{2.59a}$$

where

$$\ell' = \ell / \bar{\ell} \,. \tag{2.59b}$$

This is plotted in figure 22, where the dashed line is computed from equation 2.59, using the value recommended by Bernal of $\Sigma_\ell = 0.28$. See Roshko (1976, figure 5 and related discussion) as well as Bernal (1981, figure I.8) for a comparison with experimental data.

Equations 1.7 and 2.58 can be combined to yield an estimate for the expected distribution of the values of the entrainment ratio E. The picture to be borne in mind is one in which the entrainment ratio E corresponding to a particular large structure can be treated as more or less fixed, but that the value of E varies from structure to structure in accordance with the range of values of ℓ/x (as well as the history of ℓ/x of the structures that have amalgamated to form the ones passing through the station x). In particular, since

$$E = \left(\frac{\rho_2}{\rho_1} \right)^{1/2} \left[1 + (\bar{\ell}/x)\, \ell' \right] \,, \tag{2.60}$$

we have, for equal free stream densities,

$$p_E(E)\, dE = p_\ell[\ell'(E)] \frac{dE}{\bar{\ell}/x} \,, \quad \text{where } \ell'(E) = \frac{E-1}{\bar{\ell}/x} \,,$$

and therefore

$$p_E(E)\, dE = \frac{1}{\sqrt{2\pi}\,\Sigma_\ell} \exp\left\{ -\frac{1}{2}\left[\frac{1}{\Sigma_\ell} \ln\left(\frac{E-1}{\bar{\ell}/x} \right) + \frac{\Sigma_\ell}{2} \right]^2 \right\} \frac{dE}{E-1} \,. \tag{2.61}$$

Using similar arguments, one also obtains the distribution $p(\xi_E)$ of the corresponding values of the mixture fraction ξ_E in terms of $p_E(E)$, in particular

$$p(\xi_E)\, d\xi_E = p_E[E(\xi_E)] \frac{d\xi_E}{(1-\xi_E)^2} \,, \tag{2.62a}$$

where, inverting equation 1.8, we have

Σ_ℓ was based on structures that were more or less clear of their neighbors and of interactions with them. Evidently, a full accounting of the possible large structure spacings will contribute values of ℓ/x, which if included in the population, would tend to broaden its width. Moreover, the expression for the entrainment ratio as given by equation 2.60 and as discussed elsewhere (Dimotakis 1986) refers to the entrainment flux ratio into a single large scale structure. The composition ratio of a given large scale structure, however, is the one resulting from the amalgamation of several structures, each of which was characterized by an entrainment ratio as dictated by its local ℓ/x and its fluctuations. While this consideration does not shift the mean value of E, it can be seen that it increases the variance of E, relative to its value referenced to the fluctuations of the local ℓ/x. Accordingly, in estimating the distribution of values of the entrainment ratio E, and the resulting homogeneous composition values ξ_E, one should accept a broader distribution of values of E, which we will approximate by accepting a larger value of Σ_ℓ.

The curves depicted with the solid lines in figures 22 and 23 were computed by doubling the Bernal value of the log-normal distribution width, i.e. $\Sigma_\ell = 0.56$, as representing a reasonable estimate for that quantity in view of the preceding discussion, and are plotted for comparison. It can be seen, however, that even this factor of two increase in the width Σ_ℓ does not significantly alter the resulting probability density function width for the distribution of values of ξ_E.

Using the computed probability density function for the values of ξ_E, the problem is finally closed and we can now estimate the expected product thickness δ_P/δ in the mixing layer, i.e.

$$\frac{\delta_P}{\delta} = \langle \theta_T \rangle_{\varepsilon,E} = \int_0^1 \langle \theta_T(\xi_E) \rangle_\varepsilon \, p(\xi_E) \, d\xi_E \,, \tag{2.63}$$

where $\langle \theta_T(\xi_E) \rangle_\varepsilon$ is the expected value of the normalized chemical product, averaged over the dissipation rate fluctuations, conditional on the fixed value of ξ_E, as discussed in the preceding section.

The dependence of the resulting estimates for δ_P/δ on the possible range of values of the variance Σ_ℓ of $\ell/\bar{\ell}$ is small and confined to values of the stoichiometric mixture fraction ξ_s in the vicinity of $\xi_{\bar{E}}$. It will be discussed below in the context of the comparison of the theoretical values with the data.

3.0 RESULTS & DISCUSSION

Using the preceding formalism, one can estimate the expected volume (or mass) fraction of chemical product and molecularly mixed fluid generated within the two-dimensional turbulent shear layer wedge boundaries.

We recall here that the proposed model applies to incompressible flow, i.e. in the limit of zero Mach number. In the case of gas phase reactions, the heat release is assumed small and, in the case where the (small) temperature rise is used to label the chemical product, the heat capacities of the two free stream fluids are assumed matched. Differential diffusion effects have been ignored, i.e. all scalar species are assumed to diffuse with the same diffusivity. Also the chemical kinetics have been assumed fast. Finally, the Reynolds number has been assumed high enough for the shear layer to be in a fully developed three-dimensional turbulent state, i.e. $Re > 1.6\times10^4 - 2\times10^4$.

In evaluating the theoretical estimates, the following values will be used for the dimensionless parameters:

1. The expected value of the entrainment ratio $\bar{E}$ will be computed using equation 2.58 .

2. The fluctuations of $E / \bar{E}$ will be estimated using equation 2.61 with a variance twice the Bernal value, i.e. $\Sigma_\ell = 0.56$, as discussed in section 2.9 .

3. The value of the expected maximum contraction rate σ_c , at or below the Kolmogorov scale, will be estimated using the expression $\sigma_c t_K = 1/\beta$ with $\beta \sim 3$ (see equation 2.25 and related discussion).

4. Re_{cr} , the critical Reynolds number, will be estimated via equation 2.49c , using the mid-point of the expected dimensionless dissipation $\bar{\alpha}$ bounds (i.e. $\bar{\alpha} = 0.04$). This leads to the value of $Re_{cr} = 26$.

5. The Kolmogorov/Oboukhov coefficient μ in the variance of $\ln(\varepsilon)$ will be taken as 0.3 (equation 2.43).

6. The ratio x_D of the diffusion scale λ_D to the strain rate cut-off scale λ_c will be computed using equation 2.37 , with a value of $C_B \sim 1.6$, as discussed in section 2.6 .

and, finally,

7. The product volume fraction $\delta_{P/\delta}$ will be computed using equation 2.63 , with $< \Theta_{T(\xi E)} >_\varepsilon$ given by equations 2.56 or 2.57 (or 2.53 , 2.54), as appropriate.

We note that the results are only weakly sensitive to these choices, appearing in the final expressions, by and large, as arguments of logarithms.

3.1 Comparison with chemically reacting flow data

The proposed model predictions for the chemical product volume fraction $\delta_{p1}/\delta = \xi_\phi \delta p/\delta$, versus the stoichiometric mixture ratio ϕ, for the hydrogen-fluorine gas phase data (Mungal & Dimotakis 1984), for which $Sc = 0.8$, $U_2/U_1 = 0.40$, $\rho_2/\rho_1 = 1$, and $Re = 6.6\times10^4$, are plotted in figure 24. The predicted values are in good agreement with the gas phase chemical product volume fraction data. The essentially correct prediction of the absolute amount of product may perhaps be regarded as fortuitous but is nevertheless noteworthy.

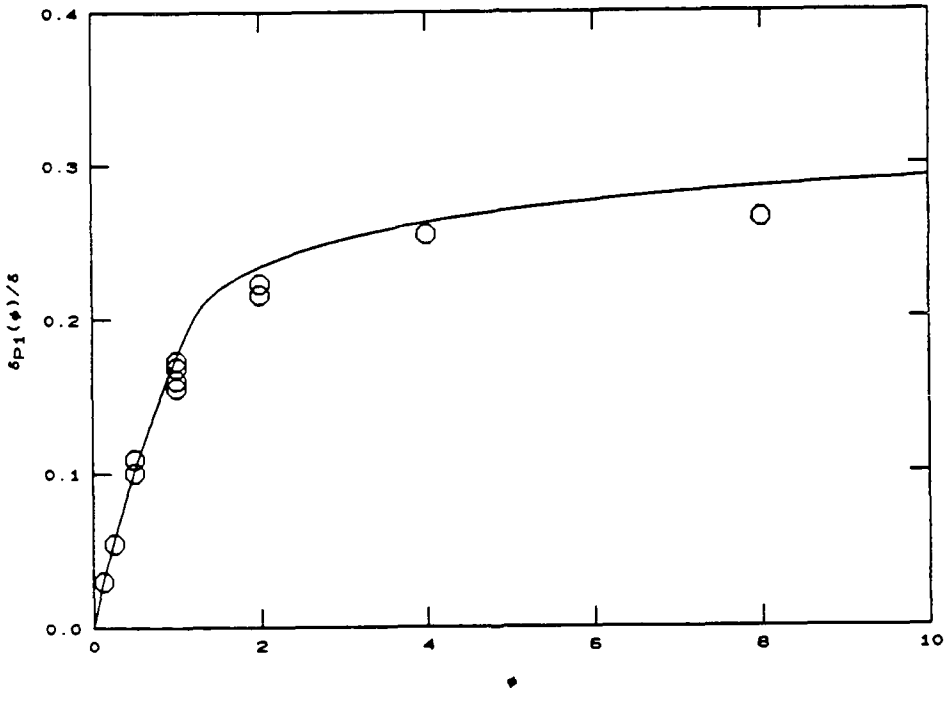

FIGURE 24. Model predictions for $\delta_{p1}(\phi)/\delta$ product thickness. Data legend as in figure 4.

A plot of the δ_p/δ predicted chemical product volume fraction, versus ξ_ϕ, appears in figure 25. The top solid curve and data points (circles) are transformed from figure 24. The corresponding predictions are also plotted for the liquid data ($Sc = 600$) of

Koochesfahani & Dimotakis (1986).

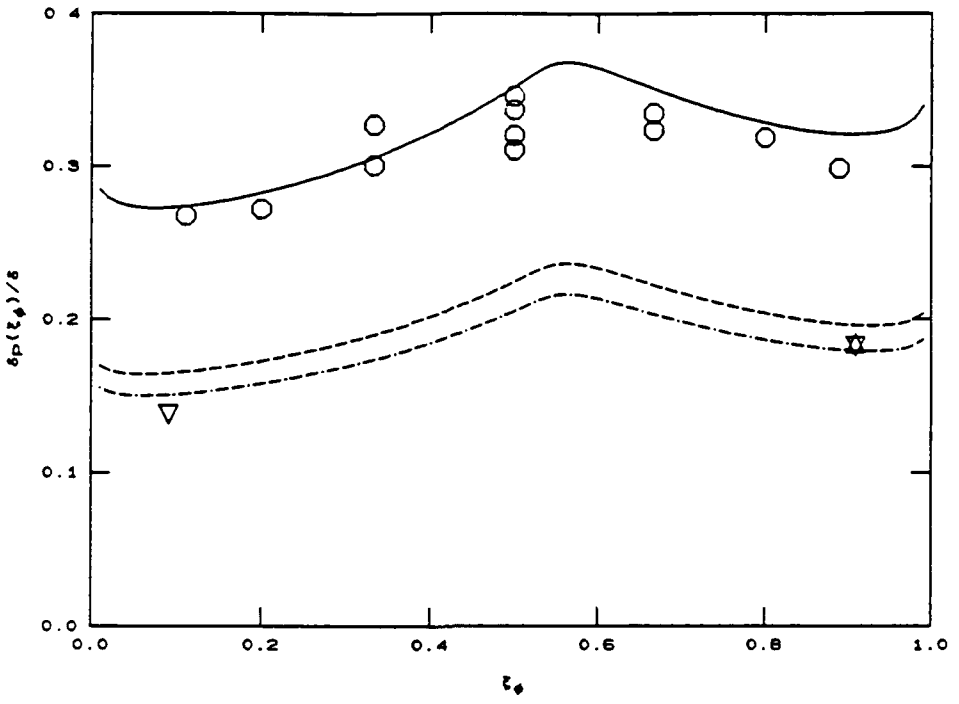

FIGURE 25. Proposed model predictions for δ_p/δ vs. ξ_ϕ data. Solid line for gas phase data (circles; Sc = 0.8, Re = 6.6×10^4, Mungal & Dimotakis 1984). Dashed line for liquid phase (Sc = 600, Koochesfahani & Dimotakis 1986) data (inverted triangles; Re = 2.3×10^4). Dot-dashed line for higher Reynolds number point (upright triangle; Re = 7.8×10^4).

As can be seen, the Schmidt number dependence of the chemical product volume fraction, at comparable Reynolds numbers, appears also to be predicted essentially correctly. The prediction for the lower Reynolds number data is a little high. As mentioned earlier, however, it may be that the Reynolds number for those data may not be high enough.

Figure 26 depicts the model predictions (solid line, Sc = 0.8) for the dependence of the product thickness δ_p/δ on Reynolds number, as compared to the gas phase data of Mungal et al (1985) and the liquid phase (dashed line, Sc = 600) data of Koochesfahani & Dimotakis (1986). As can be seen, the experimentally observed drop in the chemical product volume fraction of approximately 6% per factor of two in Reynolds number in the gas phase data, appears correctly accounted for by the proposed model. We note again that the lower Reynolds number liquid phase data point of Koochesfahani & Dimotakis may be too close to the mixing transition Reynolds number regime to be considered representative of the asymptotic behavior at large Reynolds numbers.

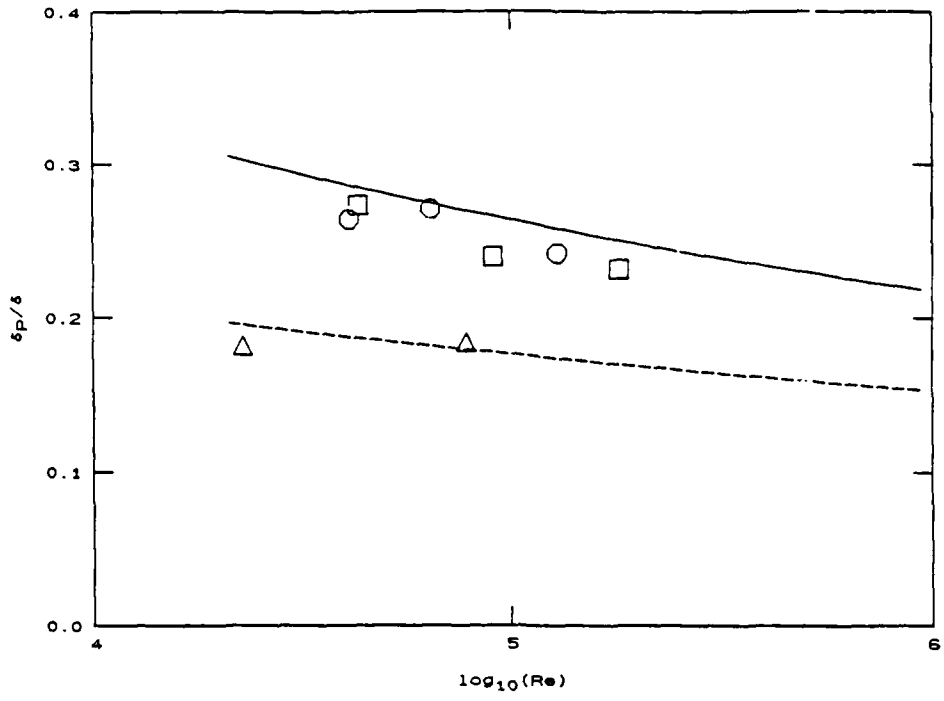

FIGURE 26. Model predictions for $\delta p/\delta$ chemical product volume fraction dependence on Reynolds number. Data as in figure 6. Solid line for gas phase data. Dashed line for liquid phase data. Data legend as in figure 6.

In figure 27, we investigate the sensitivity of the predictions on the value of the log-normal distribution width Σ_ℓ. The top cusped curve is computed for a single-valued entrainment ratio of $E = \bar{E}$, where $\bar{E}$ is given by equation 2.58, i.e. a Dirac delta function probability density function $p(\xi_E) = \delta[\xi_E - \bar{E}/(\bar{E}+1)]$, corresponding to a value for the variance of $\Sigma_\ell = 0$. The curve below the cusped curve corresponds to the Bernal value of $\Sigma_\ell = 0.28$. Finally, the bottom line corresponds to the value accepted here as representative of the entrainment ratio fluctuations as reflected in the composition within a single structure, i.e. double the Bernal value, or $\Sigma_\ell = 0.56$, and the probability density functions plotted as dashed lines in figures 22 and 23. As could have been anticipated, the effect of incorporating the expected distribution of values of the entrainment ratio is very slight and confined to the neighborhood of $\xi_\phi - \xi_{\bar{E}} = \bar{E}/(\bar{E}+1)$, corresponding to the mean entrainment ratio $\bar{E}$, and resulting in the removal of the cusp in the product thickness at $\xi_\phi = \xi_{\bar{E}}$.

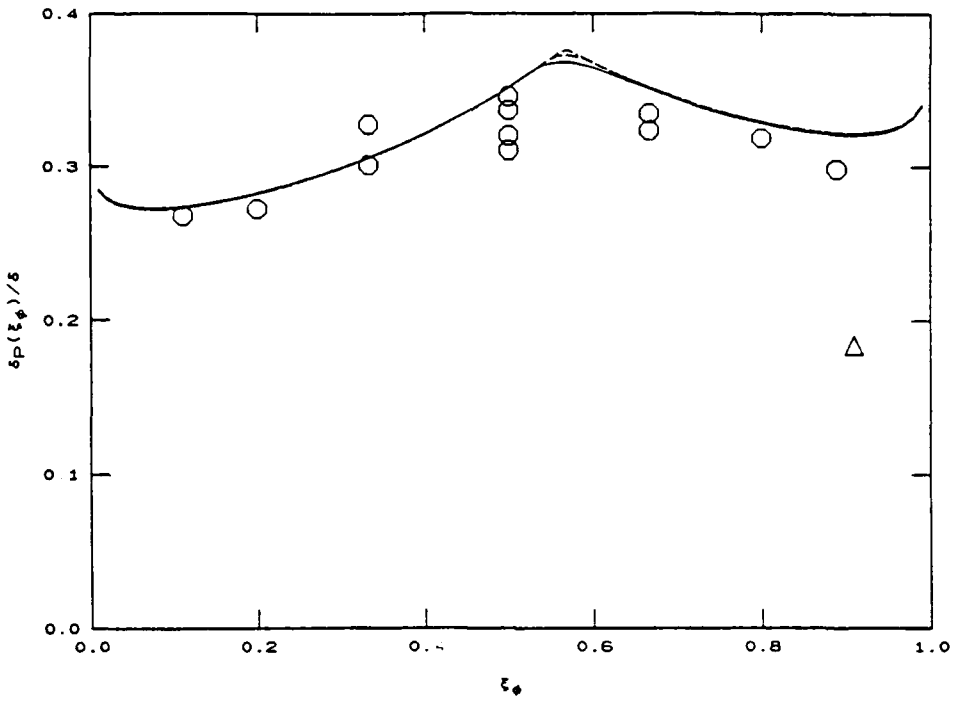

FIGURE 27. Model sensitivity to value of variance Σ_ℓ used in entrainment mixture fraction PDF. Corresponding predictions for $\delta_p(\xi_\phi)/\delta$ chemical product volume fraction. Top (cusped) curve for $\Sigma_\ell = 0$. Middle dashed curve for $\Sigma_\ell = 0.28$. Bottom (solid) curve for $\Sigma_\ell = 0.56$ used in the model.

As discussed earlier, the sensitivity of the computed values of the product volume fraction to the various choices of the flow constants is weak. By way of example, the smooth curves in figures 4 and 5, which do not differ substantially from those in figures 24 and 25, were computed using a value of $\beta = 5^\dagger$, leaving all other constants at their nominal values.

Finally, we note that the model predictions for the chemical product volume fraction tend to be a little high (see figure 25 and 26). One could argue, considering what is being attempted here with a rather simple model and no adjustable parameters, that the agreement with experiment is more than satisfactory. We also note, however, that two assumptions that were made in the analysis may not be adequately justified in the case of the hydrogen-fluorine gas phase shear layer data. One, as Broadwell & Mungal (1986) have suggested, the kinetics may not be sufficiently fast. If this is indeed the case, the chemical product would be lower than would be observed in the case of infinite kinetics. Two, we recognize that the assumption of equal diffusivities for all the reactant species

---

† Such a value is, of course, inadmissible by virtue of the bounds in inequality 2.25

is also not justified, hydrogen possessing a diffusivity roughly four times higher than the other reactants/diluents in those experiments. It is difficult to give an a priori assessment of the effects of unequal diffusivities, possibly as coupled with the effects of finite kinetics, at this time.

3.2 The mixed fluid fraction

An important quantity in turbulent mixing is the mixed fluid fraction within the turbulent zone. It is to the mixing scalar (or scalar dissipation) field what intermittency is to the turbulent velocity (or energy dissipation) field. Operationally, it can be defined through the probability density function (PDF) of the conserved scalar, i.e. $p(\xi)$, integrated across the shear layer width. In particular the quantity

$$\frac{\delta_m(Sc,Re)}{\delta} = \int_{\xi_1}^{1-\xi_1} p(\xi,Sc,Re)\, d\xi \ , \tag{3.1}$$

for some small value of ξ_1 which excludes the unmixed fluid contributions from the neighborhood of $\xi = 0$ and $\xi = 1$, represents the volume fraction occupied by molecularly mixed fluid within the transverse extent of the turbulent shear layer. This quantity can be expected to be a function of the fluid Schmidt number and the flow Reynolds number (and potentially also of the free stream density ratio and velocity ratio). In particular, we would expect that an increase in the Schmidt number, at fixed Reynolds number, should result in a decrease of δ_m/δ, which should vanish in the limit of infinite Schmidt numbers. An a priori assessment of the behavior of the mixed fluid fraction at fixed Schmidt number in the limit of very large Reynolds numbers cannot be made as readily and will be discussed separately below.

While the integral indicated in equation 3.1 can, in principle, be estimated by direct measurement of the scalar field $\xi(\underline{x},t)$, and therefore also its PDF $p(\xi)$, it was pointed out by Breidenthal (1981) and Koochesfahani & Dimotakis (1986) that, as a consequence of the inevitable experimental finite resolution difficulties at high Reynolds numbers, such measurements will generally overestimate this quantity. It was also pointed out in Koochesfahani & Dimotakis, however, that reliable estimates are possible using the results of chemically reacting experiments, namely the chemical product fractions $\delta_p(\xi_o)/\delta$ and $\delta_p(1-\xi_o)/\delta$ from a "flip" experiment conducted at ϕ_o and $1/\phi_o$, for small values of ϕ_o, corresponding to a $\xi_o = \phi_o/(1+\phi_o) \ll 1$. In particular, the mixed fluid fraction can be estimated in terms of the chemically reacting flow results by means of the relation

$$\frac{\delta_m}{\delta} = \frac{1-\xi_o}{\delta}\left[\,\delta p(\xi_o) + \delta p(1-\xi_o)\,\right] . \tag{3.2}$$

This is very close to the expression in equation 3.1 and equivalent to computing the

integral of the product of the probability density function with a "mixed fluid" function $\theta_m(\xi)$ given by,

$$\theta_m(\xi) = \begin{cases} \dfrac{\xi}{\xi_o} , & \text{for } 0 \le \xi < \xi_o , \\ 1 , & \text{for } \xi_o < \xi < 1 - \xi_o , \\ \dfrac{1-\xi}{\xi_o} , & \text{for } 1 - \xi_o < \xi < 1 \end{cases} \tag{3.3a}$$

(see figure 28), i.e.

$$\frac{\delta_m}{\delta} = \int_0^1 \theta_m(\xi)\, p(\xi)\, d\xi . \tag{3.3b}$$

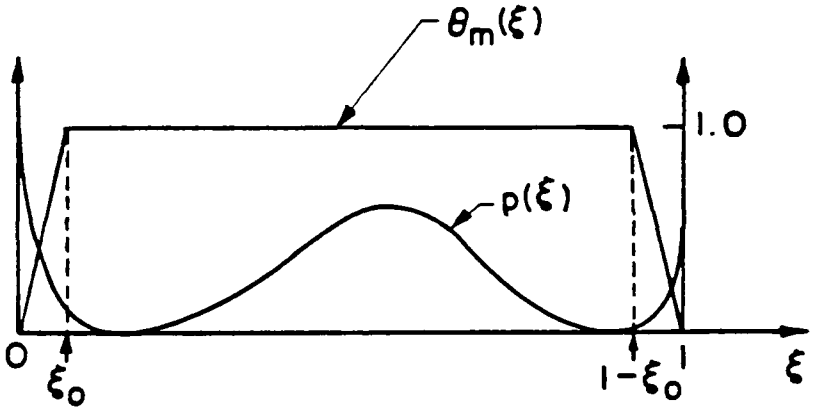

FIGURE 28. "Mixed fluid" normalized function $\theta_m(\xi)$. See equation 3.3 .

We note that if the curvature in $p(\xi)$ in the edge regions $0 < \xi < \xi_o$ and $1 - \xi_o < \xi < 1$ can be ignored, this expression reproduces the result of equation 3.1 for $\xi_1 = \xi_o/2$.

Gas phase (Sc ~ 0.8) "flip" experiments ($\phi_o = 1/8$) are available from Mungal & Dimotakis (1984) at a Reynolds number of 6.6×10^4 (see figure 25). The liquid phase (Sc ~ 600) "flip" experiments ($\phi_o = 1/10$) of Koochesfahani & Dimotakis (1986) were at a lower Reynolds number ($Re \sim 2.3 \times 10^4$). The value of δ_p/δ for their higher Reynolds number data at $\phi = 10$, however, is so close to their corresponding lower Reynolds number value (see figure 26) that the Reynolds number dependence of the liquid data can probably be ignored as a first approximation in comparing the gas phase and liquid phase results to assess the Schmidt number dependence of δ_m/δ .

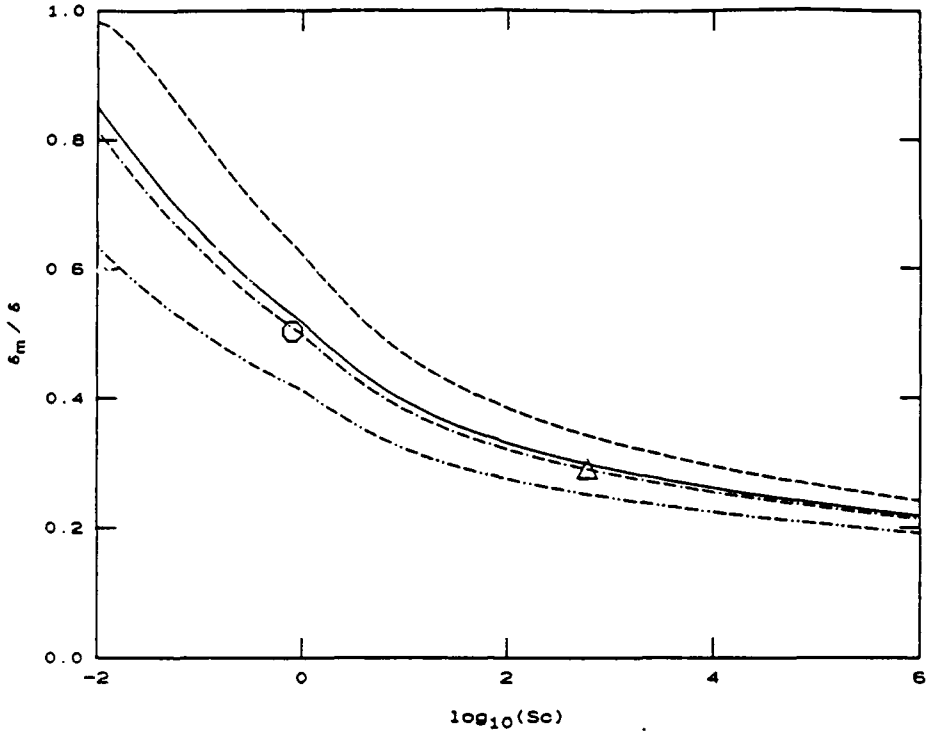

FIGURE 29. Proposed model predictions for mixed fluid volume fraction δ_m/δ as a function of Schmidt number and Reynolds number. Circle derived from Mungal & Dimotakis (1984) data. Triangle from Koochesfahani & Dimotakis (1986) data (see text). Solid curve for $Re = 6.6 \times 10^4$. Dashed curves, in order of decreasing mixed fluid volume fraction, for $Re = 10^4$, 10^5 and 10^6.

A plot of the model estimate for the mixed fluid volume fraction $\delta_m(Sc,Re)/\delta$, using a value for ϕ_o of 1/8 corresponding to the gas phase data, is depicted in figure 29 as a function of Schmidt number. For the purposes of illustration of the qualitative behavior, the plot ranges from a value of the Schmidt number of 0.01, as would be appropriate in estimating the fluid at an intermediate temperature in a two-temperature free stream shear layer in mercury, for example, to a Schmidt number of 10^6, as would be appropriate for mixing of a particulate cloud that diffuses via Brownian motion. The solid line in that figure is for $Re = 6.6 \times 10^4$ corresponding to the gas phase data. The circle represents the gas phase experimental value while the triangle represents the liquid phase data. The other dashed lines are for $Re = 10^4$, 10^5 and 10^6, respectively, in order of decreasing values of δ_m/δ. The corresponding estimates using the Broadwell-Breidenthal model, with the values of the coefficients c_H and c_F in that model derived by fitting the gas/liquid difference (at low ϕ) of these data (equation 1.13), are plotted in figure 30 for comparison.

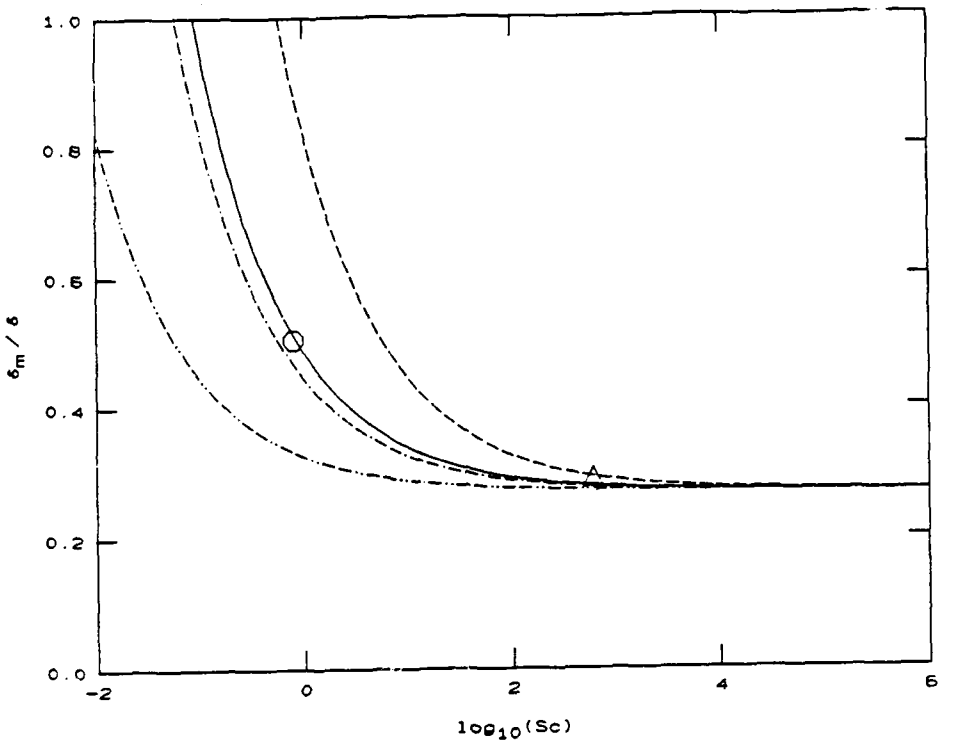

FIGURE 30. Broadwell-Breidenthal model predictions for mixed fluid volume fraction δ_m/δ as a function of Schmidt number and Reynolds number. Note Reynolds number dependence at fixed Schmidt number and asymptotic dependence for large Schmidt numbers. Data legend as in figure 29.

3.3 Discussion and conclusions

Several features of the predictions of the proposed theory for the expected mixed fluid or chemical product volume fraction, within the transverse extent of the shear layer, perhaps merit discussion.

The absolute amount of molecular mixing appears to be estimated essentially correctly, as a function of the Schmidt number and Reynolds number of the flow, with no adjustable parameters. In this context, recall that the various experimental values for the parameters used in the theory pertain to the statistics of the turbulent velocity (and dissipation) fields, which are assumed given. In particular, they are not derived from the results of mixing or chemically reacting experiments, which the theory attempts to describe. Moreover, the theory is relatively robust in that variations within the admissible range of these parameters do not have a significant effect on the predictions. The usually difficult question of an a priori estimate of intermittency, or, in the

present context, of the volume fraction in the flow occupied by unmixed (unreacted) fluid, is addressed through the normalization of the volume-filling spectrum of scales. Finally, except for switching (matched) analytical expressions, depending on the relative magnitudes of the various (inner) scales of the problem, i.e. λ_D, λ_H, λ_c, liquids and gases are treated in a unified way through the explicit dependence of the results on Schmidt number.

The theory also predicts that, at sufficiently high Reynolds numbers, the amount of mixed fluid or chemical product in a gas phase shear layer would be less than what would be observed in a liquid layer at sufficiently low Reynolds numbers (recall figure 29). In fact, the interesting and controversial prediction is that the volume fraction of the mixed fluid tends to zero with increasing Reynolds number, albeit slowly, possessing no Reynolds number independent asymptotic (non-zero) value. One might intuitively argue that as the Reynolds number increases, the interfacial surface area available for mixing must increase (under the action of the higher sustainable strain rates in the flow) and therefore also the mixing rate. This argument, however, is incomplete in that it fails to recognize that the thickness of the mixed fluid layer straddling the interface must be decreasing, in fact, approximately inversely as the interface area is increasing, by the force of the same arguments. Consequently, these two effects must approximately cancel each other. In particular, the model predicts that as the Reynolds number increases, the associated diffused layer thickness must be decreasing at a slightly faster rate, since the flow volume fraction occupied by the mixed fluid is decreasing (slowly) with increasing Reynolds number. This behavior is corroborated by the limited data available, which indicate a monotonically decreasing volume fraction of chemical product with increasing Reynolds number, in good quantitative agreement with the predicted Reynolds number dependence.

It should be noted that the prediction is not that mixing ceases in the limit of infinite Reynolds numbers. If one were to increase the Reynolds number by increasing the downstream coordinate x, for example, the integrated mixed fluid thickness $\delta_m(x)$ would increase almost proportionally to the shear layer thickness $\delta(x)$, specifically

$$\delta_m(x) \sim \frac{b_1(Sc)}{b_0(Sc) + \ln(x/x_t)}\,\delta(x) \ . \tag{3.4a}$$

Consequently, however, the mixed fluid volume fraction would decrease logarithmically, or in terms of the Reynolds number,

$$\frac{\delta_m}{\delta} \sim \frac{B_1(Sc)}{B_0(Sc) + \frac{3}{4}\left(1 - \frac{\mu}{8}\right)\ln\left(\frac{Re}{Re_{cr}}\right)} \ . \tag{3.4b}$$

This result is a direct consequence of the assumed statistical weight and normalization over the range of scales of the problem. In particular, accepting the $W(\lambda)\,d\lambda \sim d\lambda/\lambda$ statistical weight for the moment, the dependence on the local Reynolds number enters through the ratio of the outer large scale δ to the inner scale $\lambda_c = \beta^{3/2}\lambda_K$, where $\beta = 3$ and λ_K is the Kolmogorov scale, i.e.

$$\frac{\delta_m}{\delta} \sim \frac{B_1(Sc)}{B_0(Sc) + \langle \ln\left(\frac{\delta}{\lambda_c}\right)\rangle_\varepsilon}\,, \tag{3.5}$$

and where the subscripted angle brackets denote the ensemble average over the fluctuations in the local dissipation rate ε. We note that, again accepting the $W(\lambda)\,d\lambda \sim d\lambda/\lambda$ statistical weight, a non-zero asymptotic value for δ_m/δ at high Reynolds numbers would be the prediction only if $\langle \ln(\delta/\lambda_K)\rangle_\varepsilon \to$ constant, as $Re \to \infty$.

We have examples of such behavior in high Reynolds number turbulent flows. In particular, the skin friction coefficient for a turbulent boundary layer over a (smooth) flat plate at high Reynolds number appears to decrease approximately logarithmically with Reynolds number. For similar reasons, the pressure gradient coefficient for turbulent (smooth wall) pipe flow also decreases logarithmically with Reynolds number. It is interesting to note, however, that in these examples the behavior will asymptote to a Reynolds number independent regime, if the wall cannot be considered smooth compared to the smallest scales the turbulence can sustain and interferes with their participation in the dynamics, i.e. if a Reynolds number independent minimum scale is imposed on the dynamics of the flow. Analogously, in my opinion, the assignment of an Eulerian, Reynolds number independent volume fraction occupied by the homogeneously mixed fluid in the Broadwell-Breidenthal model leads perforce to a Reynolds number independent mixed fluid (and chemical product) volume fraction in the limit of large Reynolds numbers. In a free shear layer, however, in which the turbulence does not have to contend with any intruding rough walls or externally imposed minimum scales, the flow will generate its minimum (dissipation/diffusion) scales, of ever decreasing size as the Reynolds number increases, and which will participate in the mixing and dissipation dynamics unimpeded.

We recognize, however, that the Broadwell-Breidenthal argument is not Eulerian. These authors integrated the cascade time scale associated with each scale λ and concluded that the Lagrangian time to cascade to the Kolmogorov scale becomes independent of the Reynolds number at high Reynolds numbers. This is a central idea in the Broadwell-Breidenthal model. If one accepts it, one must also accept that fluid entrained at an upstream station x_1 cascades to the diffusion (Kolmogorov) scale by a station x_K, such that x_K/x_1 is independent of the Reynolds number. The argument is important and, if correct, difficult to reconcile with the proposed predicted shear layer mixing behavior at high Reynolds numbers.

We shall examine the Broadwell-Breidenthal argument by inverting equation 2.7 to yield the scaling for the differential time required to cascade from λ to $\lambda + d\lambda$. In particular, we have

$$-dt \sim \frac{1}{\sigma(\lambda)} \frac{d\lambda}{\lambda} \sim \frac{1}{\varepsilon^{1/3}} \frac{d\lambda}{\lambda^{1/3}} ,$$

where $\varepsilon = \alpha (\Delta U)^3/\delta$ is the dissipation rate. We note here that in the Broadwell-Breidenthal analysis, the dissipation rate was treated as a constant during the cascade. It can be argued that this is not a valid approximation for two reasons. First, because the distance to cascade is not small, corresponding to a non-negligible change in $\delta = \delta(x)$, and therefore $\bar{\varepsilon}$ in the process, and second, because ε must be considered as a random variable with a Reynolds number dependent variance. It is possible to respond to these objections, however, by a proper separation of the problem variables, i.e.

$$-\varepsilon^{1/3}(t)\, dt \sim \lambda^{-1/3} d\lambda .$$

Substituting for the dissipation rate and transforming to δ as the independent variable, we then obtain

$$-\alpha^{1/3}(\delta) \frac{d\delta}{\delta^{1/3}} \sim \lambda^{-1/3} d\lambda .$$

This can be integrated from a thickness $\delta_1 = \delta(x_1)$ to a thickness $\delta_K = \delta(x_K)$ to yield

$$\int_{\delta_1}^{\delta_K} \alpha^{1/3}(\delta) \frac{d\delta}{\delta^{1/3}} \sim \delta_1^{2/3} ,$$

where we have used that $\lambda_K \ll \delta_1$. To estimate the effect of the fluctuations in α we compute the expectation value of the left hand side, which for the purposes of the scaling estimate we will commute with the integration to write

$$\int_{\delta_1}^{\delta_K} \langle \alpha^{1/3} \rangle_\varepsilon \frac{d\delta}{\delta^{1/3}} \sim \delta_1^{2/3} .$$

As before, the subscripted angle brackets denote the expectation value over the distribution of values of the dissipation rate. This can be estimated using the methods outlined in section 2.7 and we obtain

$$\langle \alpha^{1/3} \rangle_\varepsilon \sim (\bar{\alpha})^{1/3} \left(\frac{Re}{Re_{cr}} \right)^{-\mu/12}$$

(recall $\mu \approx 0.3$). Substituting in our previous expression yields the desired result, i.e.

$$\frac{x_K}{x_1} \sim \frac{1}{\bar{\alpha}^{1/2}} \left(\frac{Re_1}{Re_{cr}} \right)^{\mu/8} , \qquad (3.6)$$

where Re_1 is the Reynolds number at $x = x_1$. While the preceding argument is not without its own shortcomings, if we accept $\bar{\alpha}$ as a non-increasing function of the Reynolds number, we note that the possibility that the distance to cascade is not Reynolds number independent must be entertained.

This is an interesting observation, bearing also on Saffman's (1968) concern that the available arguments in support of the assumption that $\bar{\alpha}$ itself is Reynolds number independent may not be sufficiently compelling. We note, however, that the conclusions of the present model would survive in the event (which has not been disallowed here). In particular, a weak dependence of $\bar{\alpha}$ on Reynolds number, say, $\bar{\alpha} \sim \bar{\alpha}_0 (Re/Re_0)^{-p}$, where presumably $0 < p \ll 1$, would produce only minor changes in the results (see equations 2.48 and 2.49). A weaker possible dependence, e.g. logarithmic, need not even be incorporated as a correction for any Reynolds number range of practical interest.

Finally, we return to the observation that the predicted asymptotic behavior in the limit of infinite Reynolds numbers is traceable to the assumed statistical weight distribution of scales in the inertial range, i.e. $W(\lambda)\, d\lambda \sim d\lambda/\lambda$, as discussed in section 2.6. A very small deviation from this expression, for example

$$W(\lambda)\, d\lambda \sim \left(\frac{\lambda}{\delta} \right)^r \frac{d\lambda}{\lambda} ,$$

where $|r| \ll 1$†, would produce only minor differences in the range of Reynolds numbers of practical interest, but would alter the conclusions in the limit. In particular, the mixed fluid fraction δ_m/δ would tend to a (small, order r) non-zero asymptotic value in the limit of large Reynolds numbers, or to zero with a weak power dependence on Re, depending on whether r can be taken as positive or negative, and the (possible) dependence of the scaled mean dissipation rate $\bar{\alpha}$ on the Reynolds number.

We conclude by observing that, from an engineering vantage point, the volume fraction of mixed fluid within the shear layer, i.e. δ_m/δ, is expected to possess a (broad) maximum at a Reynolds number in the range of 2×10^4 to 3×10^4 (based on the local thickness δ and velocity difference ΔU). This corresponds to the region shortly after the flow has emerged from its "mixing" transition (Bernal et al 1979) to a fully three dimensional, turbulent state.

---

† This is admissible under the revised similarity hypotheses of Kolmogorov (1962) and Oboukhov (1962), which (even if weakly) impose the outer scale δ throughout the inertial range, or the fractal iddeas put forth by Mandelbrot (e.g. 1976). On the other hand, if a power law is appropriate, the exponent r is likely to be small, since the argument of no characteristic length scale in the inertial range (leading to the $d\lambda/\lambda$ distribution) must very nearly be right.

ACKNOWLEDGEMENTS

I would like to acknowledge the many discussions within the GALCIT community, which directly or indirectly have contributed to this paper. Without wishing to imply endorsement, I would specifically like to recognize the discussions with Dr. J. Broadwell, Prof. R. Narasimha and Prof. P. Saffman. Additionally, the critical comments by Prof. A. Leonard and Mr. P. Miller contributed to many important improvements and clarifications in the final form of the text. Finally, I would like to thank Mr. C. Frieler for performing the numerical integration of the differential equation for the velocity correlation function $h(\zeta)$ in section 2.6 .

This work is part of a larger effort to investigate mixing and combustion in turbulent shear flows, sponsored by the Air Force Office of Scientific Research Contract No. F49620-79-C-0159 and Grant No. AFOSR-83-0213, whose support is gratefully acknowledged.

REFERENCES

ASHURST, W. T., KERSTEIN, A. R., KERR, R. M. and GIBSON, C. H. [1987] "Alignment of Vorticity and Scalar Gradient with Strain Rate in Simulated Navier-Stokes Turbulence", Phys. Fluids 30(8), 2343-2353.

BATCHELOR, G. K. [1959] "Small-scale variation of convected quantities like temperature in turbulent fluid. Part I. General discussion and the case of small conductivity", J. Fluid Mech. 5, 113-133.

BATCHELOR, G. K., HOWELLS, I. D. and TOWNSEND, A. A. [1959] "Small-scale variation of convected quantities like temperature in turbulent fluid. Part 2. The case of large conductivity", J. Fluid Mech. 5, 134-139.

BERNAL, L. P. [1981] The Coherent Structure of Turbulent Mixing Layers. I. Similarity of the Primary Vortex Structure, II. Secondary Streamwise Vortex Structure, Ph.D. Thesis, California Institute of Technology.

BERNAL, L. P., BREIDENTHAL, R. E., BROWN, G. L., KONRAD, J. H. and ROSHKO, A. [1979] "On the Development of Three Dimensional Small Scales in Turbulent Mixing Layers.", 2nd Symposium on Turbulent Shear Flows, 1-4 July 1979, Imperial College, England.

BETCHOV, R. [1977] "Transition", Handbook of Turbulence I (Ed. W. Frost and T. H. Moulden, Plenum Press), 147-164.

BETCHOV, R. and SZEWCZYK, A. [1963] "Stability of a shear layer between parallel streams", Phys. Fluids 6, 1391-96.

BILGER, R. W. [1980] "Turbulent Flows with Nonpremixed Reactants", Turbulent Reacting Flows (Springer-Verlag, Topics in Applied Physics 44, 1980, Ed. P. A. Libby, F. A. Williams), 65-113.

BREIDENTHAL, R. E. [1981] "Structure in Turbulent Mixing Layers and Wakes Using a Chemical Reaction", J. Fluid Mech. 109, 1-24.

BROADWELL, J. E. and BREIDENTHAL, R. E. [1982] "A Simple Model of Mixing and Chemical Reaction in a Turbulent Shear Layer", J. Fluid Mech. 125, 397-410.

BROADWELL, J. E. and DIMOTAKIS, P. E. [1986] "Implications of Recent Experimental Results for Modeling Reactions in Turbulent Flows", AIAA J. 24(6), 885-889.

BROADWELL, J. E. and MUNGAL, M. G. [1986] "The effects of Damköhler number in a turbulent shear layer", GALCIT Report FM86-01.

BROWN, G. L. and REBOLLO, M. R. [1972] "A Small, Fast-Response Probe to Measure Composition of a Binary Gas Mixture", AIAA J. 10(5), 649-652.

BROWN, G. L. and ROSHKO, A. [1974] "On Density Effects and Large Structure in Turbulent Mixing Layers", J. Fluid Mech. 64(4), 775-816.

DIMOTAKIS, P. E. [1986] "Two-Dimensional Shear-Layer Entrainment", AIAA J. 24(11), 1791-1796.

DIMOTAKIS, P. E. and BROWN, G. L. [1976] "The Mixing Layer at High Reynolds Number: Large-Structure Dynamics and Entrainment", J. Fluid Mech. 78(3), 535-560 + 2 plates.

FIEDLER, H. E. [1975] "On Turbulence Structure and Mixing Mechanism in Free Turbulent Shear Flows", from: (S. N. B. Murthy, Ed.) Turbulent Mixing in Non-Reactive and Reactive Flows (Plenum Press), 381-409.

GIBSON, C. H. [1968] "Fine Structure of Scalar Fields Mixed by Turbulence. II. Spectral Theory", Phys. Fluids 11(11), 2316-2327.

GURVICH, A. S. and YAGLOM, A. M. [1967] "Breakdown of Eddies and Probability Distributions for Small Scale Turbulence", Phys. Fluids (1967 Sup.), 59-65.

HERMANSON, J. C., MUNGAL, M. G. and DIMOTAKIS, P. E. [1987] "Heat Release Effects on Shear Layer Growth and Entrainment", AIAA J. 25(4), 578-583.

KERR, R. M. [1985] "Higher-order derivative correlations and the alignement of small-scale structures in isotropic numerical turbulence", J. Fluid Mech. 153, 31-58.

KOLLMAN, W. [1984] "Prediction of intermittency factor for turbulent shear flows", AIAA J. 22(4), 486-492.

KOLLMANN, W. and JANICKA, J. [1982] "The Probability Density Function of a Passive Scalar in Turbulent Shear Flows", Phys. Fluids 25, 1755-1769.

KOLMOGOROV, A. N. [1941] "Local structure of turbulence in an incompressible viscous fluid at very high Reynolds numbers", Dokl. Akad. Nauk SSSR 30, 299, reprinted in Usp. Fiz. Nauk 93, 476-481 (1967), transl. in Sov. Phys. Usp. 10(6), 734-736 (1968).

KOLMOGOROV, A. N. [1962] "A refinement of previous hypotheses concerning the local structure of turbulence in a viscous incompressible fluid at high Reynolds number", J. Fluid Mech 13, 82-85.

KONRAD, J. H. [1976] An Experimental Investigation of Mixing in Two-Dimensional Turbulent Shear Flows with Applications to Diffusion-Limited Chemical Reactions, Ph.D. Thesis, California Institute of Technology, and Project SQUID Technical Report CIT-8-PU (December 1976).

KOOCHESFAHANI, M. M. and DIMOTAKIS, P. E. [1986] "Mixing and chemical reactions in a turbulent liquid mixing layer", J. Fluid Mech. 170, 83-112.

LUNDGREN, T. S. [1982] "Strained Spiral Vortex Model for Turbulent Fine Structure", Phys. Fluids 25(12), 2193-2203.

LUNDGREN, T. S. [1985] "The concentration spectrum of the product of a fast bimolecular reaction", Chem. Eng. Sc. 40(9), 1641-1652.

MANDELBROT, B. [1976] "Intermittent turbulence and fractal dimension: kurtosis and the spectral exponent 5/3 + B", Turbulence and the Navier Stokes Equations (Conf. Proc., U. Paris-Sud, Orsay, 12-13 June 1975, Publ: Lecture Notes in Mathematics 565, Ed. A. Dold, B. Eckmann, Springer-Verlag), 121-145.

MARBLE, F. E. and BROADWELL, J. E. [1977] "The coherent flame model for turbulent chemical reactions", Project SQUID Technical Report TRW-9-PU.

MONIN, A. S. and YAGLOM, A. M. [1975] Statistical Fluid Mechanics: Mechanics of Turbulence 2 (English translation of the 1965 Russian text. Ed. J. L. Lumley, MIT Press).

MUNGAL, M. G. and DIMOTAKIS, P. E. [1984] "Mixing and combustion with low heat release in a turbulent mixing layer", J. Fluid Mech. 148, 349-382.

MUNGAL, M. G, HERMANSON, J. C. and DIMOTAKIS, P. E. [1985] "Reynolds Number Effects on Mixing and Combustion in a Reacting Shear Layer", AIAA J. 23(9), 1418-1423.

NOVIKOV, E. A. [1961] "Energy Spectrum of an Incompressible Fluid in Turbulent Flow", Reports Ac. Sc. USSR 139(2), 331-334, translated in Sov. Phys. Doklady 6(7), 571-573 (1962).

OBOUKHOV, A. M. [1962] "Some specific features of atmospheric turbulence", J. Fluid Mech. 13, 77-81.

POPE, S. B. [1985] "PDF Methods for Turbulent Reactive Flows", Prog. Energy Comb. Sc. 11, 119-192.

ROGERS, M. M., MOIN, P. and REYNOLDS, W. C. [1986] "The Structure and Modeling of the Hydrodynamic and Passive Scalar Fields in Homogeneous Turbulent Shear Flow", Stanford University Report TF-25.

ROSHKO, A. [1976] "Structure of Turbulent Shear Flows: A New Look", AIAA J. 14, 1349-1357, and 15, 768.

SAFFMAN, P. G. [1968] Topics in Non-Linear Physics (Ed. N. Zabusky, Springer-Verlag, Berlin), 485-614.

SPENCER, B. W. and JONES, B. G. [1971] "Statistical Investigation of Pressure and Velocity Fields in the Turbulent Two Stream Mixing Layer", AIAA Paper No. 71-613.

SREENIVASAN, K. R., TAVOULARIS, S. and CORRSIN, S. [1981] "A Test of Gradient Transport and its Generalizations", 3rd International Symposium on Turbulent Shear Flows, U. C. Davis, 9-11 September 1981 (Published by Springer-Verlag 1982, Eds. Bradbury, L. J. S., Durst, F., Launder, B. E., Schmidt, F. W. and Whitelaw, J. H. Turbulent Shear Flows 3), 96-112.

TENNEKES, H. and LUMLEY, J. L. [1972] A First Course in Turbulence (MIT Press).

TOWNSEND, A. A. [1951] "On the fine structure of turbulence" Proc. Roy. Soc. A 208, 534-542.

VAN ATTA, C. W. and ANTONIA, R. A. [1980] "Reynolds number dependence of skewness and flatness factors of velocity derivatives", Phys. Fluids 23(2), 252-257.

WYGNANSKI, I. and FIEDLER, H. E. [1970] "The Two Dimensional Mixing Region", J. Fluid Mech. 41(2), 327-361.

Appendix D

DIMOTAKIS, P. E. and HALL, J. L. [1987] "A simple model for finite chemical kinetics analysis of supersonic turbulent shear layer combustion", AIAA/SAE/ASME/ASEE 23rd Joint Propulsion Meeting (La Jolla, CA), 29 June - 1 July 1987, AIAA Paper 87-1879.

AIAA'87

AIAA-87-1879

A Simple Model for Finite Chemical Kinetics Analysis of Supersonic Turbulent Shear Layer Combustion

P. E. Dimotakis, and J. L. Hall
California Institute of
Technology, Pasadena, CA

AIAA/SAE/ASME/ASEE 23rd Joint Propulsion Conference

June 29-July 2, 1987/San Diego, California

A SIMPLE MODEL FOR FINITE CHEMICAL KINETICS ANALYSIS OF SUPERSONIC TURBULENT SHEAR LAYER COMBUSTION†

by,

Paul E. Dimotakis* and Jeffery L. Hall*

Graduate Aeronautical Laboratories
California Institute of Technology
Pasadena, California 91125

ABSTRACT

A simple flow/thermodynamic model is proposed to describe finite chemical kinetic rate combustion in a turbulent supersonic shear layer for the purposes of assessing Damköhler number effects in such flows. Sample calculations and comparisons for the $H_2/NO/F_2$ chemical system and the H_2/air system are described for a set of initial flow and thermodynamic conditions of the entrained reactants.

1. INTRODUCTION

The advent of supersonic chemical lasers and the resurgent interest in hypersonic flight has extended the range of flows for which estimates of the rate of molecular mixing and combustion are required to compressible high speed turbulent flows. In this flow environment, the chemical kinetics of fuel/oxidizer systems that are conventionally regarded as fast may find themselves in a regime where the rate of mixing, as dictated by the hydrodynamics, can overwhelm the rate of chemical product formation and associated heat release.

We can conceptually cast this discussion in terms of some characteristic fluid mechanical molecular mixing time (τ_m), and chemical reaction time (τ_χ), and their dimensionless ratio, i.e. the Damköhler number, defined by

$$Da = \frac{\tau_m}{\tau_\chi} . \qquad (1)$$

We note that in the limit of $Da \to \infty$ chemical production must be regarded as taking place in the strained diffusion layers (flame sheets) that are formed within the extent of the turbulent mixing region between the reactant-bearing fluids, which are entrained from each of the free streams; the lean entrained reactant does not have a chance to interdiffuse and homogenize on a molecular scale before it is has reacted. In that limit, therefore, the rate of chemical product formation is equal to the rate at which the lean reactant is diffusing (on a molecular scale) into fluid entrained from the other stream. In that case, the rate of chemical product formation will be dictated by the hydrodynamic entrainment and turbulent mixing processes and, in particular, will be independent of the chemical kinetics. On the other hand, we note that as the Damköhler number is decreased an increasing portion of the entrained fluids will have a chance to mix and homogenize on a molecular scale before the reactants in that portion have a chance to react. Finally, if the fluid mechanics may be treated as unaltered by variations in the chemical kinetic rate, it is evident that the chemical product formation and associated heat release attain their maximum in the limit of $Da \to \infty$. It is not possible to make any more product per unit time than the rate at which molecular diffusion of the reactants proceeds.

Efficient hypersonic propulsion requires that the associated turbulent combustion be realized in as high a Damköhler number regime as is feasible. For experiments in high Reynolds number and/or supersonic turbulence which attempt to estimate the extent of molecular mixing within the turbulent region, this is also an important regime; direct measurements of mixing, in view of the associated time and space scales, are generally out of the question. On the other hand, in a flow/kinetic rate regime in which the Damköhler number is sufficiently high, chemical reactions suggest themselves as the diagnostic probe of choice, since the heat release, or other associated chemical products, can serve as unambiguous markers for molecular mixing.

---

* Professor, Aero. & Appl. Phys. (member AIAA).

* Graduate student, Aeronautics.

A model which first considered the relative effects of mixing rate and chemical kinetic rate was formulated by Broadwell (1974) in an attempt to analyze supersonic HF chemical laser performance. In that model, "the mixing is treated in an idealized way with the rate characterized by a single parameter, the angle at which the mixing zone spreads. The mixing, the chemical reactions, and lasing are allowed to occur simultaneously". By means of this model, a serious discrepancy between the premixed (constant mass) chemical reactor models (e.g. Emanuel & Whittier 1972), which were being used to analyze the supersonic shear layer chemical laser performance, and the observed dependence of the laser power on the cavity pressure was resolved.

An important addition to this idea was contributed by Konrad (1976) who concluded, on the basis of direct measurements of composition in (subsonic) shear layers, that the fluid carried in the free streams of a shear layer is entrained into the mixing region asymmetrically; for equal density free streams, the high speed stream is entrained preferentially. An explanation for this asymmetry, and a simple model for estimating the entrainment ratio E was proposed recently (Dimotakis 1986). These considerations suggested a zeroth order model for mixing in which the principal role of turbulence, following the initial stage of entrainment into the layer, is one resulting in a homogenization of the entrained fluids (and reactants) at a composition corresponding to the entrainment ratio E, i.e. to a high speed fluid mixture fraction ξ_E, given by

$$\xi_E = \frac{E}{E+1} \,. \qquad (2)$$

This simple picture was used by Konrad to account for the dependence of his composition fluctuations on the free stream density ratio. See figure 1.

Fluid that is mixed at the composition ξ_E of equation 2 plays an important role in the Broadwell & Breidenthal model (1982), in which the mixed fluid is partitioned as comprised of homogeneously mixed fluid at this composition and also as residing in strained diffusion layers. In this partition, the homogeneously mixed fluid volume fraction is regarded as a constant of the flow, and (for a given stoichiomentric mixture ratio) the volume fraction of the fluid residing in the flame sheets is assigned a volume fraction that is inversely proportional to the square root of the product of the flow Reynolds number and the fluid Schmidt number (this was the suggestion in the revised discussion of the model in Broadwell & Mungal 1986). This model was recently used by Broadwell & Mungal (1986) as the basis for their analysis of the experimental investigation of finite Damköhler number effects in a subsonic shear layer by Mungal & Frieler (1985). Broadwell & Mungal assumed that the rate of formation of the chemical product can be similarly partitioned as taking place within a homogeneously mixed fluid fraction and a flame sheet fluid fraction, where the assignement of these fractions is the same as the one made for the amount of chemical product in the original Broadwell & Breidenthal formulation.

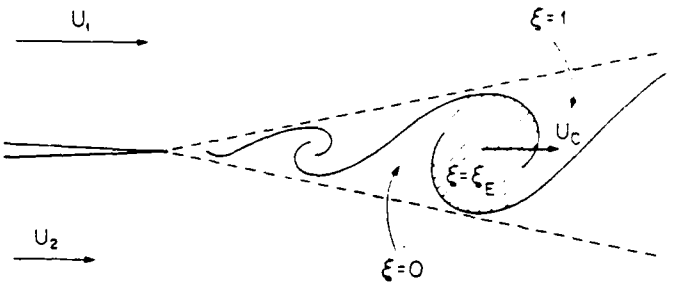

FIG. 1 Shear layer entrainment and growth.

We will not adopt the Broadwell-Mungal description of chemical product formation, primarily because it will serve our purposes to base the present discussion on an even simpler flow/thermodynamics model that will allow a realistic account of the chemical kinetics dynamics to be computed relatively readily.

2. THE PROPOSED MODEL

It is our purpose in this discussion to explore the interrelation between the rate of entrainment and mixing, and finite chemical kinetics in high Reynolds number shear layers, extending to supersonic flow. We will attempt to do this in the simplest terms that capture the salient features of this behavior, using two fuel/oxidizer systems as examples: the $H_2/NO/F_2$ system and the H_2/air system. While some of our results will be peculiar to these two systems, many of the conclusions are general and we would like to hope that the adopted simple formulation and implementation can serve as a useful guide.

The proposed scheme has three main components:

1. the entrainment/mixing model,

2. the thermodynamic model,

and

3. chemical kinetic model.

2.1 Entrainment/mixing formulation

We will adopt the simple idea suggested by Konrad (1976), namely the one which views the molecularly mixed fluid in the shear layer as homogenized at a single-valued composition dictated by the entrainment ratio E (cf. equation 2). The entrainment ratio E will, in turn, be computed using the simple ideas discussed by Dimotakis (1986). Briefly, it was argued in that discussion that the (volumetric) entrainment ratio should be approximated by

$$E = \frac{U_1 - U_c}{U_c - U_2} \left(1 + \frac{\ell}{x}\right), \qquad (3)$$

where $U_{1,2}$ are the high and low speed shear layer free stream velocities respectively, U_c is the convection velocity of the large structures in the layer, and ℓ/x is the large structure spacing to position ratio.

For subsonic flow, the convection velocity can be estimated by applying the Bernoulli equation in the large structure convection frame, in which it should (approximately) apply on the streamlines through the stagnation points in between the vortices. This yields (for equal free stream static pressures),

$$\rho_1 (U_1 - U_c)^2 = \rho_2 (U_c - U_2)^2,$$

or,

$$\frac{U_1 - U_c}{U_c - U_2} = \left(\frac{\rho_1}{\rho_2}\right)^{1/2}. \qquad (4)$$

The large structure spacing to position ratio ℓ/x is found (empirically) to be independent of the density ratio and approximately given by

$$\frac{\ell}{x} = 0.68 \frac{1 - U_2/U_1}{1 + U_2/U_1}. \qquad (5)$$

Combining these results, one then obtains an estimate for the volumetric entrainment ratio for subsonic flow given by

$$E = \left(\frac{\rho_1}{\rho_2}\right)^{1/2} \left(1 + 0.68 \frac{1 - U_2/U_1}{1 + U_2/U_1}\right). \qquad (6)$$

For supersonic flow, the convection velocity can be approximated using the isentropic relations connecting the stagnation pressure (in the vortex convection frame) and the static pressure in each of the free streams, which for equal free stream static pressures yields the implicit relation

$$\left(1 + \frac{\gamma_1 - 1}{2} M_{c1}^2\right)^{\gamma_1/(\gamma_1 - 1)} = \left(1 + \frac{\gamma_2 - 1}{2} M_{c2}^2\right)^{\gamma_2/(\gamma_2 - 1)}, \qquad (7)$$

where $\gamma_{1,2}$ are the ratios of specific heats in each of the free streams and

$$M_{c1} = \frac{U_1 - U_c}{a_1}, \qquad M_{c2} = \frac{U_c - U_2}{a_2}, \qquad (8)$$

are the convective Mach numbers, with $a_{1,2}$ the speeds of sound in the high and low speed free streams respectively. This relation was proposed by Bogdanoff (1983) on the basis of a different set of arguments. We note here that for low to moderate supersonic free stream Mach numbers $M_{1,2}$, the convective Mach numbers will not be too high and the incompressible relation (equation 4) may serve as an adequate approximation.

While there is insufficient information to establish a reliable relation for ℓ/x for supersonic flow, it is a probably a fair guess that ℓ/x will continue to be scaled by the shear layer growth rate δ/x. Additionally, it is known (Papamoschou 1986) that a supersonic shear layer at the same velocity and density ratio will, for high values of the convective Mach number, grow considerably slower (by a factor of approximately 5) than its incompressible counterpart. This suggests that, at high convective Mach numbers, ℓ/x may be estimated by

$$(\ell/x)_{M_{c1} > .5} = 0.2 \, (\ell/x)_{M_{c1} < .25}, \qquad (9)$$

where ℓ/x at low convective Mach numbers ($M_{c1} < .25$) can be estimated using equation 5. Accordingly, the second factor $(1 + \ell/x)$ in the basic relationn for the entrainment ratio (equation 3) will be much closer to unity for (high) supersonic flow ($M_{c1} \geq 0.5$) than for subsonic flow.

We can visualize the mixing process, in this picture, as the flow through two streamtubes (generally of unequal cross-section), with inlet

velocities $U_1 - U_c$ and $U_c - U_2$ respectively, filling the molecularly mixed fluid balloon (at constant pressure) with a mole rate that is the sum of the two entrainment contributions from each of the free streams. The total number of moles $n_T(t)$ in the balloon, at any one time $t = x/U_c$ represents the total number of moles of molecularly mixed fluid in the layer, corresponding to a mixed fluid thickness δ_m. This is smaller than the total shear layer thickness δ, to the extent that only a (mole) fraction δ_m/δ of the fluid within the shear layer wedge boundaries is mixed on a molecular scale. The ratio of the two entrainment feed rates $\dot{n}_{1,e}$ and $\dot{n}_{2,e}$ are then computed in accord with the entrainment ratio while the total feed rate is such as to yield the correct value of $\delta_m(t)$, at each station $x = tU_c$. See figure 2.

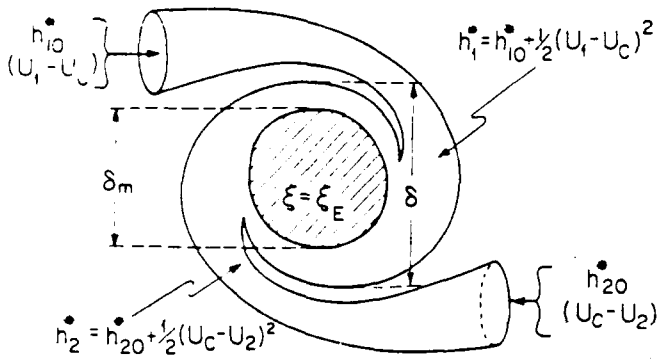

FIG. 2 Convective frame entrainment/mixing schematic.

The species composition in each of the free streams is specified via the mole fractions X_{α_i} of the species α carried by the i-th stream. This yields an entrainment feed rate for the species α from each of the free streams, given by

$$\dot{n}_{\alpha_i} = X_{\alpha_i} \dot{n}_{i,e} , \quad i = 1,2 . \tag{10}$$

The contents of the balloon are regarded as homogeneously mixed at all times, the respective feed rates guaranteeing the correct composition (equation 2) thereby. That neighboring balloons (large scale structures) coalesce from time to time to produce larger balloons of the same composition does not alter this picture as far as the chemical dynamics are concerned.

Before leaving the discussion of the entrainment/mixing component of the model, we should note that an important ingredient of the turbulent mixing process is ignored by this simple picture. It is the effect of the rapid increase in the rate of strain experienced by a particular segment of the strained reactant interface between the two entrained fluids, as it cascades in its Lagrangian frame to the smallest scales at which it ultimately homogenizes on a molecular scale. Ignoring this effect will result in an overestimation of the effective chemical kinetic rate, as we will discuss below.

2.2 Thermodynamics formulation

To compute the chemical kinetics of the system, we need to keep track of the temperature evolution in the homogeneous reactor. In particular, in addition to the heat released in the chemical reactions, we need to estimate the enthalpy flux which the entrained fluids contribute to the total enthalpy of the contents of the balloon. This will be computed by assuming that the entrained fluids are approximately brought to rest in the balloon (large scale) convection frame adiabatically. This yields an estimate for the stagnation enthalpy contributed in this frame from each of the free streams given by

$$h_{i,e}^* = h_{i,0}^* + \frac{1}{2}(U_i - U_c)^2 ,$$

where $i = 1,2$ corresponds to the high and low speed streams respectively, $h_{i,e}^*$ is the resulting specific stagnation enthalpy (J/kg) contributed by the i-th stream in the convection frame and $h_{i,0}^*$ is the specific (static) enthalpy of the i-th free stream. It will be convenient to express quantities in molar form for the chemical calculations below. Accordingly, we have for the molar enthalpy (J/kmole) of each stream

$$h_{i,e} = h_{i,0} + \frac{1}{2}\langle W \rangle_i (U_i - U_c)^2 , \tag{11}$$

where $\langle W \rangle_i$ is the (mean) molecular weight of the i-th stream.

Assuming that the balloon can be treated as an adiabatic system and that the kinetic energy of the internal motion (in the balloon convection frame) is negligible†, we obtain the energy equation (at constant pressure)

$$\dot{H}_T = \dot{H}_e = \dot{n}_{1,e} h_{1,e} + \dot{n}_{2,e} h_{2,e} . \tag{12}$$

† The latter assumption may have to be revised at very high convective Mach numbers.

where H_T is the total enthalpy of the contents of the balloon. Chemical reactions and combustion notwithstanding, the total enthalpy changes only as a consequence of the entrainment contribution.

The total enthalpy of the system is also expressible (for an ideal gas) as the sum of the molar contributions. Differentiating with respect to time, we have

$$\dot{H}_T = \sum_\alpha (\dot{n}_\alpha h_\alpha + n_\alpha \dot{h}_\alpha) .$$

We can use the relation $\dot{h}_\alpha = c_{p\alpha} \dot{T}$, where $c_{p\alpha}$ is the molar heat capacity at constant pressure of the α species and T is the balloon temperature, and combine with equation 12 to obtain the temperature evolution equation (at constant pressure), i.e.

$$C_p \dot{T} = \dot{H}_e - \sum_\alpha \dot{n}_\alpha h_\alpha , \qquad (13)$$

where C_p is the total heat capacity of the system contents at constant pressure and $\dot{n}_\alpha$ is the total rate of change of the number of moles of the α species (sum of entrainment feeds plus chemistry), i.e.

$$\dot{n}_\alpha = \dot{n}_{\alpha_1} + \dot{n}_{\alpha_2} + \dot{n}_{\alpha_\chi} . \qquad (14)$$

2.3 Chemical kinetics formulation

The chemical kinetics calculations are realized using the CHEMKIN (Kee et al 1980) code package. In particular, borrowing from their description, we have for the j-th chemical equation

$$\sum_\alpha a_{\alpha j} \chi_\alpha \rightleftarrows \sum_\alpha b_{\alpha j} \chi_\alpha , \qquad (15)$$

where the $a_{\alpha j}$ and $b_{\alpha j}$ are the (integer) stoichiometric coefficients and χ_α is the chemical symbol of the α species. The production rate [kmoles/(m^3·sec)] for the species α is then computed as the sum over all the chemical reactions, i.e.

$$\dot{\omega}_\alpha = \sum_j (b_{\alpha j} - a_{\alpha j}) q_j , \qquad (16)$$

where q_j is the rate of progress variable for the j-th chemical reaction, computed as the difference between the forward and reverse rates. For a two-body chemical reaction, this is given by

$$q_j^{(2)} = k_{f,j} \prod_\alpha [\alpha]^{a_{\alpha j}} - k_{r,j} \prod_\alpha [\alpha]^{b_{\alpha j}} , \qquad (17a)$$

where $[\alpha] = n_\alpha / V$ is the molar concentration of the α species with $V = V(t)$ the balloon volume, and $k_{f,j}$ and $k_{r,j}$ are the forward and reverse rate constants for the j-th reaction. For a three-body chemical reaction the rate of progress variable is computed as

$$q_j^{(3)} = \Big(\sum_\alpha n_{\alpha j} [\alpha] \Big) q_j^{(2)} , \qquad (17b)$$

where if all species contribute equally to the reaction (e.g. any third body M in the vernacular) the efficiency coefficients $n_{\alpha j}$ are all equal to unity and the first factor in the expression for $q_j^{(3)}$ is given by (ideal gas law)

$$\sum_\alpha n_{\alpha j} [\alpha] = \sum_\alpha [\alpha] = \frac{n_T}{V} = \frac{p}{RT} . \qquad (18)$$

The forward rate constants are computed assuming an Arrhenius temperature dependence form, i.e.

$$k_{f,j}(T) = A_j T^{\beta j} \exp\Big(-\frac{E_j}{RT}\Big) , \qquad (19)$$

while the reverse rate constants $k_{r,j}$ are related to the forward rate constants through the equilibrium constants of the j-th reaction. The coefficients A_j, β_j and E_j, as well as any non-unity three-body efficiency coefficients $n_{\alpha j}$, must be specified for each chemical reaction j.

Using equation 16 for the species production rate, we then compute the chemical rate of change of the number of moles of the species α as needed in equation 14, using the relation

$$\frac{1}{V(t)} \dot{n}_{\alpha_\chi}(t) = \dot{\omega}_\alpha(t) \qquad (20)$$

where V(t) is the volume of the balloon, computed in turn using the ideal gas law equation of state, i.e.

$$V(t) = n_T(t) \frac{RT(t)}{p} , \quad n_T(t) = \sum_\alpha n_\alpha(t) . \qquad (21)$$

The chemical reactions describing the $H_2/NO/F_2$ system are listed in the appendix, with the Arrhenius coefficients for each reaction j. The H_2/air system was used as documented in Smooke et al (1983). By way of example, if a particular species A is entrained as part of the high speed fluid with a mole fraction X_{A_1} and as part of the

low speed fluid with a mole fraction X_{A_2}, and participates in a (say, j = 1) chemical reaction

$$A + B \rightleftarrows C + D$$

its evolution equation would be given by (note that $a_{A_1} = a_{B_2} = 1$, in this case)

$$\frac{1}{V}\dot{n}_A = \frac{1}{V}\left(X_{A_1}\dot{n}_1 + X_{A_2}\dot{n}_2\right) - k_{f,1}\left(\frac{n_A}{V}\right)\left(\frac{n_B}{V}\right) + \ldots \qquad (22)$$

The manner in which the volume V = V(t) enters on the left hand side is, perhaps, noteworthy.

2.4 Model implementation

Having specified the entrainment/mixing infusion history $\dot{n}_1(t)$ and $\dot{n}_2(t)$, the temporal evolution of the flow/chemical system can be computed in the convective frame (which we can transform to the fixed shear layer combustor frame via the convective velocity, i.e. $x = t\,U_c$).

For an arbitrary history $\dot{n}_1(t)$ and $\dot{n}_2(t)$, the resulting non-linear system of equations is sufficiently complex to render drawing of general conclusions difficult. While such an arbitrary case can readily be studied numerically, it is possible to gain valuable insight by restricting the discussion to constant $\dot{n}_1$ and $\dot{n}_2$, as appropriate anyway to turbulent shear layers beyond the mixing transition (Bernal et al 1979). Additionally, in the model, we will allow the balloon reactor to be precharged with an initial amount and composition of reactants and at an initial thermodynamic state (temperature T_0) comnputed by assuming that while the entrainment has proceeded starting from t = 0, the chemistry is not initiated until a time $t = t_0 = x_0 / U_c$.

The latter provision should be a useful approximate description in the case of hypergolic (or near-hypergolic) reactants that have been entrained (but not as yet mixed) and which are mixed on a molecular scale rather abruptly as they move through the mixing transition at $x_0 = x_{tr}$, or, in the case of non-hypergolic reactants (for the flow conditions) that are allowed to mix and are ignited (by some external means) at some convective time $t_0 = t_{ig} = x_{ig} / U_c$. This is equivalent to an entrainment/mixing infusion history given by

$$\int_0^t \dot{n}_i(t')\,dt' = \begin{cases} 0, & t < t_0, \\ t\,\dot{n}_{i_\infty}, & t > t_0, \end{cases} \qquad (23)$$

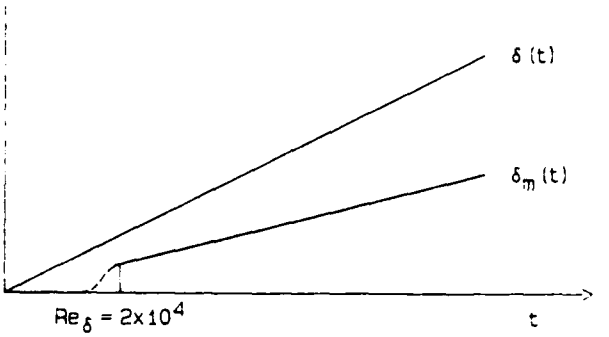

FIG. 3 Shear layer total and mixed fluid thickness.

where $\dot{n}_{i_\infty}$ corresponds to the constant entrainment/mixing infusion rate from the i-th stream, far downstream from the transition/ignition region. This situation is depicted in figure 3, and is reflected in the growing total shear layer thickness $\delta(t)$, corresponding to the constant rate (per unit time in the convective frame) at which fluid is entrained (inducted) into the layer, and $\delta_m(t)$ corresponding to the constant infusion (contribution per unit time to the mixed fluid) flux the resulting balloon reactor (molecularly mixed fluid) volume V(t). In this picture, the balloon volume V(t), per unit span of shear layer, is to be viewed as the product of a fixed streamwise thickness dx and the mixed fluid thickness $\delta_m(t)$.

Finally, we note that implicit in this discussion is the assumption that the effects of heat release on the fluid dynamics are small. In the context of the present model, the relevant question is the effect of the heat release on the entrainment ratio. At least for subsonic flow, this issue was specifically addressed in the work documented in Hermanson (1985) and Hermanson et al (1987). Based on the conclusions drawn from that work, one could certainly provide corrected estimates for $\dot{n}_1$ and $\dot{n}_2$ as a function of heat release. On the other hand, the main conclusion in that discussion was that these effects are small and would therefore be unwarranted by, and inconsistent with the spirit of the simple flow/mixing model proposed here.

3. RESULTS and DISCUSSION

3.1 General properties

Assuming that the entrainment/mixing flux $\dot{n}_i$ from the i-th stream is as described in the preceding section, we may draw the following useful conclusions.

Provided it ignites and that the entrained reactants do not quench the reaction, the system (balloon reactor contents) reaches a final equilibrium temperature T_f which is equal to the adiabatic flame temperature of a constant mass reactor at chemical equilibrium, corresponding to an atomic composition dictated by the entrainment/mixing flux ratio E. As a corollary, we have $\dot{V}$ = constant and therefore V(t) ~ t at equilibrium, since $\dot{n}_T$ = constant, p = constant, and, in the limit, T = constant.

The second important conclusion is that if the lean (or rate-limiting) reactant is entrained from, say, the high speed stream (stream 1), the evolution of the system is a function of a single dimensionless parameter

$$\Omega_1 = \frac{\dot{n}_1 \tau_\chi}{n_1(t_0^+)} , \qquad (24)$$

where $n_1(t_0^+)$ is the (precharge) number of stream 1 moles at $t = t_0^+$, $\dot{n}_1$ is the (constant) entrainment/mixing rate from stream 1, and τ_χ is the characteristic chemical time, defined here as the maximum slope thickness intercept of the T(t) curve with the $T = T_f$ line for a constant mass reactor, as will be illustrated below. In particular, for $\Omega \ll 1$, as we would expect, the system evolution is the same as that of a constant mass reactor, since the asymptotic temperature rise will be realized before any substantial amounts of entrained reacts have been added. In the opposite limit of $\Omega \gg 1$, however, the important and perhaps surprising conclusion is that not only the final equilibrium state but also the system evolution is independent of the entrainment/mixing rate $\dot{n}_1$. This behavior is depicted in figure 4, in which the scaled temperature rise in the mixed fluid reactor, i.e.

$$\frac{\Delta T(t)}{\Delta T_f} = \frac{T(t) - T_0}{T_f - T_0} , \qquad (25)$$

is plotted as a function of time, for a typical low heat release $H_2/NO/F_2$ reactant/diluent combination as used in the Mungal & Dimotakis (1984) data and in the Mungal & Frieler 1985 Damköhler number study. The solid curve corresponds to the evolution of a constant mass ($\Omega = 0$) reactor. The dashed line is the maximum slope extrapolation of that curve, used to compute the intercept with $\Delta T(t)/\Delta T_f = 1$ at the time $t = \tau_\chi$. Finally, the dot-dashed curve depicts the asymptotic, entrainment-dominated reactor (computed using a value of $\Omega = 100$). The behavior in the latter case is asymptotic in the sense that additional increases in Ω would not discernibly alter the resulting $\Delta T(t)/\Delta T_f$ curve.

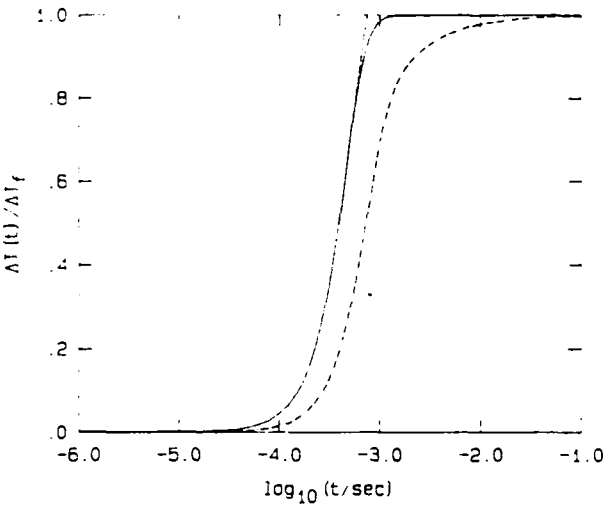

FIG. 4 Constant mass (solid line) vs. entrainment-dominated (dot-dashed line) mixed fluid reactor behavior.

3.2 Using the model

We will demonstrate the use of the proposed model by attempting a calculation of the Mungal & Frieler (1985) Damköhler number study data. In that experiment, the effective rate of reaction of the $H_2/F_2/NO$ system in the mixing zone was controlled by varying the concentration (mole fraction) of NO that was premixed with H_2 in the high speed stream. The experiments were conducted in the shear layer facility described in Mungal & Dimotakis (1984), with a free stream velocity ratio of $U_2/U_1 = 0.4$ and a density ratio $\rho_2/\rho_1 = 1$. The high speed stream was comprised of (mole fractions) 8% H_2, a nominal mole fraction of NO of $[NO]_* = 0.03\%$, and the rest N_2 at room temperature. The low speed stream was composed of 1% F_2 and 99% N_2, also at room temperature.

The H_2/F_2 reaction requires free F atoms, which under these conditions are produced via the $NO + F_2 \rightarrow NOF + F$ reaction (see Appendix A). The

kinetic rate can be reduced to zero in the absence of any free F atoms, a situation that is realized (under these conditions) if there is no premixed NO in the H_2 bearing stream. Accordingly, the kinetic rate controlling parameter in the experiments was the concentration of the premixed NO, that the authors cited normalized by the nominal concentration $[NO]_* = 0.03\%$. In particular, experiments were conducted at $[NO]/[NO]_* = 1/32$, 1/23, 1/16, 1/8, 1/4, 1/2, 1, 3/2 and 2 at the lower velocity runs ($U_1 = 22$ m/s), and at $[NO]/[NO]_* = 1/16$, 1/4, 1 and 2 at the higher Reynolds number run ($U_1 = 44$ m/s).

The experimental uncertainty in determining the amount of [NO] is estimated to be of the order of $0.03\,[NO]_*$ (laboratory record, G. Mungal private communication). The experimental uncertainty in the total amount of product, computed in those measurements as the volume fraction $\delta_p([NO])/\delta$ in the layer occupied by chemical product, was estimated to be of the order of 3% to 5%.

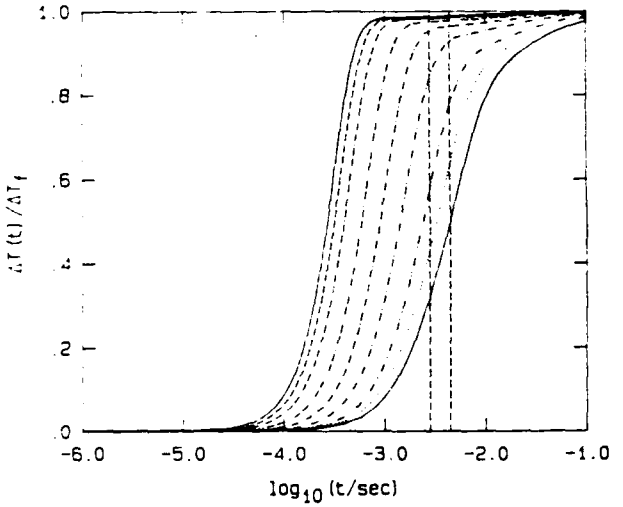

FIG. 5 $\Delta T(t)/\Delta T_f$ computed for Mungal & Frieler (1985) data. Curves from left to right for $[NO]/[NO]_*$ of 2, 3/2, 1, 1/2, 1/4, 1/8, 1/16, 1/23, 1/32. Vertical dashed lines for (scaled) times t' = 2.75 ms, 4.4 ms respectively (see text below).

The fact that the Reynolds number is different in the two sets of runs has, of course, no effect on the shape of the model $\Delta T(t)/\Delta T_f$ curves. Since other parameters were kept fixed, these curves are only a function of the $[NO]/[NO]_*$ ratio for these experiments. The results of the computations corresponding to the experimental conditions are plotted in figure 5 along with the Mungal & Frieler data and their experimental error bars.

The dependence of the chemical product δ_p/δ volume fraction on the $[NO]/[NO]_*$ ratio for the two Reynolds number runs is read off such a family of curves at a fixed Lagrangian time, which is different for each Reynolds number case. The reactor is precharged to the amount and composition corresponding to the conditions at the end of the mixing transition region, as described in section 2.4. The experimental Lagrangian time is given by

$$t = \frac{x - x_0}{U_c} , \qquad (26)$$

where x is the location of the fixed measuring station (= 45.7 cm), x_0 is taken to be at the end of the mixing transition (hypergolic reactants) at $\Delta U \cdot \delta/\nu = 2\times10^4$ (as recommended by Mungal & Frieler 1985), and U_c is the convection velocity. This yields estimates for the experimental Lagrangian time at the measuring station of t = 20.8 ms and t = 13.1 ms for the low and high Reynolds number experiments respectively.

In using the model to estimate the experimental data, we note that the reaction rate coefficients for the $H_2/NO/F_2$ system are better known than most rate coefficients. In particular, for that system they are known to within a factor of 3, or so. While it is not possible to make general statements without a specific sensitivity analysis, a qualitative estimate of the global effect of such an uncertainty on the calculated quantities can be made for the entrainment-dominated reactor ($\Omega \gg 1$) as follows. A rescaling of the reaction rate coefficients by a dimensionless scaling factor κ, i.e. $k'_{f,j} \rightarrow \kappa\, k_{f,j}$, produces the same chemical evolution as the unscaled coefficients did at a (scaled) time $t' = t/\kappa$.

There is an other, possibly more important, effect we have ignored that may have similar time-scaling consequences, namely the unsteady evolution of the rate of strain σ that is imposed by the turbulent field on the interface between the two interdiffusing fluids. In solving the unsteady diffusion problem, one can show that for times that are large compared to the reciprocal of the strain rate, i.e. for $t \gg 1/\sigma$, the solution to the unsteady diffusion problem in the presence of an imposed strain rate, tends asymptotically to those of the unsteady diffusion problem in the absence of an externally imposed strain rate, evaluated at a time $t = 1/\sigma$ (Carrier, Fendel & Marble 1975, Marble & Broadwell 1977, Dimotakis 1987). Accordingly, instead of interpreting the corresponding solutions as functions of the product of an effective kinetic rate k_* and time, i.e. $k_* t$, they should be interpreted as functions of the ratio k_*/σ. For a

two dimensional shear layer, the strain rates are scaled by $\Delta U/\delta$ and therefore $1/\sigma \sim \delta/\Delta U \sim t$. We should also mention that Broadwell & Mungal (1986), who provided an approximate solution for a finite kinetic rate analysis of a strained flame sheet using a control volume approach, also found that the solution dependence on the kinetic rate and rate of strain is via the group k_*/σ. Since the predominant fraction of molecularly mixed fluid is associated with the smallest scales of the turbulent flow, where not only the rate of strain σ is high but also the rate at which it, in turn, increases with Lagrangian time for each fluid element ($\dot{\sigma}$) is high, this effect is potentially important.

For both of these reasons we will accept an undetermined time scaling factor κ as an adjustable parameter. Uncertainties in the kinetic rate coefficients aside a more realistic hydrodynamic account of the turbulent entrainment/mixing process would hopefully remove the need for such an adjustment. We note here, however, that this is quite an aside, as many important kinetic rate coefficients are often uncertain by factors in excess of an order of magnitude.

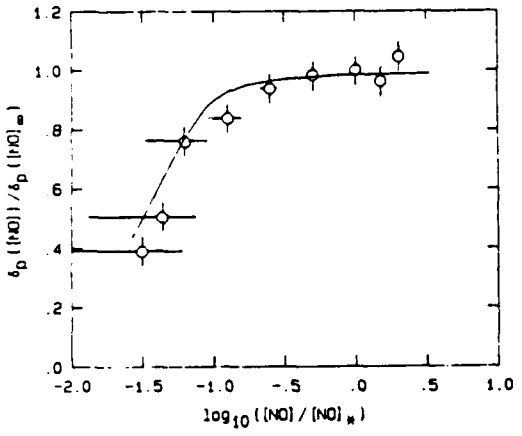

Fig 6a

The resulting computations are depicted in figures 6a and 6b, for the low and high Reynolds number runs respectively. The value of the time scaling factor used to compute these curves was $\kappa = 5$. The resulting (scaled) Lagrangian times t' corresponding to the two sets of data (t' = 4.4 ms, 2.75 ms, respectively) are indicated by the vertical dashed lines in figure 5.

Discounting for the need of the time-scaling factor κ, we see that the salient features of the data are captured correctly, especially considering the simplicity of the hydrodynamics description.

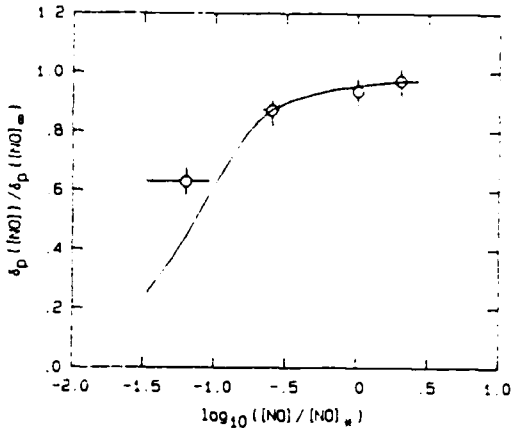

(b)

FIG. 6 $\delta_p([NO])/\delta p([NO]_*)$ for Mungal & Frieler (1985) data. (a) low Reynolds number data ($U_1 = 22$ m/s), (b) high Reynolds number data ($U_1 = 44$ m/s.

3.3 Supersonic $H_2/NO/F_2$ system calculations

Sample calculations at 1 Atm pressure for a supersonic high speed stream bearing H_2, NO and N_2 at $M_1 = 3.0$, and a subsonic low speed stream bearing F_2 and N_2 at $M_2 = 0.3$ and a stagnation temperature of 300 K were performed. The $\Delta T(t)/\Delta T_f$ evolution of the system is depicted in figure 7 for high speed stream stagnation temperatures of 300 K and 600 K at low reactant concetrations. Note that the difference in the final temperature rise ΔT_f in the two cases is due to the difference in the entrainment ratio. The increase in the effective chemical kinetic rate is manifest.

A study of an additional increase in the effective rate was undertaken by raising the reactant concentrations in both streams, keeping the stagnation temperatures for the high and low speed streams at 600 K and 300 K, respectively. The resulting calculations are depicted in figure 8.

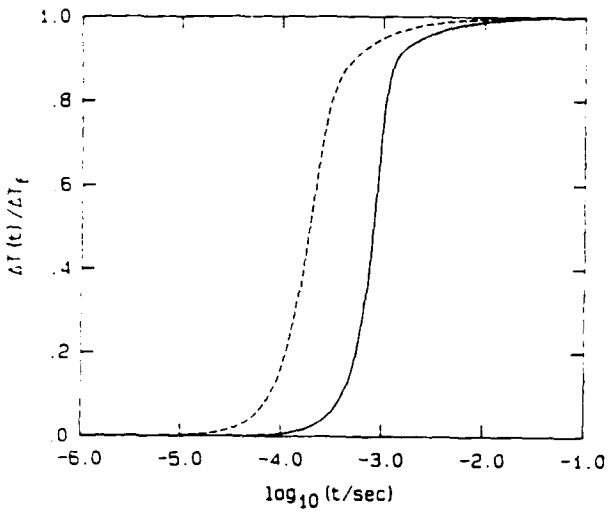

FIG. 7 $\Delta T(t)/\Delta T_f$ computed at 1 Atm (static) pressure, for a 2% H_2 / 0.1% NO / 97.9% N_2 M_1 = 3.0 stream, and a 2% F_2 / 98% N_2 stream at M_2 = 0.3 and a stagnation temperature of 300 K. Solid line and dashed line for a high speed stagnation temperature of 300 K (ΔT_f = 128 K) and 600 K (ΔT_f = 158 K) respectively.

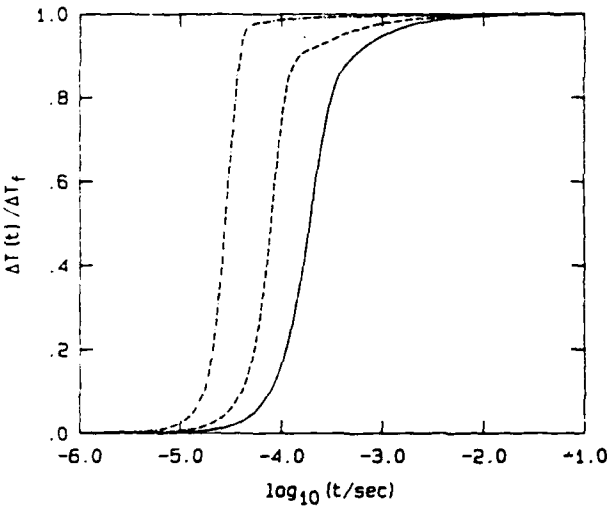

FIG. 8 $\Delta T(t)/\Delta T_f$ computed at 1 Atm (static) pressure, for a H_2/0.1%NO/N_2 stream at M_1 = 3.0 and a stagnation temperature of 600 K, and a F_2/N_2 stream at M_2 = 0.3 and a stagnation temperature of 300 K. Solid line for 2%H_2 and 2%F_2 (ΔT_f = 158 K), dashed line for 6%H_2 and 6%F_2 (ΔT_f = 459 K), dot-dashed line for 20%H_2 and 20%F_2 (ΔT_f = 1,353 K).

As can be ascertained from these calculations, characteristic chemical reaction times in the range of 10 μs to 1 ms can be attained by such means.

3.4 Supersonic H_2/air system calculations

Calculations using the H_2/air chemical system, with flow conditions for a hypothetical hypersonic vehicle are described below. It is assumed that the H_2 bearing stream has been preheated to 1,500 K, as it is utilized as a coolant, and additionally heated in a precombustion chamber using a portion of the inlet air, as required to reach a stagnation temperature of 2,200 K. It is subsequently discharged in the primary combustor at M_2 = 1.25 to form the low speed stream of a supersonic shear layer. The high speed stream is assumed to be air at a Mach number M_1 equal to 1/3 of the flight Mach number M_∞ and at a stagnation enthalpy corresponding to a static temperature of 300 K at M_∞.

Figure 9 depicts the resulting absolute temperature T(t) calculations, for a flight Mach number of M_∞ = 12 and (static) pressures in the shear layer combustion chamber of 0.75, 0.5 and 0.25 Atm. Note that whereas the reactants ignite increasingly rapidly as the pressure is raised, equilibrium is attained extremely slowly, as a consequence of energetic minor species which in turn reach their equilibrium concentrations extremely slowly (3 time decades), independently of the pressure at these conditions.

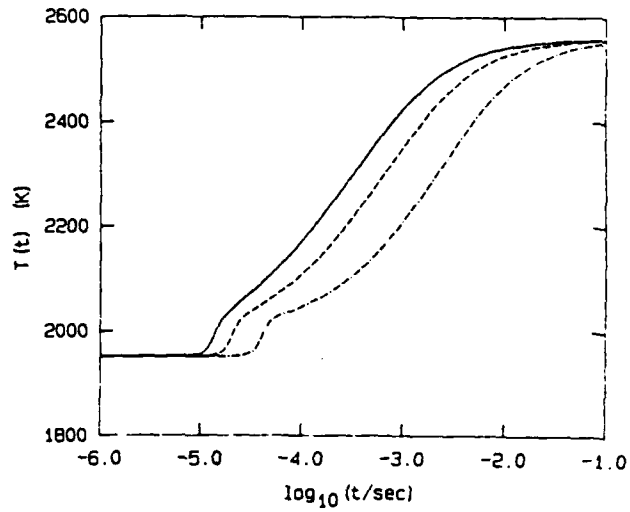

FIG. 9 T(t) computations for a hypothetical hypersonic flight vehicle at M_∞ = 12, for p = 0.75 Atm (solid line), p = 0.5 Atm (dashed line) and p = 0.25 Atm (dot-dashed line).

Calculations were also performed at a fixed static pressure of 0.5 Atm to illustrate the effect of flight Mach number M_∞. It is important to note that the main consequence of increasing M_∞ is the attendant increase in the initial mixture

temperature (T_0 in the notation of section 2.4).

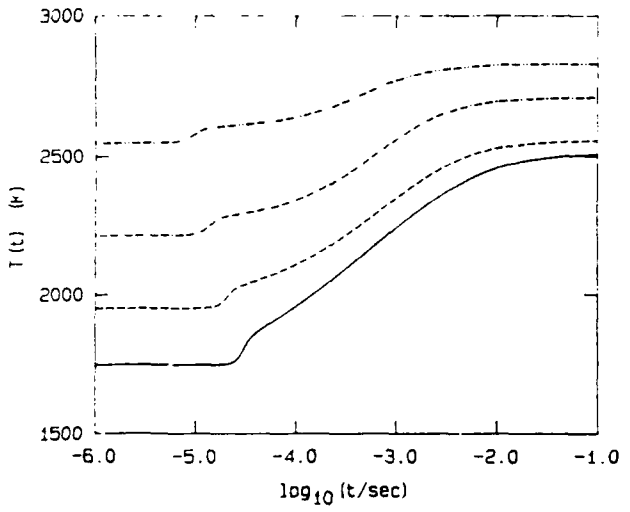

FIG. 10 T(t) computations for a hypothetical hypersonic flight vehicle at a static pressure of 0.5 Atm. Solid line for $M_\infty = 9$, dashed line for $M_\infty = 12$, dot-dashed line for $M_\infty = 15$ and dot-dot-dashed line for $M_\infty = 18$.

The conspicuous decrease in the equilibrium temperature rise ΔT_f is a consequence of the increasing participation in the final equilibrium population of energetic species, which under these *conditions of increasing absolute temperature* cannot really be considered as minor.

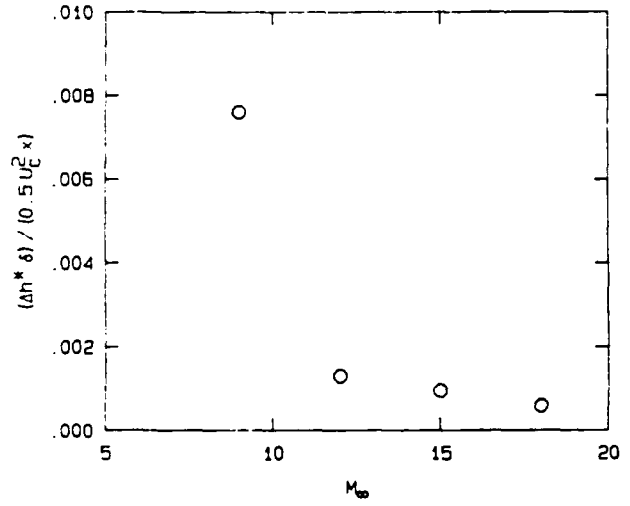

FIG. 11 Normalized specific enthalpy coefficient for hypothetical hypersonic shear layer combustor contribution.

In an effort to assess the relative contribution of the shear layer combustion to the overall enthalpy release, we have estimated the coefficient $2\Delta h^*/U_c^2$ of the specific enthalpy release at the end of a 1 meter shear layer combustor, multiplied by the estimated shear layer thickness δ/x, as computed from the data in figure 10. The results are depicted in figure 11. Note that the rapid decrease from $M_\infty = 9$ to $M_\infty = 12$ is a consequence of the transition of the δ/x growth rate to the supersonic regime ($M_{c_1} > 0.5$).

4. ACKNOWLEDGEMENTS

We would like to acknowledge the helpful discussions with Dr. G. Mungal. The work was supported by AFOSR Grant No. 83-0213.

5. REFERENCES

BAULCH, D. L., DUXBURY, J., GRANT, S. J., MONTAGUE, D. C. [1981] "Evaluated kinetic data for High Temperature Reactions", vol. 4, published in J. Phys. Chem. Ref. Data 10, Suppl. 1.

BERNAL, L. P., BREIDENTHAL, R. E., BROWN, G. L., KONRAD, J. H. and ROSHKO, A. [1979] "On the Development of Three Dimensional Small Scales in Turbulent Mixing Layers.", 2nd Symposium on Turbulent Shear Flows, 2-4 July 1979, Imperial College, England.

BOGDANOFF, D. W. [1983] "Compressibility Effects in Turbulent Shear Layers (TN)", AIAA J. 21(6), 926 - 927.

BROADWELL, J. E. [1974] "Effect of Mixing Rate on HF Chemical Laser Performance", Applied Optics 13, 962-967.

BROADWELL, J. E. and BREIDENTHAL, R. E. [1982] "A Simple Model of Mixing and Chemical Reaction in a Turbulent Shear Layer", J. Fluid Mech. 125, 397-410.

BROADWELL, J. E. and MUNGAL, M. G. [1986] "The effects of Damköhler number in a turbulent shear layer", GALCIT Report FM86-01.

CARRIER, G. F., FENDELL, F. E. and MARBLE, F. E. [1975] "The Effect of Strain on Diffusion Flames", SIAM J. Appl. Math. 29(2), 463-500.

COHEN, N. and BOTT, J. F. [1982] "Review of rate Data for reactions of Interest in HF and DF lasers", The Aerospace Corporation, report SD-TR-82-86.

DIMOTAKIS, P. E. [1986] "Two-Dimensional Shear-Layer Entrainment", AIAA J. 24(11), 1791-1796.

DIMOTAKIS, P. E. [1987] "Turbulent shear layer mixing with fast chemical reactions", US-France Workshop on Turbulent Reactive Flows, 7-10 July 1987 (Rouen, France), 9.1-106 (GALCIT Report FM87-01).

EMANUEL, G. and WHITTIER, J. S. [1972] "Closed-Form Solution to Rate Equations for an F + H_2 Laser Oscillator", Appl. Optics 11(9), 2047-2056.

KEE, R. J., MILLER, J. A., and JEFFERSON, T. H. [1980] "CHEMKIN: A General Purpose, Problem-independent, Transportable, Fortran Chemical Kinetics Code Package", SANDIA Report SAND80-8003.

KONRAD, J. H. [1976] An Experimental Investigation of Mixing in Two-Dimensional Turbulent Shear Flows with Applications to Diffusion-Limited Chemical Reactions, Ph.D. Thesis, California Institute of Technology, and Project SQUID Technical Report CIT-8-PU (December 1976).

MARBLE, F. E. and BROADWELL, J. E. [1977] "The Coherent Flame Model for Turbulent Chemical Reactions", Project SQUID TRW-9-PU.

MUNGAL, M. G. and DIMOTAKIS, P. E. [1984] "Mixing and combustion with low heat release in a turbulent mixing layer", J. Fluid Mech. 148, 349-382.

MUNGAL, M. G. and FRIELER, C. E. [1985] "Chemical reactions in a turbulent mixing layer: The effects of the reaction rate coefficient - Part I", GALCIT report FM85-01 (31-Dec-85).

PAPAMOSCHOU, D. [1986] "Experimental Investigation of Heterogeneous Compressible Shear Layers", Ph. D. thesis, California Institute of Technology.

SMOOKE, M. D., MILLER, J. A. and KEE, R. J. [1983] "Determination of Adiabatic Flame Speeds by Boundary Value Methods", Comb. Sc. & Tech. 34, 79-90.

Appendix: The $H_2/NO/F_2$ chemical system

Chemical equations

1. $NO + F_2 \rightleftharpoons NOF + F$
2. $NO + F + M \rightleftharpoons NOF + M$
3. $H + F_2 \rightleftharpoons HF + F$
4. $F + H_2 \rightleftharpoons HF + H$
5. $F_2 + M \rightleftharpoons F + F + M$
6. $HF + M \rightleftharpoons H + F + M$
7. $H_2 + M \rightleftharpoons H + H + M$

Rate Coefficients

	A	3	E
1.	4.2×10^{11}	0.0	2285
2.	3.0×10^{16}	0.0	0
3.	3.0×10^{9}	1.5	1680
4.	2.6×10^{12}	0.5	610
5.	2.1×10^{13}	0.0	33700
6.	3.1×10^{13}	0.0	125000
7.	2.2×10^{12}	0.5	92600

These values are derived from Baulch et al [1981] and Cohen et al [1982].

Appendix E

ZHUANG, M., KUBOTA, T. and DIMOTAKIS, P. E. [1987] "On the Stability of Inviscid, Compressible Free Shear Layers", Proceedings, *First National Fluid Dynamics Congress*, 25–28 July 1988 (Cincinatti, Ohio), **II**, 768–773.

AIAA'88

AIAA-88-3538-CP

On the Instability of Inviscid, Compressible Free Shear Layers

Mei Zhuang, Toshi Kubota, and Paul E. Dimotakis, Graduate Aeronautical Laboratories, California Institute of Technology, Pasadena, CA

AIAA/ASME/SIAM/APS
1st National Fluid Dynamics Congress
July 25-28, 1988/Cincinnati, Ohio

88-3538-CP

On the Instability of Inviscid, Compressible Free Shear Layers

Mei Zhuang*, Toshi Kubota° and Paul E. Dimotakis†

Graduate Aeronautical Laboratories
California Institute of Technology, Pasadena, California

Abstract

The linear spatial instability of inviscid compressible laminar mixing of two parallel streams, comprised of the same gas, has been investigated with respect to two-dimensional wave disturbances. The effects of the velocity ratio, temperature ratio, and the temperature profile across the shear layer have been examined. A nearly universal dependence of the normalized maximum amplification rate on the convective Mach number is found, with the normalized maximum amplification rate decreasing significantly with increasing convective Mach number in the subsonic region. These results are in accord with those of recent growth rate experiments in compressible turbulent free shear layers and other similar recent calculations.

Introduction

The instability of inviscid, laminar, two-dimensional shear layers in both incompressible and compressible flow has been studied in the past.

For incompressible parallel flow, the linear spatial instability of the hyperbolic tangent and Blasius mixing layers was investigated for different values of the ratio between the difference and sum of the velocities of the two co-flowing streams by Monkewitz & Huerre[1]. They found that the maximum growth rate is approximately proportional to the velocity ratio.

For compressible flow, Lessen, Fox & Zien[2] found that increasing the Mach number of the flow tends to stabilize the flow. Gropengiesser[3] studied the instability characteristics of boundary layers at various free stream Mach numbers and temperature ratios. The linear stability of a shear layer of an inviscid fluid with two-dimensional temporally growing disturbances was considered by Blumen, Drazin & Billings[4]. They showed that the flow is unstable with respect to two-dimensional disturbances at all values of the Mach number. They also showed that there exists a second unstable mode which is supersonic and decays weakly with distance from the shear layer. For compressible flow, however, the effects of shear layer Mach number, temperature ratio, velocity ratio, and temperature profile on the stability characteristics are very complicated. These authors offer no prediction about what the combined influences of these flow parameters will be. Recently, Ragab & Wu[5] studied the influence of the velocity ratio on the stability characteristics of the compressible shear layer, and they also investigated the effect of the convective Mach number, as proposed by Papamoschou & Roshko[6]. Their results indicate the convective Mach number is a parameter which correlates the compressibility effects on the spreading rate of mixing layers.

Papamoschou & Roshko performed experiments on compressible shear layers and suggested the convective Mach number (M_c) as the appropriate parameter scaling the effects of compressibility. This is defined for each stream as:

$$M_{c1} = \frac{U_1 - U_c}{a_1} , \qquad M_{c2} = \frac{U_c - U_2}{a_2} , \qquad (1)$$

where U_1, U_2 and a_1, a_2 are the free stream velocities and speeds of sound. The quantity U_c is the convective velocity of the large scale structures and was estimated as $\tilde{U}_c$ by Papamoschou & Roshko assuming that the dynamic pressure match at stagnation points in the flow (Coles[7], Dimotakis[8]). For compressible isentropic flow, i.e. (Papamoschou & Roshko)

$$\left(1 + \frac{\gamma_1 - 1}{2} \tilde{M}_{c1}^2\right)^{\frac{\gamma_1}{\gamma_1 - 1}} = \left(1 + \frac{\gamma_2 - 1}{2} \tilde{M}_{c2}^2\right)^{\frac{\gamma_2}{\gamma_2 - 1}} , \qquad (2)$$

where γ_1, γ_2 are the ratios of the specific heats of the two streams, and

$$\tilde{M}_{c1} = \frac{U_1 - \tilde{U}_c}{a_1} , \qquad \tilde{M}_{c2} = \frac{\tilde{U}_c - U_2}{a_2} . \qquad (3)$$

For γ_1 equals γ_2, $\tilde{U}_c$ can be obtained by

$$\tilde{U}_c = \frac{a_2 U_1 + a_1 U_2}{a_1 + a_2} , \qquad (4)$$

which, for equal static free stream pressures and specific heats, reduces to the incompressible expression[8]. They suggested that the growth rate of a compressible shear layer, normalized by the growth rate for an incompressible shear layer, might be expressible as a universal function of the convective Mach number $\tilde{M}_{c1}$, which is valid over a wide range of velocity and temperature ratios of a shear layer. They also found that the normalized growth rate decreases significantly with increasing $\tilde{M}_{c1}$.

The numerical calculations described here were performed under the assumptions of linear instability theory. The convective velocity is estimated as $\hat{U}_c = C_r$ (Mack[9] 1975). Therefore, a convective Mach number ($\hat{M}_c$) for each stream can be

---

* Graduate Student.
° Professor.
† Professor. Member AIAA

written as:

$$\hat{M}_{c1} = \frac{U_1 - C_r}{a_1} , \qquad \hat{M}_{c2} = \frac{C_r - U_2}{a_2} , \qquad (5)$$

where C_r is the real phase velocity of the disturbances.

The purpose of the present studies is to investigate the combined influence of the convective Mach number ($\hat{M}_c$), which is different from the one used by Ragab & Wu ($\tilde{M}_c$), the velocity and temperature ratios, and the temperature profiles of the flow on the linear stability behavior of compressible shear layers. Studies are made of the case of inviscid flow under the assumptions that the gases in the two streams are the same, the main flow can be treated parallel, and that the disturbances in the flow are of small amplitude. The range of the unstable frequencies and wave numbers were numerically calculated for a two-dimensional, spatially growing disturbance.

Basic disturbance equations

We consider a two-dimensional flow of two parallel streams. With upper stream quantities as the reference and the local layer thickness δ as the length scale, the dimensionless quantities of the flow in Cartesian co-ordinates can be written as usual

$$u_x = \bar{U} + u', \quad u_y = v', \quad T = \bar{T} + T',$$

$$\rho = \bar{\rho} + \rho', \quad p = \bar{p} + p',$$

or, for the general field quantity

$$Q(x,y,t) = \bar{Q}(y) + Q'(x,y,t),$$

where $\bar{Q}$ is a profile of the main flow, and Q' is the corresponding disturbance amplitude.

Consider now the disturbance to be a wave propagating in the x-direction. The disturbance quantities in dimensionless form can be expressed as[2]

$$(u', v', T', \rho', p') =$$

$$\left\{ f(y), \alpha\phi(y), \theta(y), r(y), \pi(y) \right\} \exp[i\alpha(x - ct)], \qquad (6)$$

where α is a complex wave number, and c is a complex wave velocity. In the case of negligible viscous effects, the linearized disturbance equations for a 2-D compressible fluid with the same gas constants and specific heats are given by[2]:

$$\text{Continuity} : i(\bar{U} - c) r + \bar{\rho}(\phi' + i f) + \bar{\rho}' \phi = 0 \qquad (7a)$$

$$\text{Momentum} : \gamma M_1^2 \bar{\rho} [i(\bar{U} - c) f + \bar{U}' \phi] = - i\pi \qquad (7b)$$

$$\gamma M_1^2 \alpha^2 \bar{\rho} [i(\bar{U} - c) \phi] = - \pi' \qquad (7c)$$

$$\text{Energy} : \bar{\rho} [i(\bar{U} - c)\theta + \bar{T}'\phi] = -(\gamma - 1)(\phi' + if) \qquad (7d)$$

$$\text{State} : \frac{\pi}{\bar{p}} = \frac{r}{\bar{\rho}} + \frac{\theta}{\bar{T}} , \qquad (7e)$$

where M_1 is the upper stream Mach number and primes here correspond to d/dy. These equations can be reduced to a second order differential equation for the pressure disturbance[2], i.e.

$$\pi'' - \left(\frac{2\bar{U}'}{\bar{U} - c} - \frac{\bar{T}'}{\bar{T}} \right) \pi' - \alpha^2 \left[1 - \frac{M_1^2}{\bar{T}} (\bar{U} - c)^2 \right] \pi = 0. \qquad (8)$$

Asymptotic Behavior of the Eigenfunctions

The asymptotic behavior of the eigenfunction $\pi(y)$ for $y \to \pm\infty$ is found from Equation (8). With $y \to \pm\infty$, $\bar{U}$ and $\bar{T}$ are constants, and $\bar{U}'$, $\bar{T}'$ are zeros. In that limit, Equation (8) becomes

$$\pi'' - \lambda_k^2 \pi = 0 , \qquad (9)$$

with

$$\lambda_k^2 = \alpha^2 \left[1 - \frac{M_1^2}{\bar{T}_k} (\bar{U}_k - c)^2 \right] = \Lambda_k = \Lambda_{kr} + i\Lambda_{ki} , \qquad (10)$$

and k = 1, 2. Therefore, from (10) we get

$$\lambda_k = \lambda_{kr} + i\lambda_{ki} = \pm \Lambda_k^{1/2}$$

and the solution for large $|y|$ can be written as

$$\pi = A_k \exp(-\lambda_k |y|) , \qquad (11)$$

where A_k is a complex constant.

Since we have only considered the case of amplified disturbances ($\alpha_i < 0$), the boundary conditions for both supersonic and subsonic disturbances can be expressed by $\pi_r(y \to \pm\infty) \to 0$ and $\pi_i(y \to \pm\infty) \to 0$. In order to satisfy the boundary conditions, we set $\lambda_{kr} > 0$, and get

$$y = y_1 \to +\infty, \qquad \pi = A_1 \exp(-\lambda_1 y) \qquad (12a)$$

$$y = y_2 \to -\infty, \qquad \pi = A_2 \exp(\lambda_2 y) , \qquad (12b)$$

where

$$\lambda_k = \lambda_{kr} + i\lambda_{ki} =$$

$$\left[\frac{1}{2} (|\Lambda_k| + \Lambda_{kr}) \right]^{1/2} + i\, \text{sign}(\Lambda_{ki}) \left[\frac{1}{2} (|\Lambda_k| - \Lambda_{kr}) \right]^{1/2} .$$

Formulation of the Eigenvalue problem

The eigenvalue problem is defined as follows. For a given real disturbance frequency β ($\beta = \alpha c$), the eigenvalues α_r and α_i are to be determined in such a way that the eigenfuctions $\pi_r(y)$ and $\pi_i(y)$ satisfy the boundary conditions. Specifically, we used a Runge-Kutta method to solve the eigenvalue equation, with (12a) and (12b) as boundary conditions. The equation was integrated from one side of the boundary ($y = y_1$) to the other side ($y = y_2$). The correct α was obtained for a given β by matching to the boundary conditions.

Velocity and Temperature Distributions

Lock's[10] numerical calculation of the velocity distribution for a compressible laminar boundary layer, suggest that the velocity profile for compressible laminar shear layers is well approximated by a hyperbolic tangent profile. So we assume that the dimensionless mean velocity profile is described by a hyperbolic tangent profile represented by the form

$$\bar{U}(y) = \eta(y) + U_R [1 - \eta(y)] , \qquad (13)$$

where $U_R = U_2/U_1$ is the velocity ratio across the shear layer, and $2\eta(y) - 1$ is approximated by a hyperbolic tangent. See mean velocity profiles $\bar{U}(y)$ in Fig. 1.

We note that the linearized flow equations do not prescribe the mean temperature profile. Accordingly, two different kinds of temperature profiles have been considered. One conforms to the Crocco-Busemann[11,12] relation, wherein the total temperature profile $T_t(y)$ for an equal ratio of the specific heats of the two free streams is represented by

$$T_t(y) = T_{t1}\,\eta(y) + T_{t2}\,[1 - \eta(y)] \,, \qquad (14)$$

where T_{t1}, T_{t2} are the free stream total temperatures. This yields the dimensionless mean static temperature profile,

$$\bar{T}(y) = c_1 + c_2\,\bar{U}(y) - \frac{(\gamma - 1)\,M_1^2}{2}\,\bar{U}^2(y) \,, \qquad (15)$$

where M_1 is the upper stream Mach number and c_1, c_2 are constants which satisfy the boundary conditions on the temperature profile. Such mean temperature profiles $\bar{T}(y)$ for $M_1 = 5$ are shown on Fig. 2. The other kind of dimensionless temperature profile is obtained by assuming that the dimensionless density distribution across the shear layer can also be approximated by a hyperbolic tangent profile, i.e.

$$\bar{\rho}(y) = \eta(y) + \rho_R\,[1 - \eta(y)] \,, \qquad (16)$$

where $\rho_R = \rho_2/\rho_1$ is the density ratio across the shear layer. Therefore, for a shear layer comprised of the same gas, the dimensionless temperature profile is $\bar{T}(y) = 1/\bar{\rho}(y)$. See Fig. 3.

Results

For a given combination of free stream Mach number M_1, temperature ratio T_R (T_2/T_1) and velocity ratio U_R, the linear instability characteristics were calculated, yielding the most unstable eigenvalue $(\alpha_m = \alpha_{mr} + i\,\alpha_{mi})$ and its corresponding real frequency β_m. The real phase velocity C_r of the disturbances was obtained as β_m/α_{mr}. This yields the convective Mach number $\hat{M}_{c1}$ and $\hat{M}_{c2}$ from Eq. (5).

Different combinations of velocity and temperature ratios using a velocity and temperature profile from Eqs. (13) and (15) were investigated for a convective Mach number $\hat{M}_{c1}$ from 0 to about 1.5. The velocity profiles for $U_R = 0.25, 0.5, 0.75$ appear in Fig. 1 and the temperature profiles for $T_R = 0.5, 1.0, 1.5$ in Fig. 2. Results shown in Figs. 4 - 9, which were obtained from nine different combinations of T_R and U_R, indicate that if the most unstable eigenvalue for a compressible shear layer is normalized by its value corresponding to an incompressible shear layer (at the same velocity and temperature ratio), the ratio is well approximated as a function of the convective Mach number only, i.e.

$$\frac{\delta_x(\hat{M}_{c1})}{\delta_x(0)} = \frac{\max\left\{-\alpha_i(U_2/U_1, T_2/T_1, \hat{M}_{c1})\right\}}{\max\left\{-\alpha_i(U_2/U_1, T_2/T_1, \hat{M}_{c1} = 0)\right\}} = F(\hat{M}_{c1}) \,, \qquad (17)$$

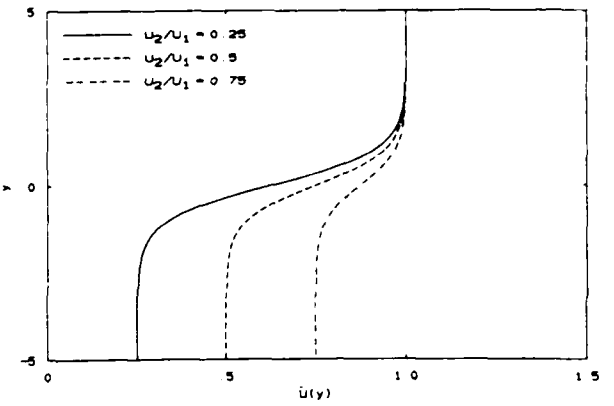

Fig. 1 Hyperbolic tangent mean velocity profiles for different values of the velocity ratio U_2/U_1.

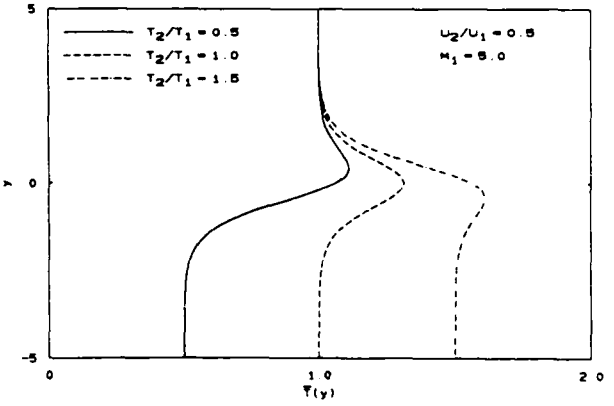

Fig. 2 Crocco-Busemann mean temperature profiles for different values of the temperature ratio T_2/T_1, for the case $U_2/U_1 = 0.5$ and $M_1 = 5.0$. —— $\hat{M}_{c1} = 1.54$, ---- $\hat{M}_{c1} = 1.13$, -·-· $\hat{M}_{c1} = 1.0$.

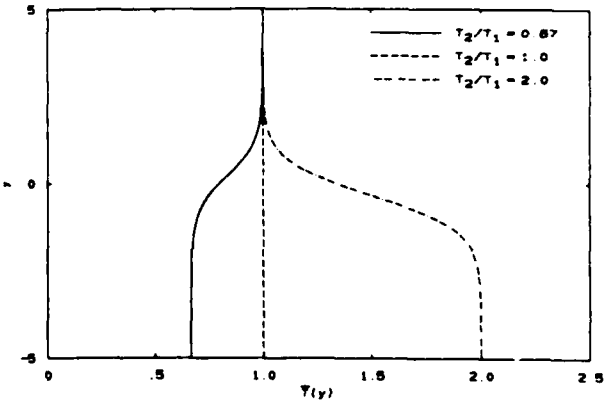

Fig. 3 Hyperbolic tangent $\bar{\rho}(y)$ mean temperature profiles for different values of the temperature ratio T_2/T_1.

where $\delta_x = d\delta/dx$ for the shear layer of the particular free stream conditions. The solid line estimate of $\delta_x(\hat{M}_{c1})/\delta_x(0)$ in Figs. 4 - 9 was computed by using all the data of the nine different cases, and least squares fitting the

normalized maximum amplification rate versus the convective Mach number $\hat{M}_{c1}$, for the range of $\hat{M}_{c1}$ from 0 to about 1.5 with a function of the form

$$\frac{\delta_x(\hat{M}_{c1})}{\delta_x(0)} = 1 + p_0\left(e^{-(p_2\hat{M}_{c1}^2 + p_3\hat{M}_{c1}^3 + p_4\hat{M}_{c1}^4)} - 1\right), \quad (18)$$

where

$$p_0 = 0.956174 \qquad p_2 = 1.53471$$
$$p_3 = -1.22389 \qquad p_4 = 1.83827 .$$

Note that $\delta_x(\hat{M}_{c1}\to\infty)/\delta_x(0) = 1 - p_0$, and that the coefficient p_2 is related to the second derivative at $\hat{M}_{c1}=0$, etc. Note also that these results suggest that $F'(\hat{M}_{c1}=0) = 0$, as might have been argued a priori. The results, shown in Figs. 4 - 9, also suggest that the normalized maximum amplification rate decreases significantly with increasing $\hat{M}_{c1}$ in the region $\hat{M}_{c1} < 1$.

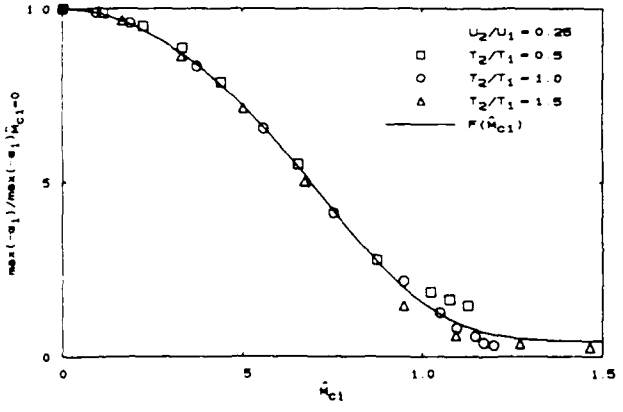

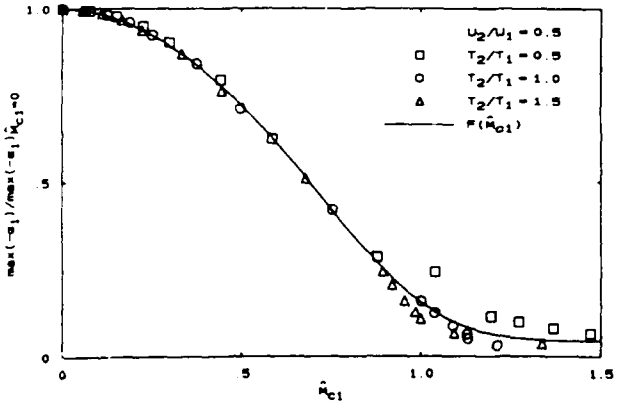

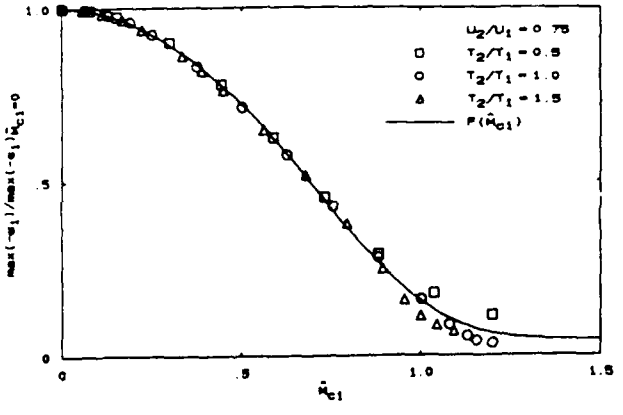

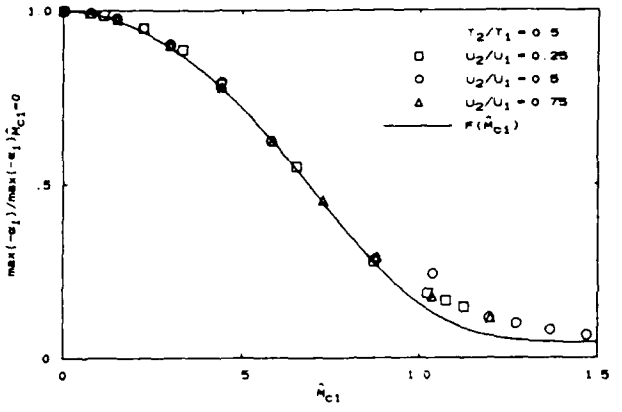

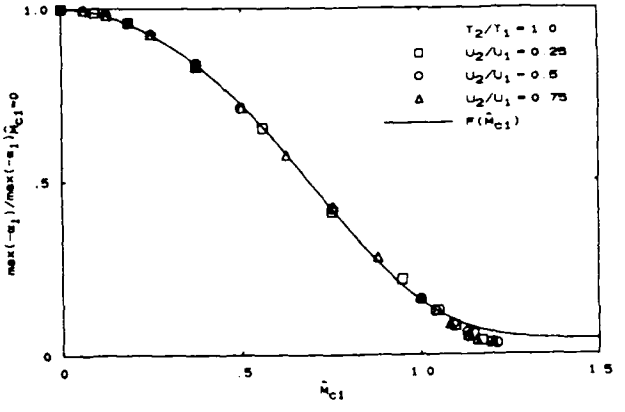

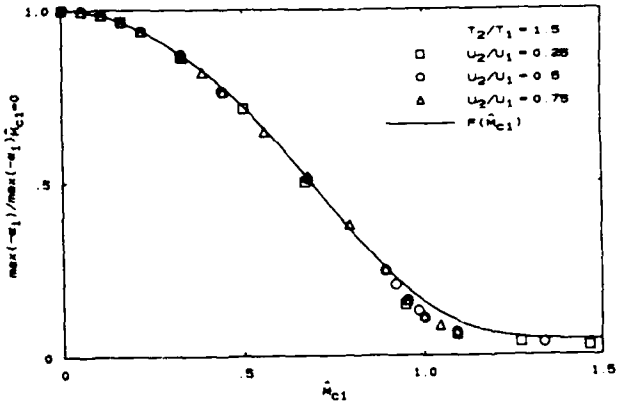

Figs. 4 - 9 Normalized maximum amplification rate vs $\hat{M}_{c1}$.

In the second set of calculations, the mean temperature profile was specified via Eq.(16), i.e. $\bar{T}(y) = 1/\bar{\rho}(y)$. The resulting temperature profiles for $T_R = 0.67$, 1, and 2 are plotted in Fig. 3. The velocity ratio $U_R = 0.5$ with each of these three temperature ratios was studied for the convective Mach number $\hat{M}_{c1}$ from 0 to about 1.5. The results, shown in Fig. 10, substantiate the convective Mach number as the relevant compressibility parameter and also display good agreement with the plot $\delta_x(\hat{M}_{c1})/\delta_x(0)$ vs. $\hat{M}_{c1}$ obtained from Eq.(18), even though these two mean

temperature profiles are very different at supersonic convective Mach numbers (see Figs 2, 3).

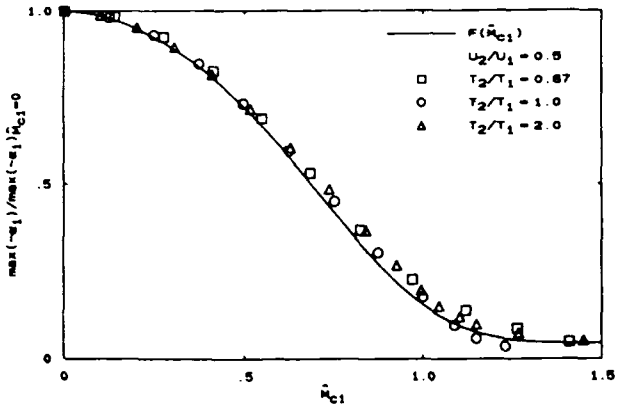

Fig. 10 Normalized maximum amplification rate vs $\hat{M}_{c1}$ for hyperbolic tangent mean temperature profiles comparison with $F(\hat{M}_{c1})$

With $\tilde{U}_c$ calculated from Eq.(4) and C_r obtained from the numerical calculations under the linear theory, $\tilde{M}_{c1}$ does not necessarily equal $\hat{M}_{c1}$. In fact, even the real phase velocity may not be unique for supersonic convective Mach number, because of the existence of a second mode. Blumen, Drazin & Billings[4] have noted this behavior for a shear layer of an inviscid fluid with two-dimensional temporally disturbances[4]. We can see that, for both temperature profiles (Eq.(15) and Eq.(16) with $\bar{T}(y) = 1/\bar{\rho}(y)$), there are very small differences between $\hat{M}_{c1}$ and $\tilde{M}_{c1}$ from the plot of $(\hat{M}_{c1} - \tilde{M}_{c1})/\hat{M}_{c1}$ vs. $\hat{M}_{c1}$ for $\hat{M}_{c1} \le 1$, but the differences only become substantial when $\hat{M}_{c1} > 1$. See Figs. 11, 12. We only studied the cases for $\hat{M}_{c1} < 1.5$, since shock waves can exist in a shear layer at high convective Mach numbers and therefore, the validity of a linear description of these phenomena would be suspect.

A comparison of our estimate of $\delta_x(\hat{M}_{c1})/\delta_x(0)$ with Ragab's numerical data and with Papamoschou's experimental data is made in Fig. 13. The data from our calculations are very close to Ragab & Wu's. The difference between $\hat{M}_{c1}$ and $\tilde{M}_{c1}$, though not small in the region $\hat{M}_{c1} > 1$, does not affect the results, since the normalized amplification rates are very small in this region. According to Papamoschou & Roshko's experimental data, the growth rate of the shear layer tapers off as the convective Mach number becomes supersonic. As opposed to their findings, however, the growth rate of our calculations decreases to zero as $\hat{M}_{c1} \gg 1$. Preliminary calculations suggest that a larger value for the growth rate at large M_{c1} is exhibited by more complex velocity and/or density profiles.

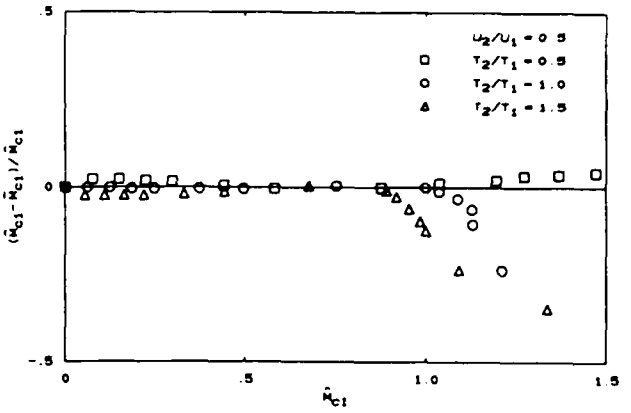

Fig. 11 Normalized difference between $\hat{M}_{c1}$ and $\tilde{M}_{c1}$ vs $\hat{M}_{c1}$.

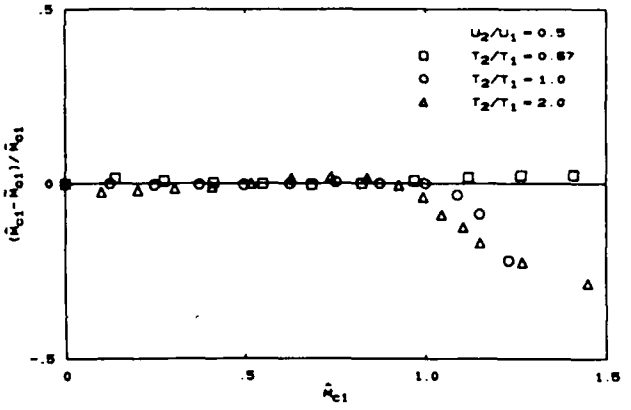

Fig. 12 Normalized difference between $\hat{M}_{c1}$ and $\tilde{M}_{c1}$ vs $\hat{M}_{c1}$ for hyperbolic tangent mean temperature profiles.

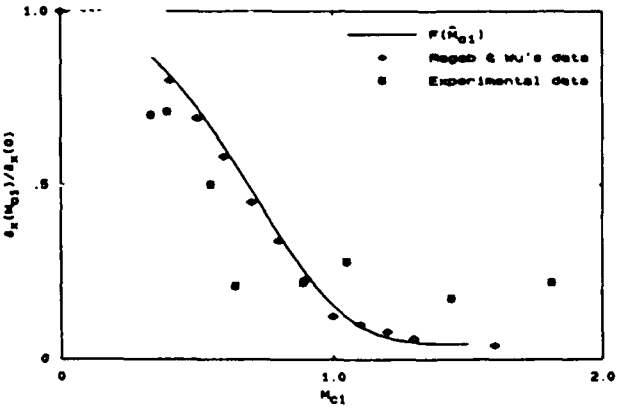

Fig. 13 A comparison of $F(\hat{M}_{c1})$ with Ragab & Wu's numerical data and with Papamoschou & Roshko's experimental data.

Conclusion

The influences of the convective Mach number, the velocity and temperature ratios and the temperature profiles of the flow on the linear spatial instability characteristics of a plane shear layer, formed by the same gas, were investigated. It was found that there is a nearly universal dependence of the normalized maximum amplificat on rate on the convective Mach number, and this amplification rate decreases significantly with increasing $\hat{M}_{c1}$ in the region of $\hat{M}_{c1} < 1$.

Acknowledgement

We would like to thank Dr. Dimitri Papamoschou, Mr. Paul Miller and Mr. Cliff Frieler for their helpful discussions and assistance. This work was supported by the Air Force Office of Scientific Research Grants No. 83 - 0213 and 88 - 0155.

References

1. MONKEWITZ, P. A. and HUERRE, P. [1982] "Influence of the Velocity Ratio on the Spatial Instability of Mixing Layers", Phys. Fluids 25(7), 1137 - 1143.

2. LESSEN, M., FOX, J. A. and ZIEN, H. M. [1965] "On the Inviscid Stability of the Laminar Mixing of Two Parallel Streams of a Compressible Fluid", J. Fluid Mech. 23, 355 - 367.

3. GROPENGIESSER, H. [1970] "Study of the Stability of the Boundary Layers in Compressible Fluids", NASA TT-F-12, 786.

4. BLUMEN, W., DRAZIN, P. G. and BILLINGS, D. F. [1975] "Shear Layer Instability of an Inviscid Compressible Fluid", J. Fluid Mech. 71, 305 - 316.

5. RAGAB, SAAD A. and WU, J. L. [1988] "Instabilities in the Free Shear Layer Formed by Two Supersonic Streams", AIAA Paper No. 88-0038.

6. PAPAMOSCHOU, D. and ROSHKO, A. [1986] "Observations of Supersonic Free Shear Layers", AIAA Paper No. 86-0162

7. DIMOTAKIS, P. E. [1986] "Two-Dimensional Shear-Layer Entrainment", AIAA J., 24(11), 1791-1796.

8. COLES, D. [1981] "Prospects for Useful Research on Coherent Structure in turbulent shear flow", Proc. Indian Acad. Sci. 4(2), 111-127.

9. MACK, L. M. [1975] "Linear Stability and the Problem of Supersonic Boundary-Layer Transition", AIAA J., 13, 278-289.

10. LOCK, R. C. [1935] "The Velocity Distribution in the Laminar Boundary Layer Between Parallel Streams", Quart. J. Mech. Appl. Math. 4, 42 - 63.

11. CROCCO, L. [1932] "Sulla trasmissione del calore da una lamina piana a un fluido scorrente ad alta velocita", L'Aerotecnica 12, 181 - 197.

12. BUSEMANN, A. [1935] "Gasstromung mit Laminarer Grenzschicht Entlang einer Platte", ZAMM 15, 23 - 25.

Appendix F

DOWLING, D. R. and DIMOTAKIS, P. E. [1988] "On Mixing and Structure of the Concentration Field of Turbulent Jets", Proceedings, *First National Fluid Dynamics Congress*, 25–28 July 1988 (Cincinatti, Ohio), **II**, 982–988.

AIAA'88

AIAA-88-3611-CP

On Mixing and Structure of the Concentration Field of Turbulent Jets

David R. Dowling and Paul E. Dimotakis, California Institute of Technology, Pasadena, CA

AIAA/ASME/SIAM/APS 1st Fluid Dynamics Congress

July 25-28, 1988/Cincinnati, Ohio

ON MIXING AND STRUCTURE OF THE CONCENTRATION FIELD OF TURBULENT JETS

88-3611-CP

David R. Dowling† and Paul E. Dimotakis*

Graduate Aeronautical Laboratories
California Institute of Technology
Pasadena, California 91125

Abstract

This work is an investigation of the mixing of the nozzle fluid of a round turbulent jet with the entrained reservoir fluid, using laser-Rayleigh scattering methods. Our measurements, at a Reynolds number of 5000, cover the axial range from 20 to 80 jet exit diameters and resolve the full range of temporal & spatial concentration scales. The measured mean & rms values of the concentration, and the mean scalar dissipation rate, when estimated from the time derivative of concentration, are consistent with jet similarity laws. Concentration fluctuation power spectra are found to be self-similar along rays emanating from the jet virtual origin. The probability density functions for the concentration, the time derivative of concentration, and the square of the time derivative of concentration, are compiled and are also self-similar along rays.

Introduction

Background

The free turbulent jet, a small source of high speed fluid issuing into a large quiescent reservoir, is one of the classical *free shear* flows. It has been the subject of experimental work for more than 50 years (Ruden[23] 1933, Kuethe[15] 1935) and has found broad application in combustion systems as a means of mixing reactants.

It is conventionally accepted that profiles of the mean jet fluid concentration are self-similar beyond about 20 jet exit diameters (Wilson & Dankwerts[27] 1964, Becker et al.[3] 1967, Birch et al.[4] 1978, Lockwood & Moneib[16] 1980). In cylindrical coordinates with the direction of the jet discharge chosen to lie along the axis of symmetry (the x-axis here), the mean profile of jet gas concentration, for example, takes the following form:

$$\overline{C}(x,r) = \frac{C_0}{x - x_0} F\left(\frac{r}{x - x_0}\right) \qquad (1)$$

where r is the radial coordinate, C_0 the jet gas concentration at the nozzle exit, F is a smooth function that is experimentally determined, x_0 is the virtual origin, and the overbar denotes a time average.

While the similarity of the mean profile is on a solid experimental footing, the picture is not yet complete. Most experimental data for the *root mean square* (rms) fluctuation can not be collapsed in the same coordinates used to collapse the mean values. Conflicts also exist between the reported rms levels from different experiments (Dahm[8] 1985). No clear consensus exists as to whether the ratio of the rms to mean concentration of the jet fluid ($C'_{rms}/\overline{C}$) is a constant in the far field of the jet (Dahm[8] 1985). These problems could arise from many sources including: Reynolds number effects, contamination of the flow by small buoyancy forces, insufficient resolution of all of the fluctuating scales, unsteadiness in the jet source or the quiescent reservoir, neglect of the effects of the molecular Schmidt number (kinematic viscosity divided by species diffusivity), or the possible failure of the chosen similarity form.

Present Experiments

The experiments described here address some of these concerns in the far-field of the jet. These experiments were designed with adequate spatial & temporal resolution, as well as dynamic range, throughout the jet to unambiguously resolve all of the diffusion scales in a purely momentum dominated flow. This meant that the Reynolds number, nozzle size, jet & reservoir gases and internal volume of the experimental enclosure were not chosen independently of each other or of the noise characteristics of the diagnostic.

This work, an experimental investigation of mixing of the jet fluid with the entrained reservoir fluid, is based on measurements of the instantaneous concentration of jet fluid, C(t). In particular, it is a study of the similarity of the mean concentration of jet fluid, $\overline{C}$, the probability density function of jet fluid concentration, the rms fluctuation level, C'_{rms}, the power spectrum of concentration fluctuations, E_C, the probability density function of the time derivative of concentration, and some of the statistical properties of the scalar dissipation rate, ε_C, as estimated from the square of the time derivative of concentration.

Experimental Technique

The Main Apparatus

These experiments were performed in the gas phase jet mixing apparatus shown schematically in Figure 1. The main apparatus consisted of a large enclosure with an interior volume of about 120 cubic feet. The jet was produced by a vertically adjustable ¾" nozzle with an 11 to 1 contraction ratio. The exit turbulence level was less than 0.2% and the exit Reynolds number ($U_0 d/\nu_\infty$) was 5000, where ν_∞ is the reservoir gas kinematic viscosity. The Taylor Reynolds number along the

† Presently, Senior Specialist Engineer,
Boeing Aerospace, P.O. Box 3999 M/S 8H-29
Seattle, Washington 98124

* Professor, Aeronautics & Applied Physics,
Member AIAA

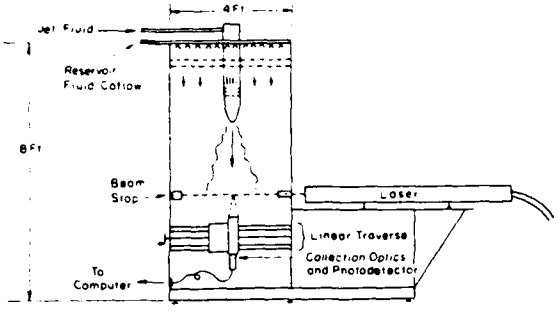

Figure 1. Experimental facility.

centerline of the jet was estimated from the formulae in Hinze[13] (1975), Equations 5 & 6 (see page 4), and a typical value for the centerline rms velocity fluctuation, $u'_{rms} = .25\,\bar{U}_{cl}$. The result being: $Re_\lambda = 100$. A uniform coflow velocity, typically about 0.006 of the jet velocity, was produced over the entire 16 ft^2 cross section of the enclosure. The volume flux of the coflow was chosen to provide the entrainment needs of the jet (Ricou & Spalding[22] 1961) to a point down below the farthest measuring station. Large 3' x 5' plexiglas windows were located on opposite sides of the enclosure to allow shadowgraph imaging of the jet. The exhaust gases from the experiment exited through the bottom of the enclosure and were collected in a large plastic bag.

The jet gas was ethylene, C_2H_4, and its flow rate was set with a single stage regulator and a metering valve. The dynamic head of the jet was measured to determine U_o. The reservoir and coflow gas was N_2. The coflow was produced by regulating the pressure of a special delivery manifold. The density ratio of ethylene to N_2 is 1.0015. An axisymmetric laminar boundary layer calculation was used to estimate boundary layer thicknesses at the nozzle exit to calculate the the momentum diameter of the nozzle, d^*, introduced in a limited way by Thring & Newby[24] (1952), used by Avery & Faeth[1] (1974), and modified by Dahm & Dimotakis[7] (1987) to:

$$d^* = \frac{2\dot{m}_o}{\sqrt{\pi \rho_\infty J_o}} \qquad (2)$$

where $\dot{m}_o$ & J_o are the nozzle mass and momentum fluxes respectively, and the density of the reservoir fluid is denoted by ρ_∞. The estimate for the nozzle conditions of these experiments was $d^* = 0.96d$. Note that the momentum diameter, d^*, reduces to the geometric exit diameter, d, for $\rho_{jet} = \rho_\infty$ and a perfect "top-hat" exit profile of velocity.

The Diagnostic

Laser-Rayleigh scattering was used to determine the concentration time history of the binary mixture of jet and reservoir gases within a small focal volume in the mixing region of the jet. This non-intrusive diagnostic has been successfully used by many previous authors (Dyer[10] 1979, Escoda & Long[11] 1983, Pitts & Kashiwagi[19] 1984, Pitts[20] 1986, and others) and will not be described here. The main difference between this work and previous implementations of this technique was the strict observance of the spatial and temporal resolution requirements imposed by the need to accurately record the smallest estimated diffusion scales of the flow.

For these experiments, the Rayleigh scattered light from a short section of an 18 Watt collimated laser beam was imaged (one to one) onto a small aperture photodiode. The diameter of the sensitive area of the photodiode was between .20 and 1.0 mm; the local resolution requirements of the jet dictating the size used in each case. The signal current from the photodiode was amplified by a low-noise transimpedance amplifier designed by Dr. Dan Lang. This signal was filtered and sent to an LSI PDP-11/73 based computer system where it was digitized and stored for subsequent processing. The sampling frequency and filter bandwidth were chosen to insure that the estimated temporal resolution requirements imposed by the jet were surpassed by more than a factor of four. The sensitivity of the whole system was calibrated by introducing pure jet and reservoir gases into the focal volume before and after each run.

Results

The Mean and RMS Profiles

The properly scaled mean and rms concentration profiles for x/d = 20, 40, 60, & 80 are shown on Figure 2. The transformation used to

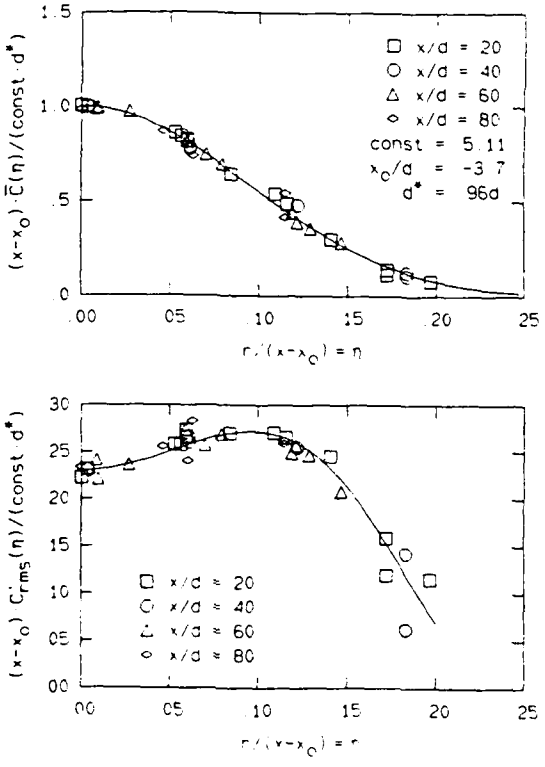

Figure 2. Mean and rms profiles of concentration.

collapse both profiles is based only on the experimentally fitted values of the virtual

origin, x_o, and the decay constant for the mean centerline concentration. Separate normalizations by the local centerline mean, centerline rms concentration, or concentration profile half radius were not necessary.

Probability Density Function of Concentration

The probability density function for the jet gas concentration was estimated by sorting the sampled data into a histogram. The results are plotted in Figures 3, 4, & 5 and display the

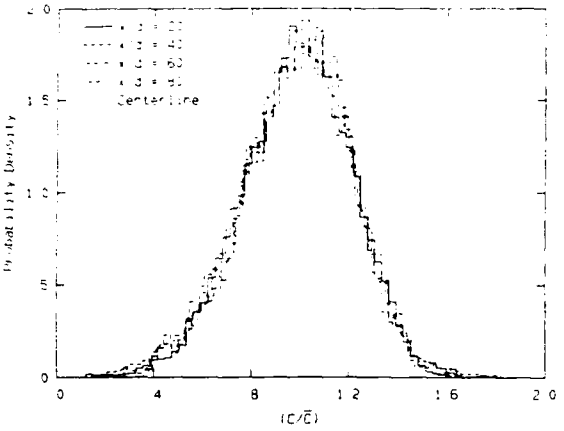

Figure 3. Probability density function of the scaled concentration on the centerline of the jet.

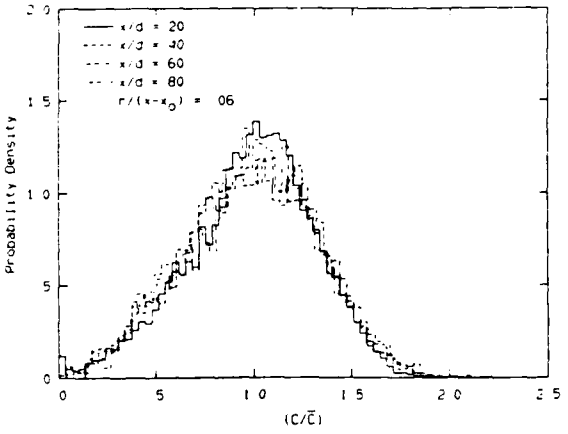

Figure 4. Probability density function of the scaled concentration 3.5° off the centerline of the jet.

similarity collapse of the concentration PDF along the centerline ray ($r/(x-x_o) = 0$), along a ray at 3.5° ($r/(x-x_o) = .06$), and along a ray at 7° ($r/(x-x_o) = .12$). The visual edge of the jet is at about 12° (White[25] 1974). Imperfections in the collapse, which are more evident as the edge of the jet is approached, are believed to be caused

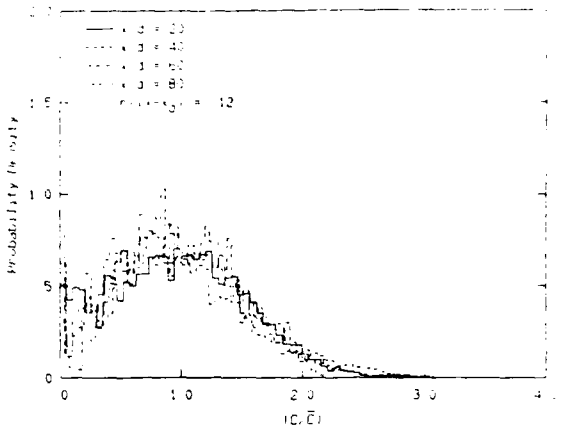

Figure 5. Probability density function of the scaled concentration 7° off the centerline of the jet.

by decreased statistical convergence. In particular, for a fixed run time, the total volume of fluid that passes through the focal volume is roughly proportional to the local mean velocity. Consequently, the effective sample size of a run is smaller near the edge of the jet.

Power Spectrum of Concentration Fluctuations

The power spectra of the concentration fluctuations were calculated from the sampled data sets for x/d = 20, 40, 60, & 80 along the three rays at $r/(x-x_o) = 0$, .06, & .12. The results are plotted in Figures 6, 7, & 8 where τ_1

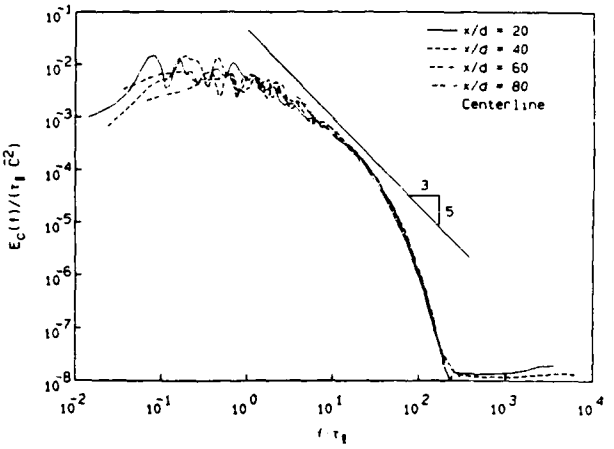

Figure 6. Scaled power spectra of the concentration fluctuations on the centerline of the jet.

(= local jet diameter/local mean centerline velocity) is the estimated large-scale time of the jet. The computed spectra satisfy the relation

$$\left[2 \int_0^\infty E_c(f)\, df \right]^{1/2} = C'_{rms} \qquad (3)$$

as an overall normalization. The flat portion of

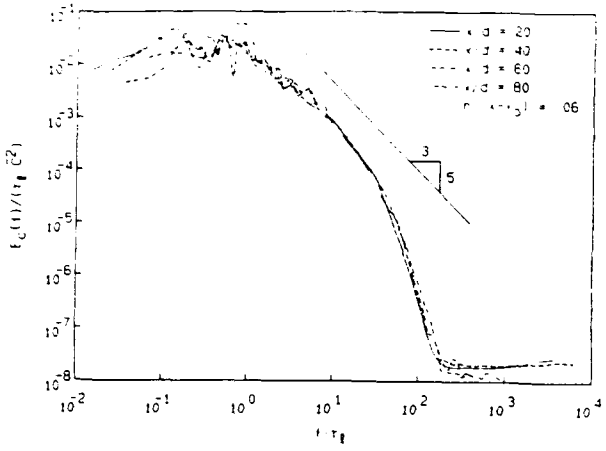

Figure 7. Scaled power spectra of the concentration fluctuations 3.5° off the centerline of the jet.

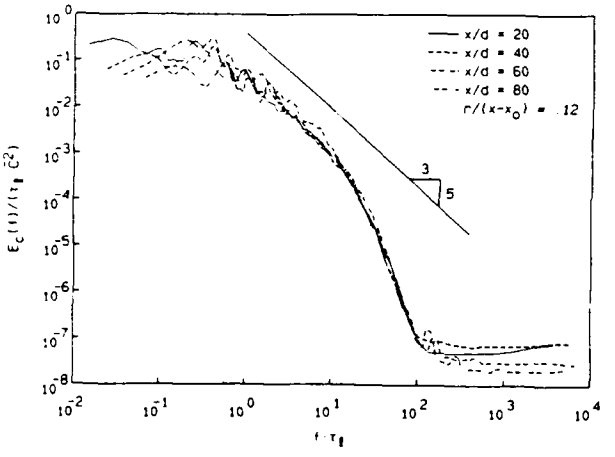

Figure 8. Scaled power spectra of the concentration fluctuations 7° off the centerline of the jet.

each spectrum at high frequencies is the noise floor produced by the measurement technique.

The spectra collapse fairly well in spite of the modest Reynolds number of the jet flow. The calculated value of the Kolmogorov passage frequency, f_K, should roughly correspond to the high frequency end of the -5/3 slope when the molecular Schmidt is of order one (Batchelor[2] 1959, Monin & Yaglom[17] 1975). To estimate f_K, the foundation of the temporal resolution requirement, the centerline energy dissipation rate in the jet, $\bar{\varepsilon}$, reported by Friehe et al.[12] (1971), and the mean centerline velocity decay law suggested by Chen & Rodi[5] (1979) were used, i.e.

$$f_K = \bar{U}_{cl} \left(\frac{\bar{\varepsilon}}{\nu_\infty^3} \right)^{1/4} \qquad (4)$$

where:

$$\bar{\varepsilon} = 48. \frac{U_\infty^3}{d} \left(\frac{x - x_o}{d} \right)^{-4}, \qquad (5)$$

$$\bar{U}_{cl} = 6.2\, U_\infty \left(\frac{x - x_o}{d} \right)^{-1}. \qquad (6)$$

These formulae and the parameters of the experiments lead to an estimate for $f_K \cdot \tau_\ell$ of about 700. While the spectra reported here do not display a -5/3 slope, the scaled frequency range in which they begin to fall more rapidly than a constant power law is at least an order of magnitude lower than 700. This discrepancy between the measured and calculated break points has also been reported by Clay[6] (1973) who worked with data from a heated air jet at a Reynolds number of almost 10^6.

It is also worth noting that although the spectra collapse along rays, the spectra are different from ray to ray. In particular, the spectra along the ray at 7° show a longer power law region with a slope closer to -5/3 than those from the inner rays. This latter behavior was also reported by Lockwood & Moneib[16] (1980) for their measurements at x/d = 20 in a heated air jet at a Reynolds number of 50,000.

The Time Derivative of Concentration

The power spectrum of each data set was used to estimate the optimal (Wiener[26] 1949) filter for that data set (see also Press et al.[21] 1986). The resulting optimal filter was used in each case to eliminate virtually all of the noise from the data, permitting a time derivative to be computed fairly reliably.

The probability density functions of the scaled time derivative were compiled. The results are displayed in Figures 9, 10, & 11. The self-similarity of the data aside, several other

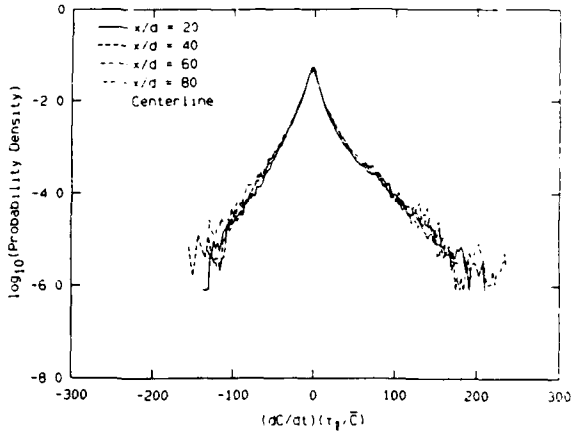

Figure 9. Probability density function of the scaled concentration time derivative on the jet centerline.

interesting points are noteworthy. All three curves are asymmetrical with the peaks slightly off center. One explanation for this is evident in the time traces of the data, which show many more large positive slopes than negative ones. In

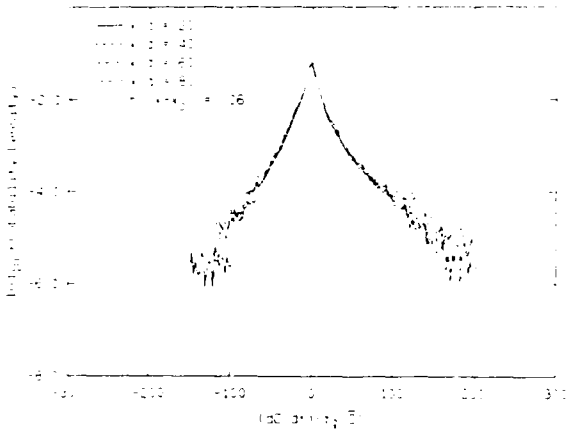

Figure 10. Probability density function of the scaled concentration time derivative 3.5° off the jet centerline.

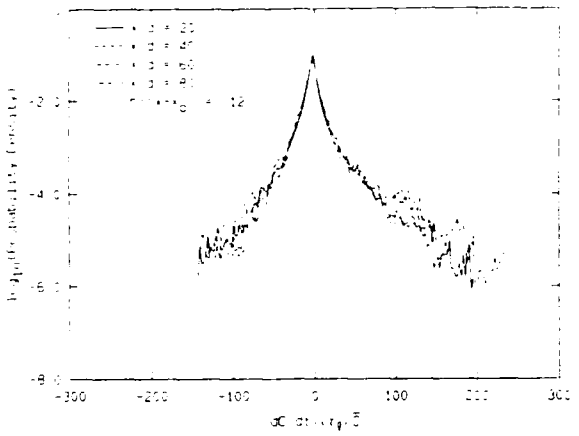

Figure 11. Probability density function of the scaled concentration time derivative 7° off the jet centerline.

fact there seems to be a "typical" large scale structure associated with the flow that takes the form of a sharp rise followed by a region where the concentration falls choatically, at a lower average rate, until the next sharp rise. Some typical data traces showing this behavior are depicted on Figure 12. The large scale time corresponding to the plotted data is estimated to be about 1.3 seconds, or about half each line's time span.

The Estimated Scalar Dissipation Rate

The scalar dissipation rate is the instantaneous rate of local mixing of the jet and reservoir gases. By squaring and scaling the concentration time derivative an estimate of the scalar dissipation rate, ε_c, can be made. Here we have used only the mean centerline velocity to

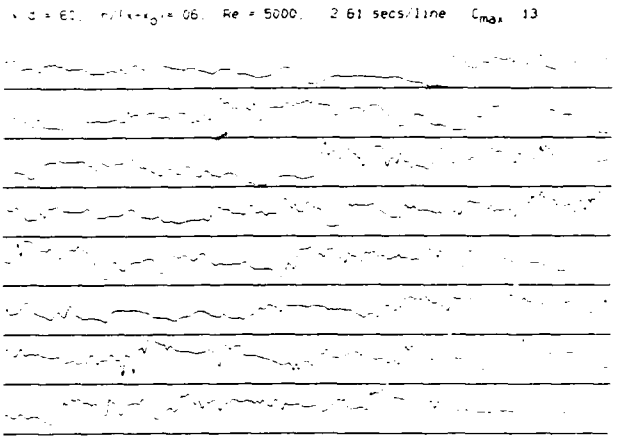

Figure 12. Time traces of the instantaneous jet gas concentration.

scale the time derivative:

$$\varepsilon_c = 3 D_{j\infty} \left(\frac{1}{\bar{U}_{c1}} \frac{dC}{dt} \right)^2 \qquad (7)$$

where $D_{j\infty}$ is the diffusivity of jet gas into reservoir gas. A plot of the mean estimated scalar dissipation rate, computed from the data along the three rays at $r/(x-x_o) = .0, .06, \& .12$, is shown on Figure 13. The scaling of the

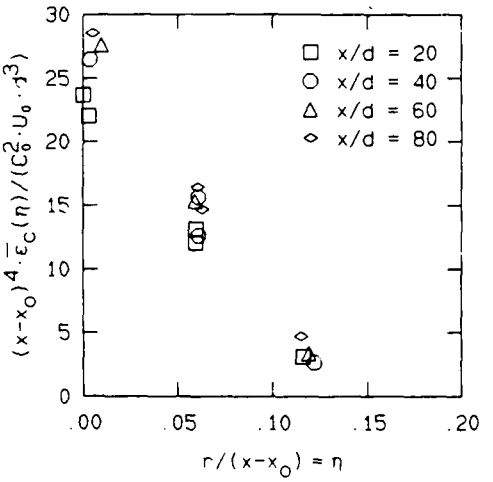

Figure 13. Scaled mean value of the scalar dissipation rate when estimated from $(dC/dt)^2$.

vertical axis is consistent with that suggested by Friehe et al.[12] (1971) for the energy dissipation rate. We note that even though this plot is severely leveraged by a factor of $(x-x_o)^4$, the collapse is acceptable, especially since the data at x/d = 20 may be contaminated by near-field effects.

Classical theories of turbulence at high Reynolds number (Kolmogorov[4] 1962, Obukhov[8] 1962) predict that the probability density function of $(dC/dt)^2$ should be log-normal. The current data are at a modest Reynolds number so they can, at most, provide a test to determine the lower Reynolds number limit of some of the classical ideas. A log-normal distribution is Gaussian when plotted verses a logarithmic abscissa and a linear ordinate. The scaled results of these experiments for $(dC/dt)^2$ are plotted in such log-linear coordinates on Figures 14, 15, and 16 for x/d = 20, 40, 60, & 80 along

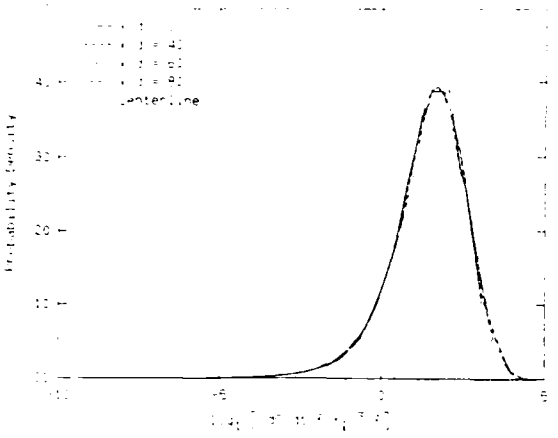

Figure 14. Probability density function of the logarithm of $(dC/dt)^2$ on the jet centerline.

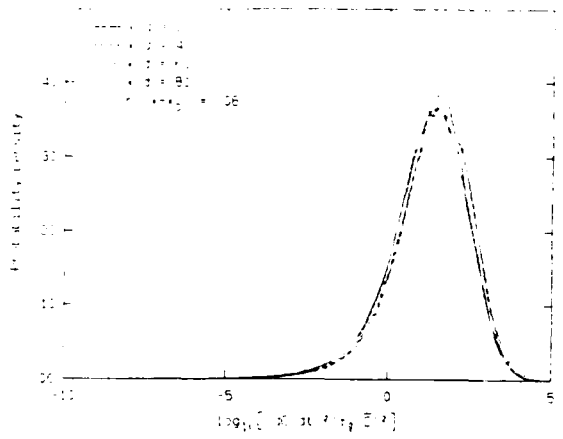

Figure 15. Probability density function of the logarithm of $(dC/dt)^2$ 3.5° off the jet centerline.

the three rays at $r/(x-x_o)$ = 0, .06, & .12. The compiled curves look approximately Gaussian but all display a relative excess at low values and a relative deficit at high values. It is also worth noting that the full width at half maximum of the distributions is typically 3 or more orders of magnitude. To the extent that $(dC/dt)^2$ scales the

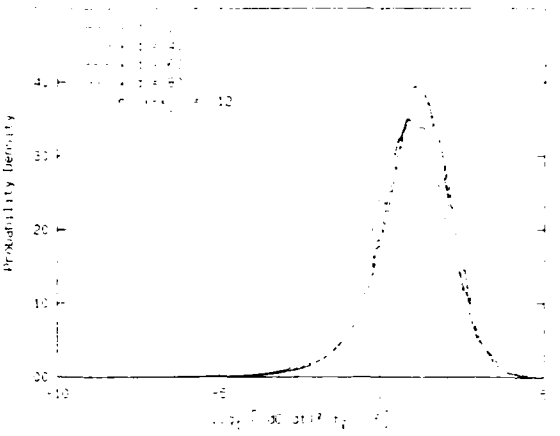

Figure 16. Probability density function of the logarithm of $(dC/dt)^2$ 7° off the jet centerline.

local mixing rate, this result has important implications for the description and modeling of turbulent mixing, with or without chemical reactions and combustion.

Conclusions

Figures 2 through 16 make a compelling case for complete similarity of the mixing at all scales in the far-field of a momentum driven jet. These plots establish that the local mean concentration and the local large-scale time can be used to collapse the statistical measures of the fluctuating concentration field of the jet at a Reynolds number of 5000. Our most recent experiments (see Dowling[9] 1988) suggest that this self-similarity extends to higher Reynolds numbers. Additionally, the measurements presented in this paper show that some of the classical theories of turbulence can be applied at Reynolds numbers which might not be considered high enough for the flow to have reached a Reynolds number independent state.

Acknowledgements

The authors wish to acknowledge Dr. Daniel B. Lang for his assistance in the design and fabrication of the whole data acquisition system. This work was supported by the Gas Research Institute grant # 5083-260-0878 and the Air Force Office of Scientific Research contract # 83-0213.

References

1. AVERY, J.F. and FAETH, G.M. 1974, "Combustion of a submerged gaseous oxidizer jet in liquid metal," Fifteenth (International) Symposium on Combustion, The Combustion Institute.

2. BATCHELOR, G.K. 1959, "Small-scale variation of convected quantities like temperature in turbulent fluid," J. Fluid Mech., 5, 113.

3. BECKER, H.A., HOTTEL, H.C. and WILLIAMS G.C. 1967, "The nozzle fluid concentration field of the round turbulent jet," J. Fluid Mech., 30, 285-303.

4. BIRCH, A.D., BROWN, D.R., DODSON, M.D., and THOMAS, J.R. 1978, "The turbulent concentration field of a methane jet," J. Fluid Mech., 88, 431-449.

5. CHEN, C.J. and RODI, W. 1980, Vertical Turbulent Buoyant Jets: A Review of Experimental Data, (Pergamon Press, New York).

6. CLAY, J.P. 1973, "Turbulent mixing of temperature in air, water and mercury," Ph.D. Thesis, University of California San Diego.

7. DAHM, W.A. and DIMOTAKIS, P.E. 1987, "Measurements of entrainment and mixing in Turbulent jets," AIAA J. 25(9), 1216-1223.

8. DAHM, W.A. 1985, "Experiments on entrainment, mixing and chemical reactions in turbulent jets at high Schmidt number," Ph.D. Thesis, Caltech.

9. DOWLING, D.R. 1988, "Mixing in gas phase turbulent jets," Ph.D. Thesis, Caltech.

10. DYER, T.M. 1979, "Rayleigh scattering measurements of time-resolved concentration in a turbulent propane jet," AIAA Journal, 17, 912.

11. ESCODA, M.C. and LONG, M.B. 1983, "Rayleigh scattering measurements of the gas concentration field in turbulent jets," AIAA Journal, 21, 81.

12. FRIEHE, C.A., VAN ATTA, C.W., and GIBSON, C.H. 1971, "Jet turbulence: dissipation rate measurements and correlations," AGARD Turbulent Shear Flows, CP-93, 18-1 to 18-7.

13. HINZE, J.O. 1975, Turbulence, 2nd ed. (McGraw-Hill Book Co., New York), p. 224-225.

14. KOLMOGOROV, A.N. 1962, "A refinement of the previous hypotheses concerning the local structure of turbulence in a viscous incompressible fluid at high Reynolds number", J. Fluid Mech. 13, 82-85.

15. KUETHE, A.M. 1935, "Investigations of the turbulent mixing regions formed by jets," Journal of Applied Mechanics, Transactions of the AMSE, Vol. 2, no. 3, 87-95.

16. LOCKWOOD, F.C. and MONIEB, H.A. 1980, "Fluctuating temperature measurements in a heated round free jet," Comb. Sci. Tech., 22, 63-81.

17. MONIN, A.S., and YAGLOM A.M. 1975, Statistical Fluid Mechanics II, (MIT Press, Cambridge), Chapter 8.

18. OBUKHOV, A.M. 1962, "Some specific features of atmospheric turbulence", J. Fluid Mech. 13, 77-81.

19. PITTS, W.M., and KASHIWAGI T. 1984, "The application of laser-induced Rayleigh light scattering to the study of turbulent mixing," J. Fluid Mech. 141, 391.

20. PITTS, W.M. 1986, "Effects of global density and Reynolds number variations on mixing in turbulent axisymmetric jets," NBSIR 86-3340.

21. PRESS, W.H., FLANNERY, B.P., TEUKOLSKY, S.A., and VETTERLING, W.T. 1986, Numerical Recipes, (Cambridge University Press, New York), p. 417-419.

22. RICOU, F.P., and SPALDING, D.B. 1961, "Measurements of entrainment by axisymmetrical turbulent jets," J. Fluid Mech. 11, 21.

23. RUDEN, P. 1933, "Turbulente aurbreitungsvorgänge im freistrahl," Die Naturwissenshaften, Jahrg. 21, Heft. 21/23, 375-378.

24. THRING, M.W. and NEWBY, M.P. 1952, "Combustion length of enclosed turbulent jet flames", Fourth (International) Symposium on Combustion, The Williams and Wilkins Co., 789.

25. WHITE, F.M. 1974, Viscous Fluid Flow, (McGraw-Hill Book Company, New York), p. 505-510.

26. WIENER, N. 1949, Extrapolation, Interpolation and Smoothing of Stationary Time Series, (Technology Press, MIT & John Wiley).

27. WILSON, R.A.M. and DANKWERTS, P.V. 1964, "Studies in turbulent mixing - II, A hot air jet," Chem. Engr. Sci. 19, 885-895.